Density-Driven Currents and Deposition of Fine Materials

Saremi, Sina

Publication date:
2014

Document Version
Publisher's PDF, also known as Version of record

Density-Driven Currents and Deposition of Fine Materials

PhD Thesis

$$(EIv'')''=q-\rho A\ddot{v}$$

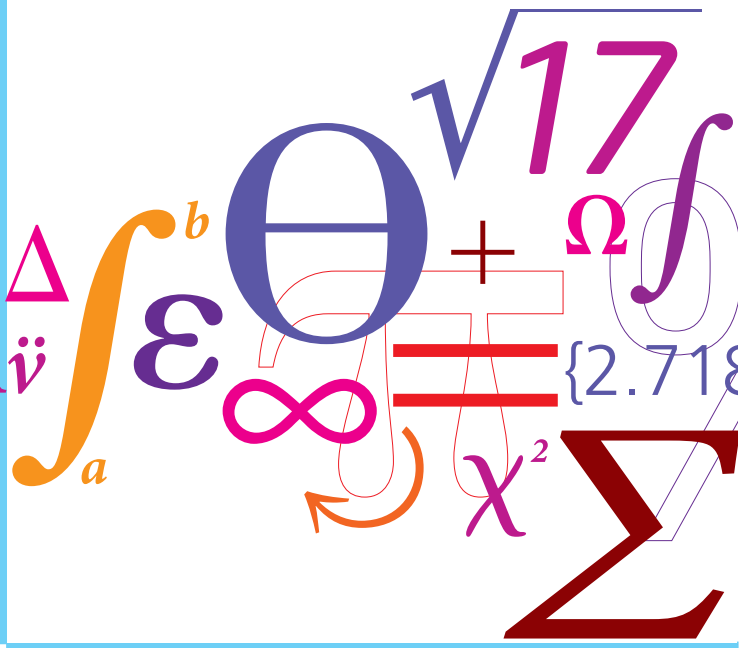

Sina Saremi
DCAMM Special Report No. S168
April 2014

DTU Mechanical Engineering
Department of Mechanical Engineering

Density-Driven Currents and Deposition of Fine Materials

Sina Saremi

Technical University of Denmark
Department of Mechanical Engineering
Section of Fluid Mechanics, Coastal and Maritime Engineering

April 30, 2014

PREFACE

The present thesis *Density-driven currents and deposition of fine materials* is submitted as one of the requirements for obtaining the degree of Ph.D. from the Technical University of Denmark. The work was performed at the Department of Mechanical Engineering, Section for Fluid Mechanics, Coastal and Maritime Engineering, under the main supervision of Associate Professor Jacob Hjelmager Jensen.

The external stay took place at the Danish Hydraulic Institute (DHI) research center in Singapore, arranged and facilitated by Ole Larsen and Thomas Hies, which is much appreciated and acknowledged. A big thanks goes to Juan Carlos Savioli, head of the department at DHI office in Kuala Lumpur , Malaysia, for the arrangement of the visit on board a TSHD at southern coast of Johor, Malaysia.

The very interesting and valuable field investigations of the sediment plumes were carried out at the southern coast of Cyprus, which the collaboration and arrangements done by Dr. Carlos Jimenez and his team from the Energy, Environment and Water Research Center (EEWRC) at The Cyprus Institute (CyI) is greatly acknowledged.

A thanks goes to my colleges in our group for any help and discussions during my three years of studies. A special thanks goes to Ph.D. Niels Gjøl Jacobsen and Ph.D. Bjarne Jensen for lots of helps and long discussions.

Several Master and Bachelor students completed their thesis under guidance of the author and the supervisor. Of relevance for the work presented here, a thanks should be given to Mr. Louis Quist Poulsen who worked on the analytical model of hopper sedimentation presented in Chapter 2, and Ms. Hale Al-Mousavi who worked on the air entrainment in overflow shafts presented in Chapter 5.

The project was founded by the Danish Ministry of Science, Technology and Innovation through the GTS grant: Fremtidens Marine Konstruktioner (Marine Structures of the Future). The support is greatly acknowledged.

Sina Saremi
30^{th} of April 2014

CONTENTS

ABSTRACT

Dredging is a key element in river, ports, coastal and offshore development. In general dredging is conducted for excavation at the river,lake or seabed, relocation of the material, maintenance of the navigation channels, mining underwater deposits, land reclamation or cleaning up the environment. Dredging activities always make changes to the environment, such as alteration of the coastal or river morphology, currents and wave climates, and water quality. Such changes may be considered improving or degrading to the environment. The type of material being dredged, type of the dredging equipment and the local conditions determine the level of environmental interference and the impacts caused by the dredging projects.

Sediment spillage from hopper overflow constitutes a source for sediment plumes and can also impact the turbidity of aquatic environments. The overflowing mixture is often different from the mixture pumped into the hopper (the inflow), because the mixture undergoes compositional transformation as a result of different timescales in the segregation of the various sediment fractions. A proper description of the compositional transformation during filling and subsequent overflow stages can be captured using a sediment budget approach, i.e., by using continuity equations for water and sediment phases. In the first part of this study, the compositional transformation and the bed height inside the hopper are obtained by solving these equations, considering monodisperse, bidisperse, and polydisperse mixtures, the former analytically. Although assumptions tied to the mathematical model are fulfilled best for hoppers rigged with a multiple-inflow system, the model accurately predicts measured concentrations in the final stage of overflow for single-inflow systems.

In the second part of this study, a 3 dimensional two-phase mixture method has been used to model the detailed processes involved in the highly concentrated mixture inside the hopper. The benefit of such model is that it takes into account important dynamic interactions and volume exchange effects due to the settling particles in the flow and the accretion of the bed layer inside the hopper. The model has been validated successfully with experiment and has been used to study different processes critical to overflow losses. The placement of the inlet pipes along the length of the hopper, which is primarily arranged to balance the load distribution in the hopper, has been studied from the perspective of dredging efficiency. The results show large influences from the arrangement of the inlet pipes on the sedimentation rates, and the overflow losses in the hopper. Natural seabed

material is composed by many fractions and the size and type of sediments change along and into the seabed. Variations in the material entering the hopper have been studied by assuming fluctuating inflow concentrations. The fluctuations impose a mean net change on the overflow concentrations.
In the third part of this study, the above described CFD model has been used to model the detailed processes involved in nearfield entrainment, dilution and settling of the turbidity plumes. In order to resolve the entrainment and dilution mechanisms, the Large Eddy Simulation (LES) method has been implemented to directly solve the major flow structures and eddies responsible for the interactions between the mixture and the ambient fluid. The effects of governing parameters on the plumes behaviour have been studied, being in density driven or the mixing regime. The main parameters are the densimetric Froude number at the discharge point below the overflow pipe, velocity ratio between the overflow jet and the ambient current, and the water depth. The results from the CFD model have shown that presence of the dredgers propeller in the vicinity of the overflow plume increases the mixing rate, drags the plume towards the surface and retards its settling rate. The results from the polydisperse model show that the dispersity in size and weight of the sediment constituents affects the fate of overflow plumes, due to dynamic and kinematic interaction between the fractions. The numerical model is a perfect tool for conducting a parametrized study on the nearfield behaviour of the plume, which then provides boundary conditions for the larger scale farfield dispersion models.
In the last part of this study, the hydraulics of the classic dropshafts (being in close resemblance to the hopper overflow structures) has been studied for better understanding of the air entrainment process and the driving parameters. The air entrainment at hopper overflow structures results in further mixing and slower settling of the sediment plume due to the positive buoyancy effects of the entrained bubbles. A two-phase numerical model, based on the Volume of Fluid (VOF) method, has been established to simulate the process of overflow and the air entrainment in circular dropshafts, which has been verified successfully with the experimental data. The model has been used to simulate the performance of the so called Green Valve, as being a mitigation method in reducing the air entrainment in overflow pipes.

RESUME

Uddybning (dredging) er et centralt element i floder-, havne-, kyst- og offshoreudvikling. Generelt udføres uddybninger af floder, søer eller havbund, ved flytning af materiale, vedligeholdelse af sejlender, minedrift, undersøiske lagring, landindvinding og ved oprensning. Graveaktiviteterne ved uddybning forårsager ofte påvirkninger på miljøet, såsom ændringer af kyst eller flodmorfologi, strøm og bølge-klima, og vandkvalitet. Ændringerne kan anses som værende forbedringer eller forringelser af miljøet. Den type materiale som opgraves, opgravningsmateriel og de lokale forhold bestemmer graden af den miljømæssige belastning.

Sedimentspild fra overløbet i den type pramme som anvendes ved uddybning udgør en kilde til sedimentskyer, og kan også påvirke turbiditeten af vandet. Blandingen af vand og sedimenter, der spildes ved overløb, er ofte forskellig fra den blanding, der pumpes ind i prammen. Det skyldes, at blandingen gennemgår en filtrering som følge af forskellige tidsskalaer i udfældelsen af de enkelte sedimentfraktioner. En nøjagtig beskrivelse af filtreringen der pågår under påfyldningen af prammen og ved det efterfølgende overløb, kan beskrives ved hjælp af et sedimentbudget, dvs. ved hjælp af kontinuitetsligningen for vand og sediment. I den første del af dette studie, er filtreringen og deponereringsmængderne i prammen beregnet ved at løse disse ligninger for situation hvor sedimentet er monodisperse, bidisperse og polydisperse. Selvom antagelserne i den matematiske model er bedst opfyldt for en pram med flere indløb kan modellen forudsige målte koncentrationer i den afsluttende fase af opfyldningen, selv for et system med kun et enkelt indløb.

I den anden del af undersøgelsen, anvendes en 3-dimensionel to-fase blandingsmodel til at studere detaljer i sedimentringsprocessen for højkoncentreret blandinger inde i prammen. Fordelen ved en sådan model er, at den tager hensyn til vigtige dynamiske og 3D-effekter. Modellen er blevet valideret ved sammenligning med forsøg, og den er blevet brugt til at studere forskellige processer, der er kritiske for overløbstabet. Placeringen af indløbsrørene langs prammen, som primært er indrettet til at fordele sedimentet i prammen, er blevet undersøgt med henblik på at studere sensitiviteten af indløbets placering på overløbskoncentrationerne. Resultaterne viser, at der er store påvirkninger fra placeringen af indløbsrørene på sedimentationsraterne og overløbstabet i prammen. Det naturlige havbundsmateriale er sammensat af mange fraktioner og størrelser, og typen af sediment ændrer sig horisontalt og vertikalt i havbunden. Effekten af overløbskoncentrationerne ved variationer i det opgravede materiale er blevet undersøgt ved at kigge på indløbskoncentrationer

der varierer i tid. Udsvingene giver ændringer af koncentrationerne.
I tredje del af dette studie, er CFD-modellen blevet anvendt til at modellere detaljerede nærfelts processer ved dumpning udgravet sediment. For at modellere medrivning og opblanding anvendes Large Eddy Simulation (LES) metoden. Denne metode løser direkte de større skalaer i turbulensen, som styrer opblandinger. Effekten af de styrende parametre for spredningen af sediment-fanen er blevet undersøgt, både i det densitetsdrevne regime og opblandingsregimet. De vigtigste parametre er det densimetriske Froude-tal ved udløbsåbningen fra overløbsrøret, forholdet mellem hastigheden i overløbsstrålen og den omgivende strøm, og vanddybden . Resultaterne fra CFD model har vist, at tilstedeværelsen af skibspropellerne på prammen i nærheden af overløbes -fanen øger opblandingen, trækker sedimentfanen mod vandoverfladen og hæmmer dens bundfældningshastighed. Resultaterne fra den polydisperse model viser, at en spredning i størrelse og vægt af sediment sammensætningen påvirker overløbs-faner, som følge af dynamisk og kinematisk samspil mellem sedimentfraktionerne. Den numeriske model er et anvendeligt værktøj til at gennemføre en parameteriseret undersøgelse af nærfeltet i udløbsfanen, som derefter kan give randbetingelser til stor-skala spredningsmodeller.
I den sidste del af denne undersøgelse er de hydrauliske forhold i en klassisk faldstamme (drop shaft) blevet undersøgt for at give en bedre forståelse af luft-medrivningsprocessen. En typisk faldstamme har stor lighed med overløbet og udløbet fra en hopper-uddybningspram. Når luften medrives i overløbet resulterer det i yderligere blanding og langsommere sedimentering af sedimentfanen på grund af opdriften fra de indblandede luftbobler. En tofase numerisk model, baseret på mængden af væske (VOF-metoden), er blevet anvendt for at simulere processen med overløb og luft-medrivning i cirkulære faldstammer. Modellen er blevet verificeret ved sammenligning med eksperimentelle data. Modellen er blevet anvendt til at simulere virkningen af de såkaldte grønne ventiler (Green Valve), som værende en metode til at reducere luft-medrivningen i overløbsrør.

CHAPTER 1

INTRODUCTION

INTRODUCTION

Dredging is a key element in river, ports, coastal and offshore development. In general dredging is conducted for excavation at the river,lake or seabed, relocation of the material, maintenance of the navigation channels, mining underwater deposits, land reclamation or cleaning up the environment. Dredging activities always make changes to the environment, such as alteration of the coastal or river morphology, currents and wave climates, and water quality. Such changes may be considered improving or degrading to the environment. The type of material being dredged, type of the dredging equipment and the local conditions determine the level of environmental interference and the impacts caused by the dredging projects.

The environmental impacts from dredging are divided into physical, chemical and biological impacts. The most pronounced physical environmental impacts of dredging are the raise in turbidity levels in the vicinity and burial of the benthic life. The former is due to spillage of dredged material, which occurs during excavation, overflow during loading or the loss of material during transport, and the latter occurs at the placement site. The duration of the mentioned impacts is also an important issue corresponding to the tolerance level of the receptors. Short periods of high turbidity could be lethal to some species but may not harm the others. As an example, the coral riffs are sensitive to the light change and disturbances from turbidity plumes or severe burial from disposal of dredged material may result in permanent devastation of them (Erftemeijer et al. 2012). However, in some areas the natural background turbidity is high and the local environment has been adapted to it, and the spillage from dredging activities is not considered as an extreme event.

Dredged material can be divided into coarse/fine and cohesive/non-cohesive types of material. Coarser material with higher falling velocities usually settle and leave the water column faster and hardly contribute to the problem of increased turbidity. On the other hand, fine sediments with smaller falling velocities remain longer in water and with the hindrance mechanisms retarding their settling rate even more, they can create long lasting turbidity plumes. The flocs of cohesive material being released into ambient water, may brake up and turn into very fine individual grains, which results in slower settling velocities and increased

(a) (b)

FIG. 1: a) Overflow turbidity plume , b) Dredged material disposal

turbidity levels. The cohesive material may also begin to flocculate and create heavier flocs with higher settling rate. However, the focus of the present study is on non-cohesive fine grains and the flocculation mechanisms are not considered.

Dredging works cover a wide range of different activities within various kinds of projects. Based on type of project, repetition and type of material being dredged, they are traditionally divided into three main groups:

- Capital dredging
- Maintenance dredging
- Remedial dredging

Capital dredging is pertained to large infrastructure projects such as bridges, tunnels, beach nourishment, creation of harbour basins and land reclamation. Therefore, it often deals with compact, undisturbed soil layers with minimum contamination contents and relocation of large quantities of material. Besides the spillage during the course of dredging and burial of benthic life at the replacement sites, such projects also result in permanent destruction of natural habitats. Maintenance dredging involves in removal of siltation from channel beds to maintain the design depth. It deals with various types of sediments possibly contaminated and less compact. Such projects often take place regularly in artificially deepened navigation channels, and there is very little concern about destruction of natural environment. However, the potential impacts from spill and disposal of dredged material still exist. Remedial dredging is exclusively done for removal of contaminated material. It deals with smaller quantities but highly contaminated material. The overall environmental impacts of such projects are considered positive, due to their cleaning purpose, but there still exists risks of spillage during dredging and at the replacement site (Bray 2008).

Besides the type of material and type of the project, the dredging equipment (type of the dredger) also affect the characteristics and the degree of the environmental impacts. Based on the method for dislodging in-situ material and horizontal transport means, there are various types of dredgers with different ca-

(a) (b)

FIG. 2: a) Trailing Suction Hopper Dredger (TSHD) , b) Mechanical Dredger

pabilities. Trailing Suction Hopper Dredger (TSHD) is a type of dredger equipped with suction pipes lowered down to the seabed with dragheads at their end. During the forward movement of the dredger the draghead scratches a thin layer of the seabed which is then sucked into the suction pipe with some water. The dredged material is pumped into the vessel's hopper. The loading continues even after the hopper is filled with the mixture of water and sediment. The heavier fractions settle in the hopper and finer fractions with the excess water flow overboard. When the desired amount of material is retained in the hopper, the dredging terminates and the TSHD navigates to the relocation site. The disposal is carried out through the bottom doors in the hopper or by pumps trough a pipeline to the relocation area. This type of dredger is often used for maintenance dredging or for winning good quality sand far out at sea for reclamation projects (Bray 2008). Mechanical dredgers, either self-propelled or pontoon-mounted, are the other major type of dredgers. A grab or bucket is used for dislodging material and transferring them into a barge. Similar to TSHDs, the loading continues until there is enough material retained inside the barge. Besides the overflow from the barge, the spillage during raising the material from seabed also may increase the local turbidity. However, the use of the recently developed closed grabs prevents the spillage during the raising phase.

The in-situ material after being dislodged from the bed, enter the hopper (or the barge) which acts as a settling basin. The concentration of the overflowing mixture (as the source of turbidity plumes) depends on the sedimentation rate of the particles and their retention time inside the hopper. The rate of sedimentation and the bed rise in the hopper is function of sediment type, hopper dimensions, inflowing concentration and inflow rate. The overflowing mixture forms a buoyant plume by entering the ambient water. The behaviour of the plume is governed both by the mixture characteristics (concentration, sediment type and discharge rate) and the local conditions, namely the ambient current, water depth and other external effects such as dredger's propeller. The overflow structure also can affect

the turbidity plumes. The overflow structures are typically a weir-type at the edge of the barge, or circular dropshafts inside the hopper, releasing the overflow from bottom of the vessel. In both cases the entrainment of the air bubbles occurs at the plunging into the ambient water surface, or at the hydraulic jump inside the overflow pipe. The bubbles mixed in the overflow mixture reduce the buoyancy and by travelling towards the surface hinder the falling of sediment grains. In overall the air entrainment decreases the settling rate of the plumes and enhance their mixing towards the surface.

In following a brief introduction to the analysis and modelling of the mentioned governing processes which influence the environmental impacts of dredging (mainly the turbidity plumes) are presented. In the end a site visit (on board a TSHD) and a field observation (material disposal) are presented, followed by the outline of the present work and further research possibilities.

SETTLING AND SEDIMENTATION OF FINE MATERIAL

The fall velocity of the grains is an important parameter in studying and modelling the processes involved during the whole dredging cycle, namely the sedimentation inside the hopper, overflow, dispersion and deposition at the seabed. The sum of forces acting on each grain determines the direction and magnitude of their velocity. Considering the predominance of drag and inertia interactions , a single fine grain in stagnant water experiences the forces; 1)drag, 2)pressure gradient in surrounding fluid, 3)added mass, 4)effect of acceleration on drag and 5) the gravitational body force (Zuber 1964). The grains reach a terminal fall velocity depending on their response time to the surrounding fluid. The ratio between the grains response time and the hydrodynamic time scale is called the Stokes number St. small Stokes number $St << 1$ shows high degree of coupling between the grains and the surrounding fluid (instantaneous reaction of grains to velocity changes in the fluid), which is the case for fine material. In suspensions with sufficiently high levels of concentration, the individual grains experience additional forces due to mutual interaction with other grains in the suspension. Each individual grain drags down certain volume of fluid while descending, and the total displaced volume of fluid (including the grains volume) creates a return flow which confronts the settling of other grains in vicinity (Batchelor 1972). The overall effect of dynamic and kinematic interactions between the grains in a suspension results in a net decrease in their fall velocity known as Hindered Settling. The variations in size and shape of grains in a suspension influence the degree of hindrance they impose on each other. The return flow from coarser grains may be large enough to change the settling of finer fractions to an upward motion. The coarser fractions also experience a medium around them with enhanced viscosity (Einstein 1906) and density due to presence of fine fractions around them (Batchelor 1982). However, in some lower levels of concentration, there is possibility of occurrence of an other phenomenon, which in contradictory to hindered settling, increases the settling rate in the suspensions; Cluster settling (Kaye and Boardman 1962), which is when group of particles settle faster due to non-homogeneous

horizontal distribution of particles and therefore the preferential return flow in regions of lower concentration.

The rate of sedimentation and deposition of particles depends on the settling velocity and the local flow conditions close to the bed. In hoppers, dredged material with high levels of concentration are introduced from above and the mixture of suspended sediment inside the hopper is overloaded which results in accretion of bed layer at the bottom of the hopper. The hindrance mechanisms result in the formation of hyper-concentrated regions above the bed (the slurry layer) which dampens out turbulence and the velocity gradients close to the bed. Therefore, the governing parameter in determining the sedimentation rate inside the hoppers is the settling rate of the grains, and the maximum packing they can reach depending on their size and shape.

The dredged material entering the hopper is combination of fluid medium (water) and discrete solid particles (sediment grains, clumps and irregular material). Numerical modelling and calculations of the flow fields and sedimentation in such two-phase environment with sharp property jumps between the solid particles and the liquid medium is a great challenge. Apparently the Lagrangian methods can be considered as a good way of approaching this problem, but the large scales being dealt with in the field of dredging, result in extensive computational costs and complexity. Dealing with fine grains, owing to their small Stokes number and relatively very small sizes in compare to major flow structures in the computational domain (the hopper), the solid phase, with good level of accuracy, can be considered as a dispersed continuum mixing in water, which is an Euler-Euler approach. The high levels of concentration inside the hopper implies that strong coupling and mutual interaction exists between the two phases, i.e., the volume occupancy (presence) and motion of each phase influences the other phase. Therefore, the common single-phase approaches such as passive modelling or the Boussinesq approximation (the density varies little, yet the buoyancy drives the flow, thus the variation in the sediment-water mixture density is neglected everywhere except in the buoyancy term) are not valid any more, and a solution which solves the conservation and force balance for both phases (coupled together) is required. The only source of drifting of fine material within a suspension is their vertical falling velocity, which is governed by range of micro-scale mechanisms, which can be approximated as function of the mixture concentration. This justifies the use of the drift-flux method (Ishii 2006) which solves the mixture as a whole, but still taking into account the volume exchange due to movement of each phase and the dynamic interaction between them. The benefit of such method is in considerably reduced computational costs and the complexities due to interface interaction terms in between the two phases solutions.

FATE AND DISPERSION OF NEGATIVELY BUOYANT PLUMES

Overflow of the highly concentrated sediment-water mixture into open water during the overflow acts as a (negative) buoyant jet, which according to its properties and the local conditions, can act as a density driven current towards the seabed, or mixes quickly and forms dispersing plumes possibly at the surface. The ambient current velocity (relative to the sailing vessel) has a considerable impact on mixing the overflow and preventing it to descend as a density current. Other parameters such as entrainment of the air bubbles at the overflow structure can also enhance the mixing rate of the overflowing mixture. The trapped bubbles flow upwards to the surface and hinder the settling rate of the fine grains. The overflow from TSHDs is also affected by the propellers of the vessel, due to the forward sailing during dredging, and therefore experiences further mixing and lift towards the surface. The mentioned parameters determine the nearfield behaviour of the overflow which influence how the farfield behaviour is going to be. The extensive mixing of fine material in nearfield results in formation of surface turbidity plumes travelling considerable distances.

The release of the dredged material in a quasi-instantaneous manner in open water, which happens at the relocation sites (e.g. from the split hoppers), acts as a (negative) buoyant plume forming a particle cloud. The behaviour of the released material can be divided into four distinct phases: 1) convective descent, 2) dynamic collapse, 3) density current over the bed and 4) passive diffusion. During the descent, the entrainment mechanisms due to the shear and density gradients incorporate the mixture in a spherical (ring) vortex resembling an upside down mushroom, which falls faster than the individual grains velocity. Provided with sufficient time (sufficient depth), the expansion and dilution of the plume reaches a point where the plume enters the dispersive phase and particles begin to rain out of the cloud (Bush et al. 2003). In this case the collapsing stage and formation of density currents over the bed do not exist. The minimum depth (the fallout height) depends on the plumes initial concentration and the fall velocity of the individual grains.

As discussed in the previous section, the numerical modelling of the highly concentrated dredged material in different processes during the dredging, overflow and disposal requires full-coupling of the two phases involved. Therefore, the nearfiled behaviour of the overflow and disposal plumes can be perfectly simulated by the mixture method. The most important parameter which determines the rate of dilution and settling of the plume, is the entrainment mechanism due to the eddies and velocity/density fluctuations during the decent of the plume. Therefore, detailed modelling and resolving the flow structures is necessary for simulating the behaviour of the plumes. The Large Eddy Simulation method (Sagaut 2002), which resolves the major structures in the flow, is an adequate approach in modelling the overflow and disposal plumes, otherwise by using the averaging models, the main features of the plume will be dismissed.

SITE VISIT ON BOARD A TSHD

As part of studying the processes involved during dredging and the overflow from the hoppers, the author, during his external research period at the Danish Hydraulic Institute (DHI) research center in Singapore, had a visit on board a trailing suction hopper dredger with 20,000 m^3 hopper capacity, in a sand mining project (for land reclamation) off the southern coast of Johor, Malaysia.

(a)

(b)

FIG. 3: a) The visited TSHD , b) Overview of the hopper

The dredger is equipped with two suction pipes on each side with dragheads at their ends (figure 4b), and it had two overflow shafts at one end of the hopper which their height were controlled by hydraulic jacks (figure 4a). The TSHD had a trailing speed of about 12 knots during the dredging operation under calm sea conditions. The hopper was initially almost empty and the whole dredging took around 4 hours.

(a) (b)

FIG. 4: a) Overflow shaft , b) Draghead at the suction pipe

The inlet configuration was composed of a main inlet at one end of the hopper and few secondary inlets distributed along the length of the hopper. During the course of dredging, due to controlling the load distribution over the hopper, the inlets were used in different combinations in time.

(a) (b)

FIG. 5: Inlet configuration , a) Main inlet , b) One of the secondary inlets

During most of the filling period, only one of the overflow pipes was in use. By the onset of the overflow, the turbidity plume is appeared at the surface, meaning that the overflow mixture undergoes significant amount of mixing and reaches the surface instantaneously, as it can be seen in figure 6b, where the plume appears at the surface from the side of the hopper close to the position of the overflow pipes. The overflow structure was equipped with the Green valve (see chapter 5 for definition of the Green valve), and as a result (also can be seen in figure 6a) the water level inside the overflow shaft is high and almost close to the water level inside the hopper. Therefore, the effect of air entrainment is insignificant. The relative velocity of the hopper and the local currents can be one of the main reasons for enhanced mixing of the overflow plume.

(a)

(b)

FIG. 6: a) Overflow pipe during dredging , b) Overflow plume

The mixture inside the hopper was fully turbulent and well-mixed all along the hopper (figure 7a). The surface turbidity plume appeared behind the hopper, however, was a clear representation of the environmental impact, as can be seen in figure 7b.

(a)

(b)

FIG. 7: a) Mixture inside the hopper , b) Overflow plume behind the TSHD

The second overflow pipe was activated at the final stage, by the onset of the constant tonnage period, where both of the overflow pipes were used maintaining the hopper's weight. This phase starts when the ship has reached its maximum draught. The overflow weir is automatically lowered such that a constant hopper

mass is maintained. In this phase the overflow losses are typically higher ,and it continues until the losses become so high that it is no longer economically feasible to continue dredging, or the sand bed has reached the overflow weir (Braaksma 2008). The termination time of dredging has always been a point of debate between the environmentalists and the dredging contractors, due to the augmented impacts of the overflow plume during the final stages of infilling. In figure 8 the raised bed level inside the hopper after termination is shown. The depression under one of the secondary inlets is visible in figure 8b, which is due to retarded settling because of highly turbulent flow in that region.

(a) (b)

FIG. 8: sand bed inside the hopper after the termination of dredging

FIELD OBSERVATIONS OF THE DISPERSION FROM SEDIMENT DISPOSAL

Hereby, the observations made during a field investigation campaign on the nearfiled dispersion and settling of sediment disposal, off the southern coast of Cyprus, in collaboration with Energy, Environment and Water research Center (EEWRC) of the Cyprus Institute, are presented. The high-resolution underwater footage of the plumes in an unscaled environment close to field conditions has provided valuable insights on the processes involved in dispersion and settling of negatively buoyant plumes of sediment-water mixture. The experiments were carried out in an area sheltered from waves and currents, with a depth of around 9 meters. Different types of sediment have been used in terms of size and density. The two major fractions used during the experiments are described in table 1 below.

TABLE 1: Properties of sand types

Description	$D_{50}(mm)$	Relative density	Color
Fine well-sorted beach sand (mostly quartz)	0.19	2.5	Yellowish
Coarser well-sorted beach sand (igneous rock)	1.49	2.8	Black/greyish

The sediment mixture was prepared in buckets with 20 Litres volume. The payload of the buckets had both single sediment type and mix of fine and coarse types. The concentration of the mixtures were around 50%, resembling the conditions at disposal sites. The mixture was kept fully homogeneous by continuous stirring until the releasing time. The release was done by instantaneous depletion of the bucket just above the water surface.

The evolution of the plume from the very beginning at the release point until the final dispersive phases was recorded in detail, from three different angles and vertical positions (close to surface, at mid-depth and from bottom at the bed). The footage clearly shows the initial descent stage, where due to entrainment of the surrounding fluid, the plume begins to expand and creates a vortex ring, which looks like an upside down mushroom (figure 9a). The fine fractions have fallout heights greater than the available depth and therefore the plume is sustained until the collapsing stage and creates a density current over the bed (figure 9b). The final phase is the diffusion phase, where the plume has diluted and part of it settles and the rest remains in suspension for longer periods just above the bed.

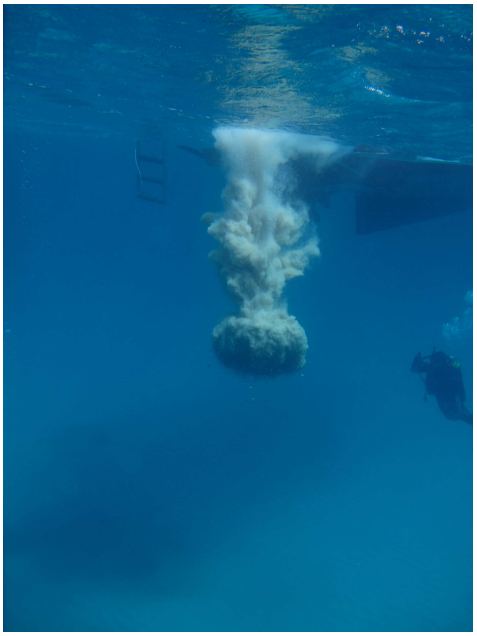

(a)

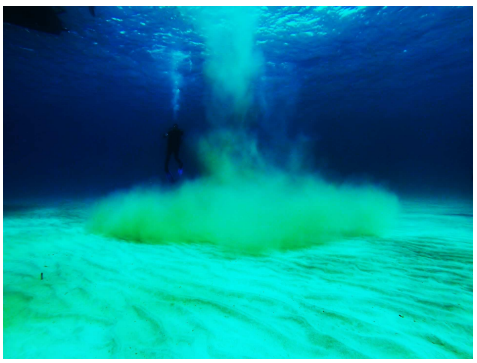

(b)

FIG. 9: a) Formation of the plume after release, b) Density current over the bed after colliding the bed

The effect of size variation on the plumes behaviour could clearly be seen from the tests with mixtures of both the fine (yellowish) grains and the coarse (black) grains. The coarser grains, owing to their higher fall velocities, fallout from the plume (rain out) very soon (figure 10a). The downward current induced by the coarser grains, drags down the fines in the center of the plume, whereas the strong return flow which is created by the coarse grains, pushes up the fines

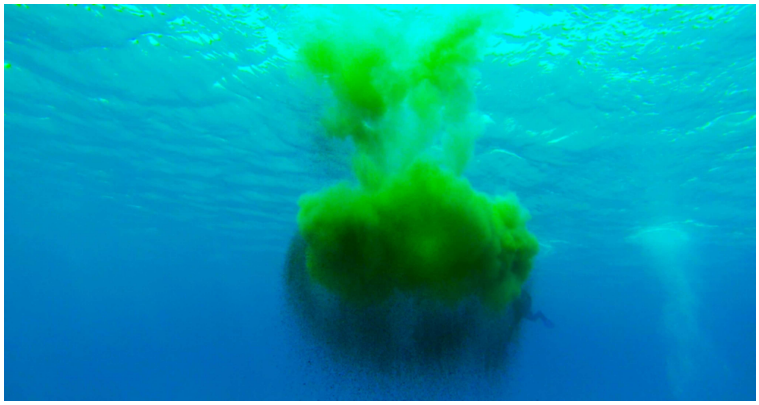

(a)

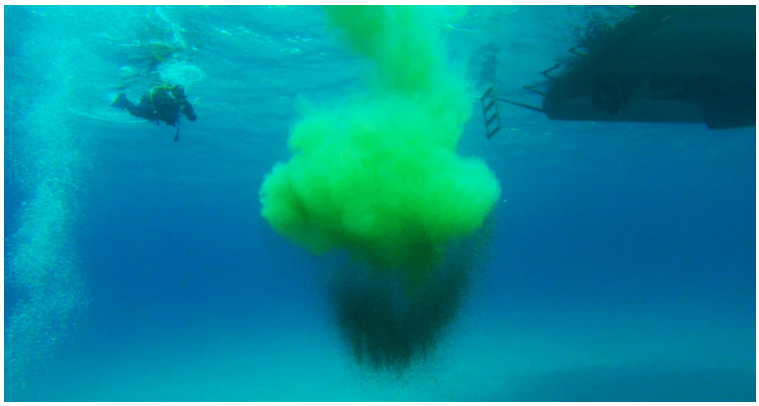

(b)

FIG. 10: Fallout of the coarser grains from the multifraction plume

from the sides, retarding their settling (figure 10b). In overall, the coarser fractions dilute the fines further over the depth and alleviate the downward density driven flow of finer fractions. This causes the finer fractions to remain longer in suspension and maintain the higher turbidity. The observations presented here are part of detailed investigations on the plumes behaviour and testing various mitigation methods on dispersion rates of the plumes, which is under preparation for submission as a scientific article.

OUTLINE OF THE PRESENT WORK

The work presented in this thesis covers the sequences of studies carried out in understanding and investigating the processes involved in dispersion and sedimentation of fine dredged material since being pumped into the hopper until the final dispersive stages after being overflowed or disposed in open waters. By understanding the physics of the governing mechanisms, and the degree of their influence, a firm base is provided for incorporating more sophisticated numerical approach in modelling and simulating the processes during dredging, overflow and disposal of fine, non-cohesive material. The following four chapters include four articles, which are either published or are going to be submitted soon.

The first paper is an analytical study of the sedimentation inside the hoppers and the overflow concentrations. A model based on the continuity equations of sediment and water is developed within a sediment budget approach, considering mono- and polydisperse mixtures. Although assumptions tied to the mathematical model are fulfilled best for hoppers rigged with a multiple-inflow system, the model accurately predicts measured concentrations in the final stage of overflow for single-inflow systems. The model can be used as a preprocessing tool for engineering plume models, providing source specifications for overflow spill and for the subsequent dumping of hopper loads.

In the second paper, a 3 dimensional two-phase mixture CFD model has been used to model the detailed sedimentation and mixing processes involved inside the hopper. The benefit of such model is that it takes into account important dynamic interactions and volume exchange effects due to the settling particles in the flow and the accretion of the bed layer. The model has been validated successfully with experiment and has been used to study different processes critical to overflow losses. The capability of the model in resolving the slurry layer above the bed elucidates the behaviour of the overflow at the final stages of the filling cycle and assists the determination of when to terminate infilling. The placement of the inlet pipes along the length of the hopper, which is primarily arranged to balance the load distribution in the hopper, has been studied. The results show large influences from the arrangement of the inlet pipes on the sedimentation rates, and the overflow losses in the hopper. Variations in the material entering the hopper have been studied by assuming fluctuating inflow concentrations. The fluctuations impose a mean net change on the overflow concentrations.

In the third paper, the mixture model has been used to study the detailed processes involved in nearfield entrainment, dilution and settling of the turbidity plumes from the overflow. In order to resolve the entrainment and dilution mechanisms, the Large Eddy Simulation (LES) method has been implemented to directly solve the major flow structures and eddies responsible for the interactions between the mixture and the ambient fluid. The model, verified successfully with experiments, is used to study the effects of governing parameters on the plumes behaviour in either density driven or mixing regime. The influence of the dredgers propeller and the size variations in the overflowing mixture have been investigated and discussed. The nearfield model is a perfect tool in providing boundary con-

ditions for the larger scale farfield dispersion models.

In the fourth paper, the hydraulics of the classic drop shafts (being in close resemblance to the hopper overflow structures) has been studied for better understanding of the air entrainment process and the driving parameters. A two-phase numerical model, based on the Volume of Fluid (VOF) method, has been established to simulate the process of overflow and the air entrainment in circular drop shafts, which has been verified successfully with the experimental data. The model has been used to simulate the performance of the so called Green Valve, as being a mitigation method in reducing the air entrainment in overflow pipes. The numerical results confirm the effectiveness of the valve in reducing the rate of entrainment of the air bubbles into the overflowing material. The model also provides information about the draw backs of this mitigation method, which is mainly the reduced rate of the overflow.

proposals for future works

Many possible avenues for advancement were touched upon during the current work, but not pursued due to the lack of time. Hereby few of them are pointed out as the possibilities for further investigations.

The mixture approach is an excellent tool for simulating the multiphase flows when phases are dispersed into each other. For including the the effects of the free-surface (for example the impingement of the inflow jets inside the hopper and flow field at the overflow), a more sophisticated model which takes into account both the dispersed sediments and the sharp interface between the air and the mixture should be developed. Detailed representation of the air phase will also enable the modelling of the trapped air bubbles dispersed into the overflow plumes (which was not possible in chapter 4). In order to correctly resolve the processes involved in deposition of the dredged material over the seabed, the model should be able to capture the grain-grain interactions and the interactions between the bed and the density current flowing over it. The model is best suited for fine material (fine sand and smaller). However, in the current study, the cohesive behavior of the clay/silt particles is not included. It can be done by including the (often case specific and empirical) relations for predicting the cohesive behavior of the particles in the multifraction model equations. The LES method is necessary for resolving the flow structures governing the rate of dispersion and the dilution in the plumes. Further investigations on using it in more optimized and cost-effective way should be carried out. In addition to the processes and parameters studied in the present work, there still exists other factors which may affect the sedimentation inside the hopper, and the dispersion of the plumes. For example, the configuration of the overflow structures placed in multi-inlet hoppers and the shape of the hopper could be investigated.

REFERENCES

Batchelor, G. (1972). "Sedimentation in a dilute dispersion of spheres." *Journal of fluid mechanics*, 52(02), 245–268.

Batchelor, G. (1982). "Sedimentation in a dilute polydisperse system of interacting spheres. Part 1. General theory." *Journal of Fluid Mechanics*, 119.

Braaksma, J. (2008). "Model-based control of hopper dredgers." Ph.D. thesis, Ph.D. thesis.

Bray, R. (2008). *Environmental aspects of dredging*. CRC Press.

Bush, J. W. M., Thurber, B. a., and Blanchette, F. (2003). "Particle clouds in homogeneous and stratified environments." *Journal of Fluid Mechanics*, 489, 29–54.

Einstein, A. (1906). "A new determination of molecular dimensions." *Ann. Phys*, 19(2), 289–306.

Erftemeijer, P. L. a., Riegl, B., Hoeksema, B. W., and Todd, P. a. (2012). "Environmental impacts of dredging and other sediment disturbances on corals: a review.." *Marine pollution bulletin*, 64(9), 1737–65.

Ishii, M. (2006). *Thermo-Fluid Dynamics of Two-Phase Flow*. Springer US, Boston, MA.

Kaye, B. and Boardman, R. (1962). "Cluster formation in dilute suspensions." *Proceedings, Symposium on the Interactions between fluids and particles*.

Sagaut, P. (2002). *Large eddy simulation for incompressible flows*. Springer.

Zuber, N. (1964). "On the dispersed two-phase flow in the laminar flow regime." *Chemical Engineering Science*, 19(11), 897–917.

CHAPTER 2

OVERFLOW CONCENTRATION AND SEDIMENTATION IN HOPPERS

Originally published as:
Jensen, J. H. and Saremi, S. (2014). Overflow Concentration and Sedimentation in Hoppers. Journal of Waterway, Port, Coastal, and Ocean Engineering. DOI:10.1061/(ASCE)WW.1943-5460.0000250.

OVERFLOW CONCENTRATION AND SEDIMENTATION IN HOPPERS

Jacob Hjelmager Jensen and Sina Saremi

ABSTRACT

Sediment spillage from hopper overflow constitutes a source for sediment plumes and can also impact the turbidity of aquatic environments. The overflowing mixture is often different from the mixture pumped into the hopper (the inflow), because the mixture undergoes compositional transformation as a result of different timescales in the segregation of the various sediment fractions. The heavier constituents in a mixture will have had time to settle, and overflowing sediments are therefore primarily composed of the finer and lighter constituents, whose concentrations potentially exceed those at the inflow. The hopper constitutes a complex system despite its geometrical regularity; the complexities are largely from the settling processes in concentrated polydisperse mixtures. These settling processes can, however, be captured by employing available settling formulas applicable for multifractional sediment mixtures (i.e., polydispersions). Strictly speaking, these formulas have been validated for homogeneous and unenergetic mixtures only, but the hopper system fulfills these criteria reasonably well. A proper description of the compositional transformation during filling and subsequent overflow stages can be captured using a sediment budget approach, i.e., by using continuity equations for water and sediment phases. In this study, the compositional transformation and the bed height inside the hopper are obtained by solving these equations, considering monodisperse, bidisperse, and polydisperse mixtures, the former analytically. Although assumptions tied to the mathematical model are fulfilled best for hoppers rigged with a multiple-inflow system, the model accurately predicts measured concentrations in the final stage of overflow for single-inflow systems. The model can be used as a preprocessing tool for engineering plume models, providing source specifications for overflow spill and for the subsequent dumping of hopper loads.

Keywords: Overflow, Hopper, Dredging, Sedimentation, Spill, Barge

INTRODUCTION

During marine dredging operations,fines are emitted into the nearshore environment, and the scale of the emissions may lead to the formation of depth-penetrating sediment plumes. Far-reaching and persistent plume excursions may impact the environment beyond the near-shore zone, and the quantification of its

range, strength, and duration constitutes an important input to most environmental impact assessment (EIA) studies. The use of detailed mathematical modeling to delineate impacts of, e.g., dredging activities, sediment disposal, leaching of fines, reclamation works, and sediment replacement, are essential as a platform to encapsulate and integrate complex advection, dispersion, and sedimentation processes occurring in the sea.

A key input to any engineering plume model is the source specification, i.e., the amount and distribution of fines spilled into the environment as well as the duration of the spill. One of the largest sources related to dredging operations is from overflow spill and subsequent hopper load dumping. Its estimation, however, is normally assigned in an ad hoc manner. A common practice in hydraulic engineering, when estimating the overflow source, is simply to resort to sediment samples and/or bore logs of the undisturbed bed to provide input to the fraction distribution and to rely on hands-on guidelines for the part of the sediment distribution that overflows. Typically, a certain percentage of fines are assumed to overflow, but simple rules, such as sediments finer than $75\mu m$ will overflow, are also widely used (Vlasblom 2003). In some cases, the distribution of fines can be obtained from the discharge point of the dredge pipe, as this is often a standard on-board data requisition. Direct measurements of concentrations at the source of the overflow are, however, typically not taken. At the EIA stage, estimates are particularly rough, because dredging has not begun, and often, equipment is not yet defined in detail, as dredging contractors have only rarely been appointed.

Adopting data directly from the seabed or at the dredger-pipe discharge points is not free of problems, because the particle size distribution (PSD) here is not well correlated to the material eventually forming the dredge plume. First, sediment undergoes a series of mechanical processes during the dredging stage that change its characteristics. The mechanical impacts of passing through the drag head, pumps, and dredger pipes will typically dislodge coherent structures in the seabed material. Consolidated seabed material is likely to create lumps in dredge spoils, and if the parent material has significant clay content, a degree of cohesive structure is likely to remain in the dredge spoil within the hopper, i.e., there will not be full disaggregation and dispersion of clay platelets.

Second, certain fractions of the dredged material will be trapped in the retaining hopper, whereas some fractions are lost through overflow. Only a fraction of the overflow material will form the suspension sediment cloud, because heavier constituents in the overflow redeposit in the immediate area of the dredging.

Last,flocculation (for clay fractions) in the overflow stage and immediate spill area can significantly change the settling characteristics of spilled sediments. Clay platelets bond together to form larger particles (flocs) that settle more quickly than individual clay platelets. If the mud content is significant, then flocculation can rapidly increase the overall settling characteristics.

Significant differences in dispersity of the parent material and the spill are thus expected. The compositional transformation from mechanical impacts is treated in Braaksma (2008). In general, however, the first two stages are, as

mentioned previously, often ignored by the hydraulic engineer in place of hand-waving guidelines, whereas the latter stage should be accounted for directly in the plume model itself. This work considers the part of the transformation occurring inside the hoppers. The following outlines a method to coherently derive the sources for plume modeling from the dredging activity, which includes overflow and the subsequent dumping of the hopper load.

PREVIOUS WORKS

Only a few journal papers have been published on the topic of overflow concentrations from hoppers. Instead, work in this field has been released primarily through conference papers. Most of this work takes a starting point in the work of Camp (1946), who studied sedimentation processes in closed idealized containers of constant volume, with inlet and outlet sections located at the front and back ends of the container, for the purpose of designing water treatment tanks. Camps design tool is built on simple considerations of the trapping efficiency: (1) the adaptation process for suspended sediment is obtained by assuming that sediments undergo pure advection by horizontal velocities, and (2) velocities attain a profile of uniform flow.

Koning (1977) and later Vlasblom and Miedema (1995) migrated concepts from the design model of Camp (1946)for water treatment tanks to a model describing sedimentation inside hoppers. The novelty of their model was two-fold; the importance of hindered settling and the influence of diffusivity on adaptation processes were recognized. Accumulation of sediments at the bottom of the hopper, i.e., the presence of a packed layer, was also accounted for. The model, however, retained the simple flow description of Camp (1946). The adopted simplified flow reflects a certain (single) inflow arrangement and hopper geometry. In Ooijens (1999), further modifications are made to the hopper model, wherein the unsteadiness of the mixture concentration is introduced, allowing the mixture to store sediment, thus introducing additional phase-lag effects in the system. Ooijens model, however, also retains the simple prescribed flow field of Camp (1946), i.e., the simple inlet/outlet arrangement.

In Miedema (2009a), a descriptive overview of infilling stages (four stages identified) in single-inflow arrangements is provided, and some nice gimmicks for unsteady inflow conditions are presented in which varying inflow conditions inherent to real operations are displayed. In that work, a slight improvement of the flow description is presented by including the total head associated with the overflow, thus accounting for the extra water level inside the hopper. The simple inlet/outlet arrangement used in previous works is, however, maintained. It can be argued that the trapping efficiency is not fully correlated to the length of the hopper but rather to the time that the sediment is retained inside the hopper.

The simple models rooted in the Camp model seem to be tied, more than necessary, to the container geometry. For a single-inflow system, the length-scale model of Miedema (2009a) performs well, as demonstrated by Rhee (2002), but predictions will likely be inaccurate for cases with multiple-inflow systems,

where streamlines along which sediments are advected become complicated (and stochastic in cases of unsteady inflow and pronounced three dimensionality). Choosing a geometrical length scale as a scale for adaptation is not straightforward.

In Miedema and Rhee (2007), the model sophistication is increased by modeling the flow and concentration processes in the context of one dimensional (1D) and two-dimensional (2D) depth-resolving models, where the distributions of the flow and concentrations are liberated. Reference is made to Rhee (2002) for details on the 1D and 2D models, noting, however, that the 2D model is based on the Reynolds averaged Navier-Stokes equations with a standard $k - \epsilon$ model to promote turbulence, thereby ignoring important interactions between concentration and turbulence on one hand and between turbulence and settling on the other hand. Nonetheless, the model provides a more accurate description of the hopper system. The improvement is partly achieved through adoption of the settling method for polydisperse mixtures, as originally described in Masliyah (1979), involving the kinematic coupling between settling of individual fractions, as opposed to treating fractions independently as if they were part of an isolated monodispersion. The two-dimensionality of the model is, however, challenged by the use of hindered settling formulas, which assume mixture homogeneity (statistically). In general, depth-resolving models improve the description of local flow and sediment processes inside the hopper. The models bring an increased flexibility in the modeling of more complex hopper arrangements and can thus be perceived ultimately as supporting the design and optimization of hopper configurations. The 1D and 2D models reproduced overflow concentrations measured in scaled laboratory single inlet hopper settings well. The good agreement was attributed to limited horizontal variability in concentrations observed inside the laboratory hopper, even for the single-inlet arrangement, and it was concluded that turbulence plays a secondary role in overall hopper processes. The role of turbulence was, however, studied thoroughly in the laboratory, the argument being that turbulence would be underestimated at laboratory scale. These measurements were part of a comprehensive laboratory campaign reported by Rhee (2002), which provides valuable and detailed observations of processes inside and at the overflow of the hopper. Throughout this paper, the authors will return continually to these experiments, as they define a well-documented baseline for discussion.

Braaksma (2008) and Miedema (2009b) returned to the less sophisticated modeling of overflow spill, arguing that depth resolving models are not operationally efficient, need calibration, and lack the transparency provided by simple models. In Braaksma (2008), a model based on mass balance equations inside the hopper was proposed, leaving most of the parameters related to sediment characteristics to be calibrated by on-site measurements. The model was developed as a real-time control and optimization tool. The formulation was tested with varying concentration profiles, including exponential,linear, and constant profiles over hopper depth. Braaksma adopted the latter profile, providing overflow concen-

trations in good agreement with test rig data. The success of the elected uniform profile was consistent with findings by Rhee (2002).

PRESENT WORK

With the purpose of developing a robust model for common hopper configurations and inflow arrangements and furthermore finding evidence in experimental results of Rhee (2002) of limited dimensionality governing sediment transport processes (even with single-inlet arrangements), it seems logical to approach the problem from an integrated angle. In particular, pronounced horizontal and vertical uniformity observed in concentrations can be utilized, e.g., by adopting available settling formulas established for homogeneous mixtures. A theoretical footing resembling, to some extent, that of the Braaksma model is the starting point for the present investigation. The target of the present work is to develop a preprocessing tool that can provide source conditions for engineering plume models. The source conditions comprise

- The PSD of the spill during overflow (at the overflow site)
- The PSD of the material in the hopper-bed layer (for disposal)
- Duration of the spill and the loading to provide input to dredge plans and preliminary spill budgets.

By resolving the PSDs, detailed estimates of both the duration of the spill and the actual source strength during the overflow (spill) and at dumping (disposal of the hopper load) are acquired. Because the two sources (from the mixture and the hopper bed) are determined concurrently (through the laws of conservation), the conservative approach of using an identical source at the dumping and the spill sites is avoided. (The fines emitted at the spill are not also emitted at disposal.) The hopper tool has been developed in response to demands made over the course of many large EIA studies involving plume-excursion modeling (carried out by the first author).

Monodisperse mixtures (uniform sediments) are considered first to provide insight into the processes governing the transformation occurring inside the hoppers. Second, multifractional mixtures are considered. These include the canonical case of bidisperse mixtures and the polydisperse mixtures described by a continuous PSD curve. Results of the model are compared with measurements.

DEFINITION OF THE PROBLEM

Often hoppers are used for the temporary retainment of dredged seabed material. The material is transferred from the seabed to the hopper by pumping it through connecting dredger pipes. To ease the pumping, seabed material is fluidized with seawater, and a resulting mixture of high concentration enters the hopper through multiple dredger-pipe valves. An example of multiple valves (discharging above the surface) loading a hopper is shown in Fig.1a. As a basis

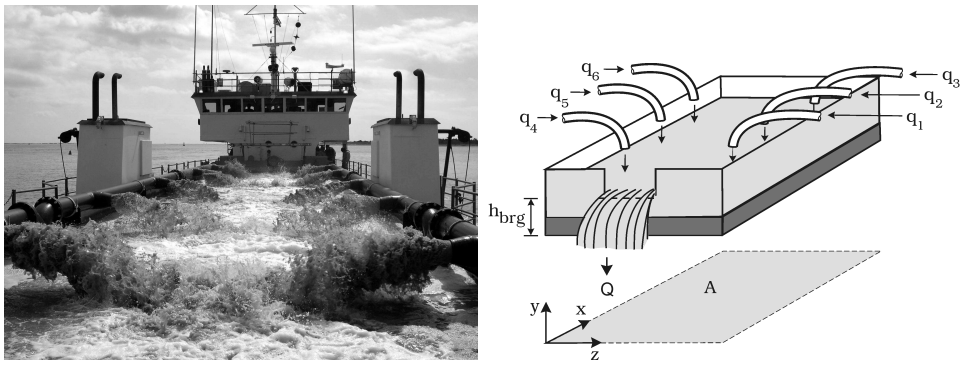

(a) (b)

FIG. 1: (a) Multiple-inflow arrangement (courtesy of Hank Heusinkveld, U.S. Army Corps of Engineers); (b) definition sketch of hopper parameters with overflow from the back and with indication of mixture (light gray) and bed (dark gray) layers

for discussions and the underlying assumption in the Two-Layer Model section, please take note of the foam/turbulence on the water surface of the hopper.

Inside the hopper, the mixture cannot sustain the sediment suspension. Sediments will segregate from the mixture and accumulate in a packed layer at the bottom of the hopper (the bed). This layer will consist primarily of fractions that segregate quickly (typically larger particle sizes), whereas slower separating constituents remain in the mixture layer for a prolonged period of time. The bed typically thickens rapidly during most of the loading process. The segregation of water and especially fine sediments occurring in the hopper is the core of the problem, because the segregation process is incomplete, owing to the finite size of the hopper and the time scale of the settling of the fines. The challenge is to control segregation inside the hopper, which for sand mining infers that only larger constituents of the seabed material are retained, i.e., the leaching of fines is optimized. In most dredging works, however, the environmental agenda takes precedence, which means that the reintroduction of seabed sediments (especially fines) in the marine environment, through overflow spill, is minimized. Under certain (rare) conditions, any spill at the dredging location is not tolerated, and a restrictive no-spill practice is enforced. This is typically adopted when dredging is carried out within very sensitive environmental zones. In these cases, loading operations terminate when the total volume of mixture pumped into the hopper reaches the actual hopper capacity; thus, only a limited seabed volume can be transported per load. A more common practice is a continuous loading operation beyond the hopper capacity, which terminates when the bed reaches a certain height. In the continuous loading mode, the mixture overflows when the hopper is full, and as a consequence, spillage occurs for a certain period of time. The

concentration of fines in the overflow spill can be partly controlled (minimized), noting inherent uncertainties in the composition of seabed sediments. One way of reducing sediment spill is by controlling the carrying capacity of the mixture by either adjusting the degree of fluidization (within pumping limits) or regulating the pumping rate. Limiting the pumping rate can increase retention times and thus allow more sediment to settle, whereas fluidization can be used to saturate the mixture to overwhelm and dampen turbulence (see Appendix). Another way of reducing spill is through the choice of hopper equipment, arrangement, and configuration. This is, to a large extent, reflected in hopper designs; examples of rational designs include the use of shallow hoppers with large planform dimensions, which are ideal for capturing suspended sediments, as well as multiple-dredge pipe discharge arrangements, which are often preferred over single-inflow arrangements, because of improved trapping, promotion of more uniform concentrations over the length of the hopper, which promotes a more leveled fill and higher growth rates, and additional flexibility for the operation. An appraisal of hopper designs (size, width-to-length ratios, and inflow and overflow structures) is provided in Vlasblom (2003). Optimization of the operation has been examined by, e.g., (Miedema 2009a). In the following, hoppers are assumed to be in the shape of rectangular cuboids of height h_{brg} and with planform area A such that the available volume or hopper capacity,V_{brg}, equals Ah_{brg}. In Fig.1b, a definition sketch of the hopper parameters is presented. The rate of overflow (here from the back of the hopper) is denoted Q. From continuity, the overflow equals the net inflow, which for multiple-valve arrangements, as indicated in Fig.1, equals the sum of inflows from individual pipes, i.e.,$Q = \Sigma q_i$, where q_i is the inflow from the ith pipe.

GOVERNING PROCESSES IN HOPPERS

Before proceeding to the formulation of the governing equations for hopper concentrations, it is beneficial to discuss fundamental processes that are key to the distribution of sediments in the hopper and to the compositional filtering.

Destratification and consolidation effects are not considered to be key processes in hoppers, because the concentration varies little in the vertical direction (this is discussed in the Appendix), and consolidation occurs on timescales much larger than the timescale of the loading. Flocculation is also neglected, assuming the seabed material to be composed of noncohesive sediments. This is a limitation of the model, because dredged sediments are just as often cohesive and, as mentioned in the Introduction section, can potentially play a role in the transformation. The focus of the discussion will be on the role of settling and turbulence in monodisperse and polydisperse mixtures of noncohesive sediments and how these adapt in hoppers of different dimensions and to inflow conditions (discharge rate, inflow concentration, and particle dispersity).

Timescales

A few key timescales for the processes taking place inside the hopper during loading can be identified. The retention time,t_w, is the average period of time

that particles entering a hopper are retained within that hopper, which can be expressed as follows:

$$t_w = \frac{V_{brg} - V_b}{Q} = \frac{V}{Q}$$

where V_b =volume of the bed, which typically equals zero at the onset of loading; and V =volume of the mixture. As the hopper is being filled, the mixture volume V and thus the retention time decrease. The period of time,T_{fill},of no overflow can be determined as follows:

$$T_{fill} = \frac{V_{brg} - V_0}{Q} = T_w - \frac{V_0}{Q}\,, \qquad T_w = \frac{V_{brg}}{Q}$$

where V_0 =ballast (preload) volume; and T_w =potential value of t_w. Note that t_w is a bulk measure for the retention time, disregarding detailed geometry and flow within hoppers and thus disregarding the existence of dead zones. Dead zones are the ineffective sections of hoppers from, e.g., the presence of recirculating currents. Dead zones can, according to Camp, occupy approximately 30% of the settling tank volume, resulting in a comparable reduction in retention time. The focus of Camps investigations was settling tank setups, which are characterized as single-inlet systems. In this study, multiple-inlet arrangements are (primarily) considered, and because dead zones are known to be reduced with the number of dredger-pipe valves, a more even loading and thus better utilization of the hopper are anticipated. The loading is terminated when V_b reaches some fraction of V_{brg}. In the section Duration of Loading and Spill, the loading time and the duration of the overflow are estimated.

The residence time,t_s, defines another important timescale, giving the time required for sediments to settle over the depth of the mixture as follows:

$$t_s = \frac{h_{brg} - h_b}{U_c} = T_s - \frac{V_b}{U_c A}\,, \qquad T_s = \frac{h_{brg}}{U_c} = \frac{V_{brg}}{U_c A}$$

where U_c =settling velocity; and T_s =potential value of t_s. The residence time decreases with decreasing mixture volume (i.e., height). The spatial analogy to this parameter is the adaptation length; however, an adaptation length requires specification of relevant velocity scales, which can be difficult to characterize in hoppers rigged with more complex dredger-pipe and overflow arrangements.

The concentration of the overflowing mixture is different from that pumped into the hopper because of the retention and settling timescales. A fundamental parameter for trapping sediment in hoppers is the ratio of the two timescales, expressed as follows:

$$\beta' = \frac{t_w}{t_s} = \frac{T_w}{T_s} = \frac{U_c A}{Q} \tag{1}$$

This parameter constitutes a measure for the probability for a given particle to deposit and will emerge as a significant number in the governing equations

and their solutions. Samples of sediment from natural seabeds (or from hoppers) will typically comprise a wide range of fractions, each having a unique value of T_s and thus β'. Fractions thus accommodate differently within the retention time (because of differences in segregation timescales of the various fractions), and consequently, some fractions will deposit, whereas others remain in suspension and risk overflow. In a given hopper, particles with β' larger than unity are more likely to deposit, regardless of their position above the bed, whereas particles with β' smaller than unity are less likely to deposit, because only particles within a certain distance from the bed can reach the bed. The rationale behind hoppers having large planform areas can thus be explained by enhanced trapping efficiency, corresponding to a large β'. In the following, a simple version of the parameter will be adopted as follows:

$$\beta = \frac{U_T A}{Q} \qquad (\beta' = \beta \frac{U_c}{U_T}) \tag{2}$$

which is based on U_T rather than U_c, the former being the settling velocity for isolated particles (as if settling in clear water). A similar parameter, labeled removal, was presented in Camp (1946).

Settling

The hopper floor is solid, which conforms to a condition at the bed of zero flux (through a horizontal plane), and the flux of volume of one phase will induce a compensating inverse flux of volume of the other phase. In hoppers, the settling of suspended sediment entails accretion of particles at or supported by the floor and an upward displacement of water. The upward displacement or reflux of water is forced into the mixture as an interstitial vertical velocity opposing the settling of sediments and thus impeding settling throughout the mixture. In otherwise homogeneous mixtures, this velocity is vertical and constant, and its magnitude,v, can be derived explicitly for both polydisperse and monodisperse mixtures using the equations of continuity (the zero-flux condition) as follows:

$$\sum_{i=1}^{N} U_{c,i} c_i - v(1 - \sum_{i=1}^{N} c_i) = 0, \quad for N = 1, \;\; U_c c - v(1-c) = 0 \tag{3}$$

where index $i = i$th constituent in a polydisperse mixture containing N constituents (of different size); c_i =fractional concentration; and velocities are relative to the hopper coordinates (x, y, z), as shown in Fig.1. Other vertical velocities, i.e., in addition to that from the exchange of volume, are introduced in the governing equations presented in the Two-Layer Model section. As proposed by Masliyah (1979), the settling velocity can be found by subtracting the opposing interstitial velocity determined from Eq.3 from the slip velocity,w_s , as follows:

$$U_{c,i} = w_{s,i} - v \tag{4}$$

Combining Eq.3 and Eq.4 leads to the following system of equations for the settling velocities of the N constituents:

$$\beta_i \frac{U_{c,i}}{U_{T,i}}(1+\frac{c_i}{1-c}) + \sum_{j=1,j\neq i}^{N} \beta_j \frac{U_{c,j}}{U_{T,j}} \frac{c_j}{1-c} = \beta_i \frac{w_{s,i}}{U_{T,i}} \ , \qquad c = \sum_{i=1}^{N} c_i \tag{5}$$

where c =total concentration. Eq.5 can be solved with a matrix solver, whereby settling of an individual particle depends on all the other particles. The settling of a constituent in a polydispersion is thus more complex compared with settling in monodispersions because of the battle between constituents. In polydisperse mixtures, finer fractions can, e.g., be lifted upward by the vertical velocity imposed primarily by the settling of the coarser fractions. Upward movement of finer fractions is associated with a downward displacement of water, and these fractions therefore impede the (dominating) vertical velocity induced by the coarser fractions. From pure kinematic considerations, however, it can be shown (using Eq.20 and Eq.21) that no particle in a suspension will be advected upward faster than the bed, implying that all particles move downward relative to the bed and will thus ultimately be engulfed by the bed.

Nonspherical particle shapes may affect the return flow, as an additional amount of water may potentially remain with the particle as it settles. In his experiments, Steinour (1944) estimated the additional volume to be approximately 20% for angular, as compared with spherical, particles. In principle, this increase in displacement volume can be accounted for by adding the additional volume to the concentration in Eq.3.

To solve Eq.5, the slip velocity must be known. The slip velocity depends on the actual flow and force fields in the interstitial fluid induced by the settling particles. The interstitial flow and forces further impede settling and constitute, together with the reflux effect outlined previously, the hindered settling effects. In general, slip velocities have been studied for homogeneous and unenergetic mixtures, often by considering Stokes-sized and spherical-shaped sediments only. Theoretical derivation of the slip velocity and a discussion of effects in a dilute mixture are presented in the authoritative contribution by Batchelor (1982). In the present work, closure is obtained by using the semiempirical formula for polydisperse mixtures proposed in Davis and Gecol (1994). This formula can be interpreted as an extrapolation of the empirical formula of Richardson and Zaki (1954), which is valid for monodispersions of high concentration, by the theoretical findings for dilute polydisperse mixtures (here reduced to equidensity mixtures) of Batchelor (1982), and reads

$$\begin{aligned} \frac{w_{s,i}}{U_{T,i}} &= (1-c)^{m-1}[1 + \sum_{j=1,j\neq i}^{N} (m - m_{ij})c_j], \\ m_{ij} &= 3.5 + 1.1\lambda + 1.02\lambda^2 + 0.002\lambda^3, \qquad \lambda = \frac{d_i}{d_j} \end{aligned} \tag{6}$$

where λ =particle size ratio between the jth and the ith constituents; and $m = 5.622$, which is valid for the range of Reynolds number (R) considered. In general, m depends on the shape of particles and on the R(Garside and Al-Dibouni 1977). The slip velocity of a given particle in a polydispersion depends on all the smaller particles surrounding it. The velocity for isolated settling is described as follows:

$$U_{T,i} = \frac{\psi U_{T0,i}}{1 + 0.15R^{0.687}} , \qquad R = \frac{U_{T,i} d_i}{\nu} \tag{7}$$

where U_{T0} =Stokes settling velocity; ψ =nonspherical shape factor; d =grain size; and ν =kinematic viscosity. The denominator is a fitting function that extends the applicability to R up to 500 (Schiller and Naumann 1933).

The applied settling formulas in Eq.5 and Eq.6 are applicable for limited levels of ambient turbulence and homogeneous dispersion. These assumptions are compatible with actual conditions inside hoppers, and the settling theory is thus tailored for the present applications. The effects of turbulence on settling are discussed in the Turbulence section.

Turbulence

To facilitate discussions on the distribution of mixture concentrations in hoppers, being a system with a high degree of saturation per se, a few important observations on turbulence are subsequently highlighted.

The distribution of turbulence and flow structures are likely to display some degree of three-dimensionality. With respect to turbulence, three significant sources can be identified:

1. pipe turbulence is introduced into the hopper mixture at the discharge points. Generally, this turbulence is short-lived outside the pipe and, therefore, most pronounced across the surface layers, dispersing rapidly as it penetrates to the lower layers of the mixture.

2. Turbulence is generated along the sheared perimeter of the inflow jet and from the air entrainment from plunging. This turbulence is also short-lived and confined to the inlet sections and the near-surface layers.

3. Turbulence is generated by the net flow through the hopper (water moving from the inflows to the overflows).

The impinging turbulence from the first and second sources is spatially confined; the former decays rapidly over a distance of 5-10 pipe diameters. The impacts of these sources are evident in the experiments of Rhee (2002), where the bed growth is retarded at the inlet section, likely because turbulence in single-inlet systems is more concentrated. In comparison with the overall dimensions of the hopper, impacts are moderate. In the case of multiple inlets, turbulence is introduced and dispersed over a larger area, where the first and, to a larger

degree, the second sources act as horizontal mixers of sediments across the surface layers of the mixture. This is shown in Fig.1 as formation of foam on the surface.

Source 3 possesses the largest capacity for near-bed turbulence and is not confined to inlet sections but affects the entire hopper. The source may become important in the late stage of loading where the mixture height is small and the flows are representatively larger. The β'-parameter can, for an otherwise stationary loading operation, be considered constant throughout loading, because it remains invariant to the height of the mixture by virtue of it being a settling parameter. (Note that height can be significant for the stability of barges.) Because settling is sensitive to turbulence, at least three turbulence-related effects on β' can be identified: (1) Stokes-sized particles are coupled to small-scale turbulence structures, leading to particle congregation and downward sweeping, effectively increasing settling by up to 50% (Wang and Maxey 1993); (2) flocculation of sediments increases settling; and (3) more energetic scales of turbulence govern diffusive fluxes of sediment in the vertical direction. As dispersions inside hoppers are often nearly homogeneous, upward and downward fluxes will nearly cancel (see Appendix). Stratification in hoppers occurs when the influx of sediment changes (and is perhaps also prone to exist in some single-inlet systems). In such cases, turbulence can play a role, as demonstrated in the laboratory flume investigations by Rhee (2002).

The level of turbulence in hoppers is a function not only of the sources outlined previously but also of its decay. The turbulence decay is particularly efficient in mixtures of high concentration as a consequence of sediment-induced turbulence damping. Significant turbulence damping and thus reduction in the carrying capacity occur from the mere presence of suspended sediments. In Thompson et al. (2006), a decrease in bed shear stresses of up to 50-70% in homogeneous (i.e., nonstratified) dispersion of fine sediments is observed.

With this discussion in mind and with van Rhees findings that turbulent diffusion is dismissible, it seems reasonable that near-bed turbulence in a hopper environment can be assumed secondary to other processes.

TWO-LAYER MODEL

The mixture is fueled from above by inflow sediments. Inflow density currents may form in the initial phase (Rhee 2002), but generally, sediment is dispersed rapidly in the surface layers by horizontal mixing from the first and second turbulence sources discussed in the Turbulence section. This phenomenon manifests itself in the pronounced horizontal uniformity of near-surface concentrations. Therefore, if the flux of sediment through the surface remains the only source of sediment, then profiles of concentration are approximately constant over depth (see Appendix). In systems similar to that presented in Fig.1, with multiple inlets, the concentration is particularly uniform. The homogeneity of the dispersion is in agreement with the experimental and numerical findings of Rhee (2002), which considered single-inlet systems that are not necessarily prone to uniform concentrations to the same degree expected in multiple-inlet systems. The mea-

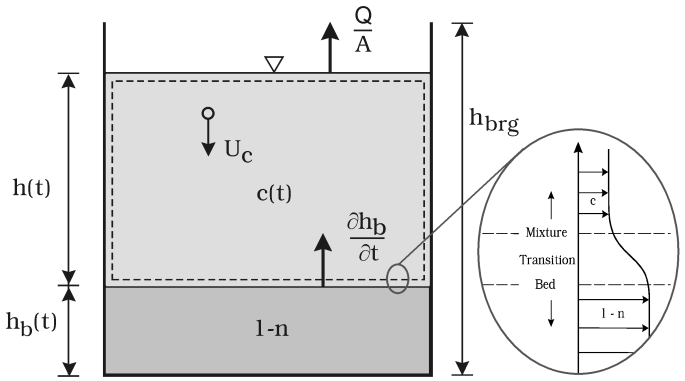

FIG. 2: Cross-sectional view of the hopper prior to overflow, showing the governing parameters and layers

surements show that, even though the flow and turbulence structures display pronounced three dimensionality, sediments segregate with little regard to near bed flow structures as long as the sediment mixture remains homogeneous.

A model for the bed height and the mixture concentration is developed for a hopper system based on a sediment budget established for each fraction in the mixture. The model uses a two-layer representation of the hopper content as follows:

- Mixture layer: This layer contains suspended sediments, and concentrations are assumed homogeneous throughout the layer (averaged over hopper volume). Concentrations and mixture heights are denoted $c(t)$ and $h(t)$, respectively, where t is the time. The sediments are input evenly across the surface of the mixture.

- The packed layer (bed): This layer contains the deposited sediments. The height of the bed is denoted $h_b(t)$, and the concentration in the bed attains a value of $1 - n$, where n is the porosity. The bed defines the zone where settling is partially or fully terminated. The value of n is assumed constant and in the range of 0.4-0.5, which reflects a looser packing than the parent seabed (typically $n = 0.4$) because of the sediment segregation and a lack of consolidation.

A cross-sectional view of a hopper is shown in Fig.2 prior to overflow, presenting the two main layers and their surface elevations. During overflow, the bed grows until it reaches its final height.

A two-layer representation of the hopper content is an approximation. A slurry layer that transitions from the bed layer to the mixture layer will appear as a consequence of hindered settling; the height of which, however, is small compared with the height of the hopper, as shown in Fig. 2. The slurry remains passive

with respect to the processes occurring in the mixture and the bed layer and may therefore be ignored in the present investigation. The limited interaction with the mixture layer was observed in Rhee (2002) (Test08), where the concentration of the mixture layer persists right up to the point where the slurry is exposed to the overflow. The slurry will, on the other hand, tend to even out the bed undulations under the action of gravity. In single-inlet systems, a distinct bump is often created in the central part of the hopper, and bed leveling from slurry avalanching becomes more pronounced (Rhee 2002). In multiple-inlet systems, the bed develops more evenly (Vlasblom 2003), and the slurry is less dynamic. If loading is continued up to the point in time where the slurry becomes exposed, then the two-layer model takes overflow concentrations (in this short stage) to be equal to the average of the mixture concentration (i.e.,c) and the bed layer concentration (i.e., $1-n$). If loading is continued beyond this point, overflow concentrations will equal c_0, corresponding to the exceedance of hopper loading capacity. Results presented in the next section consider loading terminated prior to exposing the slurry to overflow, and overflow concentrations are assumed equal to c.

Interface Flux (Monodispersion)

The flux of sediment through the interface separating the mixture and the bed layer is given as follows:

$$\Gamma = c(U_c + \frac{\partial h_b}{\partial t})A \tag{8}$$

which accounts for the continuous advance of the interface (the second term on the right-hand side). The interface flux is based on the volume averaged concentration, c, utilizing that the diffusive flux in the homogeneous mixture is negligible (see Appendix).

Sediment budgets for the two layers are established using the conservation of volume, i.e., based on the interchange of sediments between layers (Γ) and fluxes associated with inflows and overflows. From the budgets, equations for the concentration in the mixture layer and for the bed layer height are derived. Equations are derived for two stages of loading: before and during overflow. The amount of sediment in suspension and in the packed layer is, at any time, measured against the total amount of sediment fluxed into the system to ensure that overall continuity is satisfied.

Bed Height (Monodispersion)

The rate of change in bed height reads (for $\lambda = 1$) as follows:

$$\begin{aligned} &\frac{\partial V_b}{\partial t}(1-n) = \Gamma, \\ &i.e., \frac{\partial h_b}{\partial t} = \frac{c}{1-n}(U_c + \frac{\partial h_b}{\partial t}) \Rightarrow \frac{\partial h_b}{\partial t} = \frac{cU_c}{1-n-c} \end{aligned} \tag{9}$$

where the bed volume is corrected for porosity, i.e., by the amount of water trapped between sediment deposits. This relation was previously reported by Kynch (1952). The expression is a reflection of the kinematic balance in a system, where the effect of settling on the reflux of water is related to the growth of the bed. In monodispersions, combining Eq.4 with Eq.3 and Eq.6 leads to the following:

$$U_c = U_T(1-c)^{m-1} - v \ , \qquad v = \frac{U_c c}{1-c} \Rightarrow \frac{U_c}{U_T} = (1-c)^m \tag{10}$$

In nondimensional form, the equation reads as follows:

$$\begin{aligned} &\frac{\partial \tilde{h}_b}{\partial \tilde{t}} = \beta \frac{U_c}{U_T} \frac{c}{1-n-c} \ , \\ &where \quad \tilde{h}_b = \frac{h_b}{h_{brg}} \ , \qquad \tilde{t} = \frac{t}{Ah_{brg}/Q} = \frac{t}{T_w} \end{aligned} \tag{11}$$

The hopper may contain an initial bed layer of height $\tilde{h}_{b0}$ prior to loading $[\tilde{h}_b(0) = \tilde{h}_{b0}]$. In the following,$\tilde{h}_{b0}$ is taken equal to zero. The experiments conducted by Rhee (2002) showed a depression in the bed near the inflow section and a bump in the central section of the hopper during initial infill stages. These details in morphology are not resolved by the integrated approach.

Preoverflow Concentrations (Monodispersion)

Prior to overflow, the surface of the mixture and the bed are rising at different rates (see the dashed control volume in Fig.2), and the rate of change in the preoverflow mixture height reads as follows:

$$\frac{\partial h}{\partial t} = \frac{Q}{A} - \frac{\partial h_b}{\partial t} \tag{12}$$

In general, the rate of change is positive, i.e., the height of the mixture is increasing. The preoverflow sediment budget is composed of sediment fluxes into the hopper and to the bed layer (Fig.3) and reads as follows:

$$\frac{\partial Vc}{\partial t} = \Gamma_{in} - \Gamma \ , \qquad V = h(t)A \ , \qquad \Gamma_{in} = \Sigma q_k c_k = Qc_0 \tag{13}$$

where the first term on the left-hand side embodies the volume expansion and storage effects, and the first term on the right-hand side represents the inflow. The expansion term (stretching/contracting of the water column) effectively increases/reduces the retention time. The inflow is composed of discharges from k inlets with inflow concentrations c_k, which can be represented by the total discharge Q times c_0 (i.e. c_0 can be interpreted as the weighted mean).

A differential equation for concentration is obtained by differentiating Eq.13 (recall that A is constant over depth) and using Eq.8 and Eq.12 as follows:

$$h\frac{\partial c}{\partial t} = \frac{Q}{A}c_0 - c(U_c + \frac{Q}{A}) \tag{14}$$

In nondimensional form, Eq.12) and Eq.14 read (for $\lambda = 1$) as follows:

$$\frac{\partial \tilde{h}}{\partial \tilde{t}} = 1 - \frac{\partial \tilde{h}_b}{\partial \tilde{t}} \ , \qquad \tilde{h}\frac{\partial c}{\partial \tilde{t}} = c_0 - c(1 + \beta\frac{U_c}{U_T}) \ , \qquad 0 < \tilde{t} \leq \tilde{T}_{fill} \tag{15}$$

where $\tilde{h} = \frac{h}{h_{brg}}$. In general, hoppers contain a certain volume of often-clear ballast water prior to loading, the height of which is denoted $h_0 (= V_0/A)$. Initial conditions for the differential equations are therefore $\tilde{h}(0) = \tilde{h}_0$ and $c(0) = 0$. By solving Eq.11 and Eq.15 as coupled differential equations, the evolution of preoverflow concentration and bed height can be derived.

Overflow Concentrations (Monodispersion)

During overflow, the surface of the mixture remains fixed at a level located slightly above h_{brg}, and the rate of overflow equals the rate of inflow,Q. The components of the sediment budget during this stage, outlined in Fig.4, are as follows:

$$\frac{\partial Vc}{\partial t} = \Gamma_{in} - \Gamma_{out} - \Gamma \ , \qquad \Gamma_{out} = Qc$$

The coupled differential equations for the overflow concentration and the bed height therefore become the following:

$$\frac{\partial h}{\partial t} = -\frac{\partial h_b}{\partial t} \ , \qquad h\frac{\partial c}{\partial t} = \frac{Q}{A}c_0 - c(U_c + \frac{Q}{A}) \tag{16}$$

In nondimensional form, the set of equations (Eq.16) reads (for $\lambda = 1$) as follows:

$$\frac{\partial \tilde{h}}{\partial \tilde{t}} = -\frac{\partial \tilde{h}_b}{\partial \tilde{t}} \ , \qquad \tilde{h}\frac{\partial c}{\partial \tilde{t}} = c_0 - c(1 + \beta\frac{U_c}{U_T}) \ , \qquad \tilde{T}_{fill} < \tilde{t} \leq \tilde{T}_{ter} \tag{17}$$

where $\tilde{T}_{fill} = 1 - \tilde{h}_0$; and $\tilde{T}_{ter}$ corresponds to the point in time where $\tilde{h}_b$ reaches a certain (prespecified) height, often close to $\tilde{h}_{brg}$.Initial conditions for the differential equations are as follows:

$$\tilde{h}(\tilde{T}_{fill}) = \tilde{h}_{\oslash} \ , \qquad c(\tilde{T}_{fill}) = c_{\oslash}$$

where $\tilde{h}_{\oslash}$ and $c_{\oslash}$ =height and concentration of the mixture at the onset of overflow, obtained from the final stage of the preoverflow solution [i.e., from Eq.15]. By solving Eq.11 and Eq.17 as coupled differential equations, the overflow concentration and the bed height is determined.

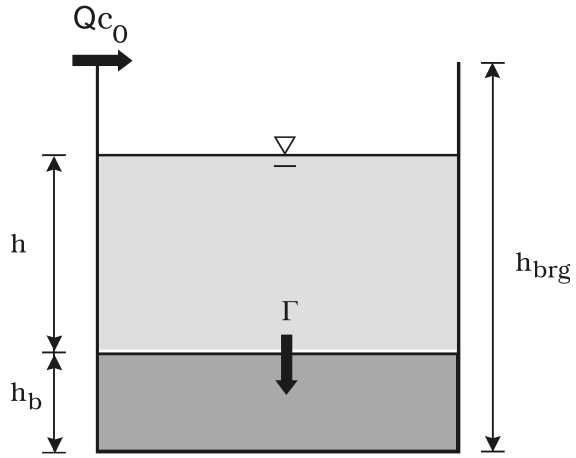

FIG. 3: Preoverflow sediment budget components for the hopper

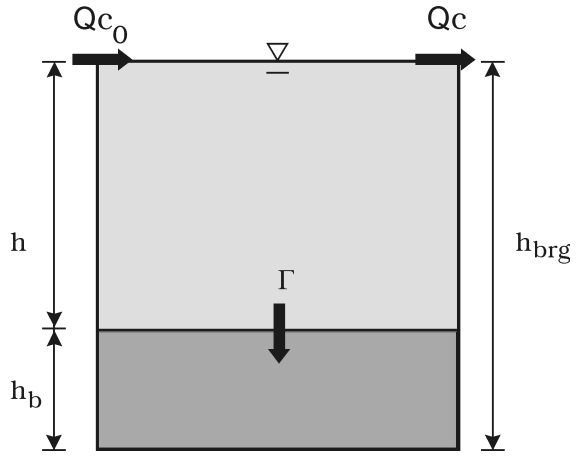

FIG. 4: Sediment budget components for the hopper during overflow

Sediment Deficit Equation

Useful equations can be derived by subtracting the two equations in Eq.15 and the two equations in Eq.17. The resulting equations keep track of the volume potentially available to sediment in the mixture layer; the potential volume is the difference between the concentration in the packed layer and the concentration in the mixture. These equations thus express the deficit of sediment in the mixture. The deficit equations before and during overflow and their initial conditions are as follows:

$$\frac{\partial \tilde{h}(1-n-c)}{\partial \tilde{t}} = 1-n-c_0 \ , \qquad \tilde{h}(1-n-c) \mid_{\tilde{t}=0} = \tilde{h}_0(1-n)$$
$$\frac{\partial \tilde{h}(1-n-c)}{\partial \tilde{t}} = c-c_0 \ ,$$
$$\tilde{h}(1-n-c) \mid_{\tilde{t}=\tilde{T}_{fill}} = \tilde{h}_{\oslash}(1-n-c_{\oslash}) = (1-n-c_0) + \tilde{h}_0 c_0$$

The initial condition for the latter equation is obtained by solving the former (preoverflow) equation, the solution of which reads as follows:

$$\underbrace{\tilde{h}(1-n-c)}_{\substack{\text{Available volume for} \\ \text{sediment in mixture layer}}} = \underbrace{(1-n-c_0)\tilde{t}}_{\text{Deficit in influx}} + \underbrace{\tilde{h}_0(1-n)}_{\text{Deficit in initial volume}} \Rightarrow \tilde{h}_{\oslash} = \frac{(1-n-c_0)+\tilde{h}_0 c_0}{(1-n-c_{\oslash})} \tag{19}$$

using $\tilde{T}_{fill} = 1 - \tilde{h}_0$

Concentrations and Bed Height (Polydispersion)

The polydispersion is composed of N fractions; thus the system can be represented by $N+1$ equations. Preoverflow equations for the bed height and the concentration of the ith constituent read as follows:

$$\frac{\partial \tilde{h}}{\partial \tilde{t}} = 1 - \frac{\sum_{i=1}^{N} \beta_i \frac{U_{c,i}}{U_{T,i}} c_i}{1-n-c} \ , \qquad \tilde{h}\frac{\partial c_i}{\partial \tilde{t}} = c_{0,i} - c_i(1+\beta_i \frac{U_{c,i}}{U_{T,i}}) \ , \qquad \beta_i = \frac{U_{T,i} A}{Q} \tag{20}$$

where $c_{0,i}$ = inflow concentration of the ith constituent; and $U_{c,i}$ is obtained from Eq.5 with Eq.6. Equations for the bed height and the concentration of the ith constituent during overflow read as follows:

$$\frac{\partial \tilde{h}}{\partial \tilde{t}} = -\frac{\sum_{i=1}^{N} \beta_i \frac{U_{c,i}}{U_{T,i}} c_i}{1-n-c} \ , \qquad \tilde{h}\frac{\partial c_i}{\partial \tilde{t}} = c_{0,i} - c_i(1+\beta_i \frac{U_{c,i}}{U_{T,i}}) \tag{21}$$

Once the PSD of the inflow is defined, then solutions to Eq.20 and Eq.21 can be obtained. The model can readily adopt any distribution (e.g., measured), but for reasons of simplicity, a lognormal probability density function has been prescribed in this study as follows:

$$f(d) = \frac{1}{\sqrt{2\pi} d ln(\sigma)} exp\{-\frac{1}{2}[\frac{ln(\frac{d}{d_{50}})}{ln(\sigma)}]^2\} \ , \qquad \sigma = \sqrt{\frac{d_{84}}{d_{16}}} \tag{22}$$

expressing the percentage of concentration of sediments smaller than a given grain size, d. In Eq.22, d_{50} is the mean grain size of the distribution, and σ is a

measure of the mixture dispersity (based on d_{84} and d_{16}), where parameters have values such that R (Eq.7) based on d_{84} remains below 10. The values of β_i and $c_{0,i}$ are derived from the PSD; the latter is defined as follows:

$$c_{0,i} = c_0 \int_{d_i}^{d_{i+1}} f(d)dd \tag{23}$$

The coupled equations for concentration and bed height can, combined with Eq.5, be solved numerically. For sufficiently large values of N, the mixture will behave as if the PSD follows the continuous curve of Eq.22 (i.e., becomes independent of N). A sensitivity analysis shows that the independence of N is achieved with logarithmic discretization for values of $N > 20 - 50$, depending on dispersity. In the following sections, all results are carried out with $N = 100$, because N has little effect on computational time. The strength of this model is its ability to provide results for a full PSD curve without the rough discretization that computational fluid dynamic (CFD) models resort to.

HOPPER CONCENTRATIONS

Solutions to monodisperse and bidisperse mixtures are presented prior to that of polydisperse mixtures. The former is obtained analytically to convey the underlying behavior of hopper systems and to facilitate the interpretation of results of the more complex polydispersions.

Monodisperse Mixtures

Numerical solutions for monodisperse mixtures are presented in Fig.5 as functions of time for different values of $\tilde{h}_0$ and with fixed values of β,n,m, and c_0. Calculations are terminated when the bed occupies 90% of the hopper volume. The dashed curves indicate the preoverflow stage, and the solid curves indicate the overflow stage. The inflow concentration, c_0, is highlighted in the figure. The hopper concentrations rise from the initial value of zero (as specified) to an equilibrium value, c_∞. The adaptation toward the equilibrium concentration depends on the preload height, $\tilde{h}_0$. When the volume of the ballast water is large, overflow begins prior to reaching the equilibrium concentration. According to Eq.11, the bed growth is constant when the concentration attains its (constant) equilibrium value. However, throughout loading, the bed exhibits quasilinear growth, which is also evident from the results presented in Fig.5.

Equilibrium Concentrations

Equilibrium concentrations can be obtained directly from Eq.17 by taking $dc/d\tilde{t} = 0$ as follows:

$$\frac{c_\infty}{c_0} = \frac{1}{1+\beta'} = \frac{1}{1+\beta\frac{U_c}{U_T}}\,, \qquad \frac{U_c}{U_T} = (1 - c_0\frac{c_\infty}{c_0})^m \tag{24}$$

where $\frac{c_\infty}{c_0} = \frac{c_\infty}{c_0}(c_0, \beta, m)$. The value of c_∞, obtained by iterating Eq.24, increases as m and c_0 increase and decreases as β increases. Whereas equilibrium

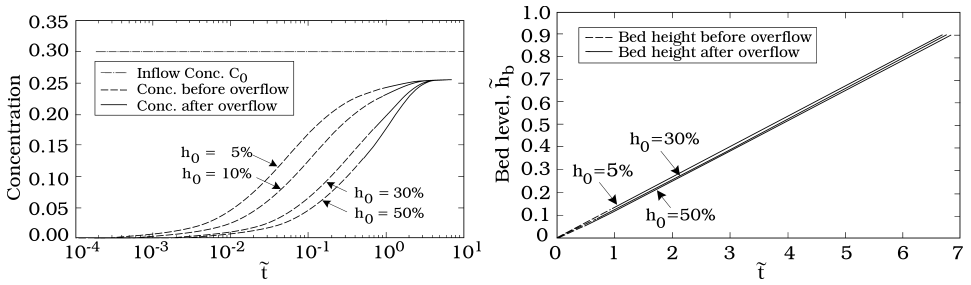

(a) (b)

FIG. 5: Changes in (a) concentration (note the logarithmic scale) and (b) bed height during loading; dashed lines indicate preoverflow, whereas solid lines indicate during overflow

concentrations are not a function of porosity (for obvious reasons), the equilibrium bed growth is, as also seen from the following:

$$\frac{\partial \tilde{h}_b}{\partial \tilde{t}} \mid_\infty = \beta \frac{U_c}{U_T} \frac{c_\infty}{1-n-c_\infty} , \qquad \frac{\partial \tilde{h}_b}{\partial \tilde{t}} \mid_\infty = \frac{\partial \tilde{h}_b}{\partial \tilde{t}} \mid_\infty (\beta, c_0, m, n) \tag{25}$$

Eq.25 shows that the bed growth becomes constant when processes in the mixture are in equilibrium.

Timescale of the Hopper Concentration to Reach Equilibrium

The computed evolution of bed height and mixture concentrations presented previously is compared with an analytical solution. The solution is obtained by assuming linear growth of the bed height while evaluating hindered settling as if in a dispersion of the constant concentration,c_∞. The solution reads as follows:

$$\begin{aligned} & c = c_\infty [1 - (\frac{\tilde{t} + \tilde{t}_0}{\tilde{t}_0})^{-p}] \\ & preoverflow: \qquad p = \frac{c_0}{c_\infty} \frac{1-n-c_\infty}{1-n-c_0} > 1 , \qquad \tilde{t}_0 = \tilde{h}_0 \frac{1-n-c_\infty}{1-n-c_0} \\ & during\ \ overflow: \qquad p = -\frac{c_0}{c_\infty} \frac{1-n-c_\infty}{c_0-c_\infty} , \qquad \tilde{t}_0 = -\tilde{h}_0 \frac{1-n-c_\infty}{c_0-c_\infty} \end{aligned} \tag{26}$$

The solution illustrates the increase in concentration toward c_∞ by a power function and how nondimensional parameters animate this adaptation. A timescale, $\tilde{T}$, for the adaptation of concentration can be derived from Eq.26 and reads as follows:

$$\tilde{T} = (\frac{1}{c_\infty} \frac{\partial c}{\partial \tilde{t}} \mid_{\tilde{t}=0})^{-1} = \frac{\tilde{t}_0}{p} = \frac{c_\infty}{c_0} \tilde{h}_0 = \frac{\tilde{h}_0}{1 + \beta \frac{U_c}{U_T}} \tag{27}$$

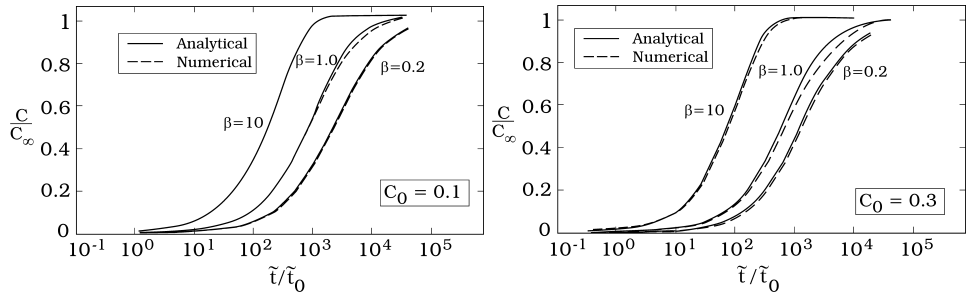

FIG. 6: Comparison between the mixture concentrations obtained analytically and numerically

which is a measure of the time required for the mixture concentration to reach equilibrium. This timescale of adaptation is proportional to the initial water height and inversely proportional to the inflow concentration and thus β. Not surprisingly, the concentration reaches its equilibrium value instantaneously when the initial height (and thus the dilution) is zero. If $\tilde{T}$ is larger than $\tilde{T}_{fill}$, then hopper concentrations may not have reached their equilibrium before overflow as shown in Fig.5.

Moreover, the concentration at the onset of overflow,c_{Tw}, relative to the equilibrium concentration can be derived as follows:

$$\frac{c_{Tw}}{c_\infty} = 1 - (\frac{1 - \tilde{h}_0 + \tilde{t}_0}{\tilde{t}_0})^{-p} \tag{28}$$

using $\tilde{T}_{fill} = 1 - \tilde{h}_0$. From Eq.28, $c_{Tw} \to c_\infty$ when c_0 and β increase and h_0 decreases. In contrast to c_∞, the porosity and the preload height influence c_{Tw}.

In Fig.6, the analytical solution Eq.26 and solutions obtained numerically by solving the coupled system are shown. Solutions for various values of β are shown with $c_0 = 0.1$ and 0.3, with $n = 0.4$. The small departure between the analytical and numerical solutions, which peak for $\beta = 1$, lie primarily in the linearization of hindered settling in the analytical model (i.e., evaluating hindered settling as if $c = c_\infty$).

Duration of Loading and Spill

The time required to pack the hopper is another important parameter in plume modeling. The duration of the loading can be estimated by using the sediment deficit equations (Eq.18). By assuming that $c_\oslash \approx c_\infty$ at $\tilde{t} = \tilde{T}_{fill}$, which according to Eq.28 is often a good approximation, Eq.19 returns the following:

$$\tilde{h}_\oslash = \frac{(1 - n - c_0) + \tilde{h}_0 c_0}{1 - n - c_\infty} \tag{29}$$

With $h_{\oslash}$ given, and $c_{\oslash} = c_{\infty}$, a solution to the deficit equation during overflow is straightforward. The loading is typically terminated when the bed height reaches a predefined level (or weight) and the duration of the loading,$\tilde{T}_{ter}$, is obtained from this termination height (where the mixture height is assumed to be zero) as follows:

$$\tilde{T}_{ter} = \frac{(1 - n - c_{\infty}) + \tilde{h}_0 c_{\infty}}{c_0 - c_{\infty}} \tag{30}$$

This expression shows that the time required to pack the hopper decreases with n and β, attains a minimum for a given c_0, and, more interestingly, increases with $\tilde{h}_0$. The duration of the spill is as follows:

$$\tilde{T}_{spill} = \tilde{T}_{ter} - \tilde{T}_{fill}$$

Influence of Variable Inflow Conditions

The composition of seabed material varies enormously, both horizontally and through subsurface layers; therefore variations in inflow concentration are an unavoidable part of any dredging operation. The model presented previously is used to exploit the effects of mixture concentration by superimposing a fluctuating component, c_0', on the mean inflow concentration, $\overline{c}_0$. Whereas Q is maintained as a constant, the inflow concentration is assumed to vary sinusoidally with amplitude ϵ and cyclic frequency ω as follows:

$$c_0(\tilde{t}) = \overline{c}_0 + c_0' = \overline{c}_0 + \epsilon sin(\omega \tilde{t}) \tag{31}$$

The fluctuating inflow concentrations will result in larger (mean) values of the settling timescale, T_s, when compared with the case with no fluctuations, because hindered settling is a nonlinear function of concentration (Eq.6). The influence of a fluctuating inflow concentration can be analyzed by considering Eq.19 for the situation described in Eq.31 as follows:

$$\tilde{h}(1 - n - c) = (1 - n - c_0)\tilde{t} + \tilde{h}_0(1 - n) - \frac{\epsilon}{\omega}[1 - cos(\omega \tilde{t})]$$

The deficit in the preoverflow mixture concentration is less when a fluctuating component is added to $\overline{c}_0$. It follows that the preoverflow mixture concentrations are smaller without than with oscillations.

In Fig.7, the calculated mixture concentrations for the case with $c_0 = 0.3$ and $\beta = 0.25$ are presented with and without fluctuations; the latter is presented for a reference. The result for the oscillating case is obtained with $\epsilon = 0.1$ and illustrates that the preoverflow concentrations exceed those of the nonoscillating case ($\epsilon = 0$). The results show that during overflow and in the closing stage of loading, when the mixture is in equilibrium and the mixture height is small, the time-averaged concentrations are only slightly more than the concentrations without oscillations. This increase is a function of β, however.

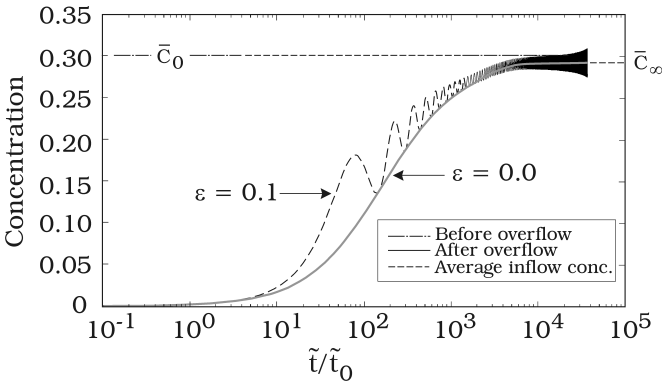

FIG. 7: Changes in mixture concentration with and without fluctuating inflow concentration for $\beta = 0.25$

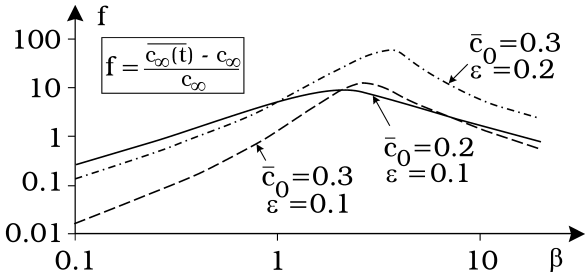

FIG. 8: Percentage increase in c_∞ from fluctuating inflow concentrations with β when h is small

During overflow, the mixture concentrations reach a quasistationary level. This is observed in Fig.7. In the final stage of loading, when the mixture height is small, Eq.17 reduces to the following:

$$\tilde{h}\frac{\partial c}{\partial \tilde{t}} \mid_{\approx 0} = c_0(\tilde{t}) - c(1 + \beta\frac{U_c}{U_T}) \Rightarrow c = \frac{c_0(\tilde{t})}{1 + \beta\frac{U_c}{U_T}} \tag{32}$$

The equilibrium concentration for a stationary inflow (Eq.24) is compared with the time-averaged value of the concentration in Eq.32(with Eq.31). In Fig.8, the percentage change between these concentrations is shown for different values of c_0 and ϵ as functions of β. In the limiting cases of β, the mixture concentrations are not affected. For small β, particles have no time to settle or to hinder settling, whereas time allows all sediments to deposit for large β. For intermediate β, the effects of fluctuations on the time averaged mixture concentration become evident and pronounced for$\beta \sim 3 - 5$. An increase in hopper concentration of up to 10% is observed for moderate fluctuations and up to 50% when oscillations represent a considerable part of the inflow concentration.

Effects in Bidisperse Mixtures

In multifractional mixtures, the vertical velocity is governed primarily by the settling of larger (heavier) particles, and the concentration of fines can increase. This property of multifractional mixtures will be discussed in the Polydisperse Mixtures section but can be illustrated scholastically by considering the canonical case of bidisperse mixtures, i.e., mixtures containing two constituents. In Fig.9, two cases are sketched, one in which both fractions are in suspension, and one in which the larger sediments have settled out while the fines remain in suspension. The latter case applies for large values of λ, where the vertical velocity induced by the coarse fraction elevates fines.

In the first case, where both fractions are in suspension, the total concentration, c, and the concentration of fines, c_{fines} ,at $t = t_0$ are the following:

$$c = c_1 + c_2 \ , \qquad c_{fines} = c_2$$

where c_1 and c_2 = concentrations of the large fraction and fine fraction at $t = t_0$, respectively. The concentrations at $t = t_0 + \Delta t$ are as follows:

$$\begin{aligned} c = c_{fines} &= \frac{c_2}{1 - \frac{c_1}{1-n}} \approx c_2[1 + c_1(1+n)] \\ &= c_2 + \Delta c_2 \quad \Rightarrow \quad \Delta c_2 \approx c_2 c_1 (1+n) \end{aligned}$$

In this case, the concentrations of fines increase by approximately Δc_2 (using a Taylor expansion). The change in total concentration can also be derived as follows:

$$\Delta c \approx \frac{c_2}{1 - \frac{c_1}{1-n}} - (c_2 + c_1)$$

For the total concentration to increase, the following is required (at least):

$$\Delta c > 0 \quad \Rightarrow \quad c_2 > 1 - n - c_1$$

which depends on porosity, i.e., on the degree to which water is retained in the bed. For typical values of n or even values representing unconsolidated and uniform beds, an increase in total concentration is not realistic.

The adaptation of bidisperse mixture concentrations containing fractional concentrations c_1 and c_2 is shown in Fig.10, including the equilibrium concentrations of the two fractions. Two cases are considered. In Fig.10(a), the adaptation of concentrations from nonzero and nonequal initial (ballast) concentrations is shown [i.e., $c_1(0) \neq c_2(0) \neq 0$], whereas Fig.10(b)shows the increase in mixture concentrations in response to initial concentrations equal to zero [i.e., $c_1(0) = c_2(0) = 0$]. In both cases, the initial ballast height is $\tilde{h}_0 = 0.1$. The inflow concentration, c_0, is composed of c_{01} and c_{02}, and these are assumed to be constant throughout the loading with $c_{01} = c_{02} = (1/2)c_0$ (where $c_0 = c_{01} + c_{02}$). The equilibrium concentration of the fine fraction exceeds that of the inflow concentration, as Fig.9 also shows is probable.

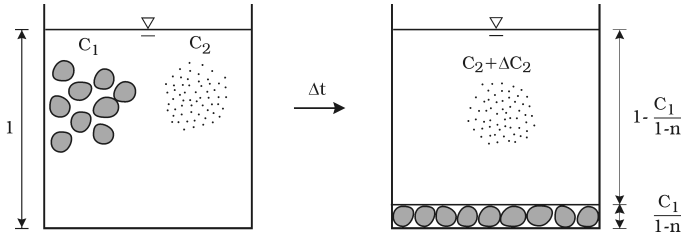

FIG. 9: Bidisperse mixture: (a) both fractions in suspension; (b) only the fine fraction remains in suspension

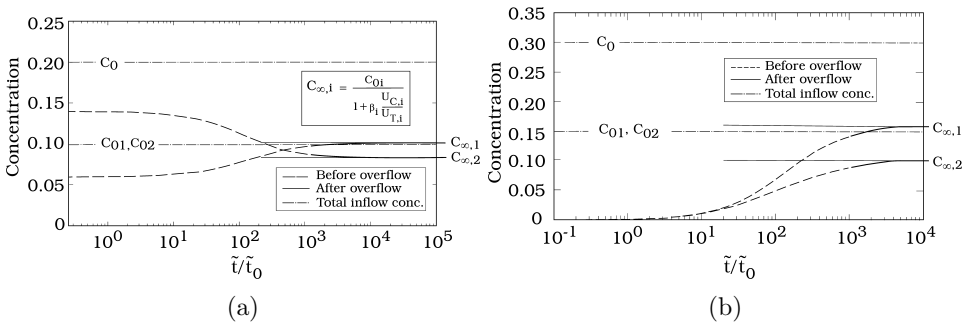

FIG. 10: Bidisperse mixture with fractional concentrations c_1(fine) and c_2 (coarse) for $\tilde{h}_0 = 0.1$ and $\lambda = 8$; (a)$c_0 = 0.2$,$c_1(0) = 0.06$ and $c_2(0) = 0.14$; (b)$c_0 = 0.3$ and $c_1(0) = c_2(0) = 0$

Polydisperse Mixtures

The concentrations in bidisperse and polydisperse mixtures, where inflow concentrations are constant, behave in a similar way to those of monodispersions, i.e., with an asymptotic evolution of the concentration toward an equilibrium. In polydispersions, the PSD of the inflow thus adapts within the hopper but on a timescale prolonged by the settling battle occurring between the individual fractions.

Solutions

Typical examples of the sediment distributions at inflow, at the time of overflow ($\tilde{t} = \tilde{T}_{fill}$), and for the equilibrium stage are shown in Fig.11. The results are obtained by numerical solution of the hopper equations. Each constituent has its unique β_i, and the difference in segregation of coarser and finer constituents therefore creates a distribution in the mixture that departs from the lognormal distribution of the inflow. The dispersity of the mixture changes with time, and the distribution becomes increasingly skewed with only finer fractions remaining in suspension. Concentrations of finer constituents exceed those of the inflow,

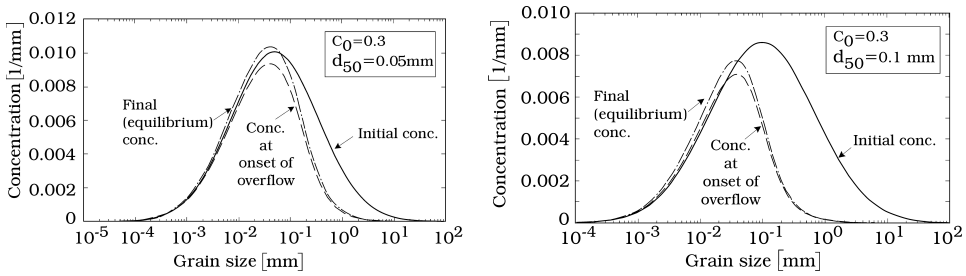

(a) (b)

FIG. 11: Inflow concentrations, concentrations at the onset of overflow, and concentrations at equilibrium with $\sigma = 7$; (a)$\overline{\beta} = 0.2$; (b)$\overline{\beta} = 3.0$

a property of polydispersions that was discussed previously. The resulting segregation timescales lead to the deposition of the coarser material, whereas finer fractions remain in the suspension and in the overflow. The PSD of the bed deposits varies with time also (i.e., it changes over the depth of the bed) and can be derived by subtracting the PSD curve of the mixture (corrected for the mixture volume) from that of the inflow.

The model thus converts the PSD at inflow, which typically becomes available as part of the data measured on-board, to the actual PSD at overflow and in the hopper bed, which are typically not directly measured.

As an alternative to the numerical solution presented previously, an analytical solution for mixture concentrations can be obtained by superimposing solutions for each individual constituent, per Eq.26. Such a solution to a polydisperse mixture reads as follows:

$$c = \Sigma_{i=1}^{N} c_i = \Sigma_{i=1}^{N} c_{\infty,i}[1 - (\frac{\tilde{t} + \tilde{t}_{0,i}}{\tilde{t}_{0,i}})^{-p_i}] \tag{33}$$

where $c_{\infty,i}$ in $\tilde{t}_{0,i}$ and p_i are obtained discretely from Eq.24. Upon comparing the distribution of concentrations between numerical and analytical (using Eq.33) solutions, only small differences are found; the largest are observed at the onset of overflow and are similar in magnitude to those shown in Fig.6.

Verification of the Model

First, the polydispersion model was subjected to an intermodel validation test, where results from numerical calculations of mixtures containing (1)$N = 100$ identical fractions (i.e.,$\lambda = 1$), each with an inflow concentration corresponding to c_0/N, were compared with (2) a single fraction with inflow concentration c_0. The mixture concentration and bed height were identical in these two test calculations.

Second, the model was compared against the following sets of published measurements:

- Laboratory measurements of overflow concentrations during the loading of a test hopper by Rhee (2002) (Tests 5 and 6);
- Laboratory measurements of bed heights during the loading of a test hopper, as presented in Braaksma (2008);
- Measurements of bed heights inside a full-scale hopper, as reported in Rhee (2002).

The first campaign was carried out in a single inflow/outflow system, whereas the last two have more elaborate inflow/outflow systems. Although the latter only offers two data points during the entire loading operation, it provides an opportunity for verification against full-scale conditions.

In Fig.12, the simulated and the measured concentrations at inflow (from $t = 0s$) and overflow (initiated at $t \approx 400s$) from Rhee (2002) are presented. The simulations assume a quasistationary value of c_0, which seems reasonable, having appraised the variability in measured inflow concentrations. The concentrations are modeled up to the time where the hoppers are loaded to 90% of their capacity. The parameters for the discharge rate, the hopper dimensions, the ψ-factor, and the porosity were derived from Rhee (2002). A distribution curve based on available information on grain sizes was constructed for each test. The difference between the modeled volume-averaged (mixture) concentrations and the measured overflow concentrations at the onset of overflow is attributed to the 3D phenomena of venting, where a pocket of clear water is pushed toward the outlet. The venting effect is pronounced in the experiment because of the single inflow/outflow arrangement, the use of large grain sizes (sand), and the relatively large ($\tilde{h}_0 = 0.55$) initial clear water volume. As venting completes, the measured overflow concentrations approach the modeled (volume-averaged) concentrations. The measurements of van Rhee thus confirm that the mixture concentrations increase and reach equilibrium and that, despite the setup, a certain degree of uniformity is achieved. The modeled and measured equilibrium concentrations are nearly identical, demonstrating that postventing concentrations are, in fact, uniform inside the hopper - a property also seen directly from the measured concentration profiles in Rhee (2002). A tendency for slight underestimation is attributed to using a constant (rather than fluctuating) inflow concentration as well as ignoring the effect of dead zones. The presence of dead zones implies that measured concentration levels will be slightly higher than those simulated, because the model assumes full utilization of the hopper volume. Dead zones are, however, limited in the experiments, as both inflow and overflow occur over the entire width of the experimental hopper. Predictions of the simple overflow model of Vlasblom and Miedema (1995), which conform to the experimental setup of van Rhee, are included in Fig.12. Turbulence factors (including their scour formulation) and hindered settling (using the total inflow concentration) are employed per Miedema (2009a). The model predicts lower overflow concen-

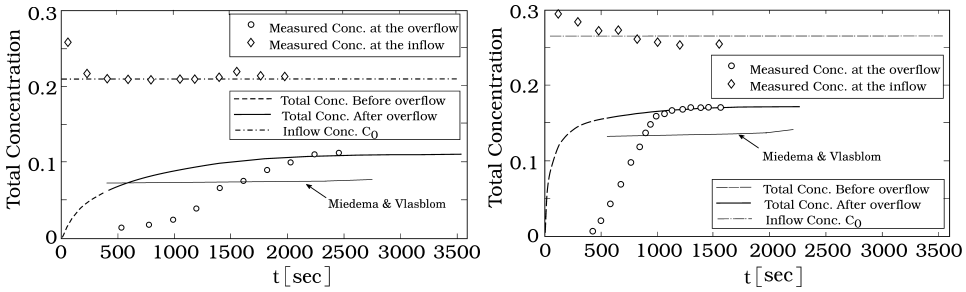

FIG. 12: Modeled (solid lines) and measured (circles) overflow concentrations for (a) Test 5 and (b) Test 6 of van Rhee (2002); dashed lines and diamonds (measured) show inflow concentrations; preoverflow concentrations are shown as dot-dashed lines

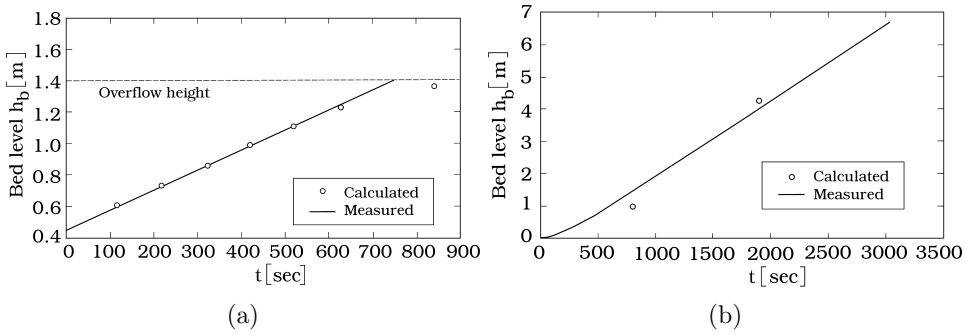

FIG. 13: (a) Test rig measurements; (b) full-scale measurements

trations in the equilibrium stage by approximately 25% as compared with the measurements.

Measurements of bed heights during the loading of a test rig were presented by Braaksma (2008), where parameters for the discharge, the hopper dimensions, the inflow concentrations, and the porosity are provided. The test rig setup generates a complex flow pattern, because the inflow is placed in the central part of the hopper and two overflow weirs are used. The comparison between the modeled and the measured bed heights during overflow is shown in Fig.13(a). The model is in excellent agreement with the measurements, which is attributed to reduced venting, because of the more complex inflow/ outflow structures and because the ballast water occupied a relatively small fraction of the hopper volume. The bed grows linearly, in agreement with previous findings.

The comparison between the modeled and the measured bed heights for the loading of a full-scale hopper is shown in Fig.13(b). In this case, the hopper has

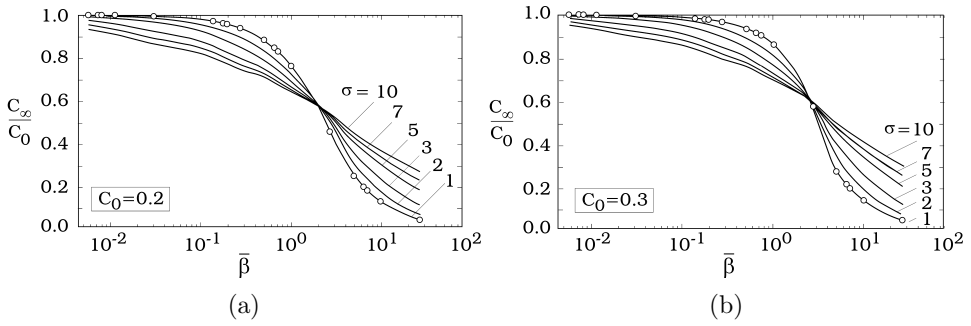

FIG. 14: Equilibrium concentrations normalized by the inflow concentration; lines denote numerical results and dots denote the analytical solution

a circular cross section or silo-shaped (Rhee 2002). Measured bed heights inside the silo-shaped hopper have been converted geometrically to an equivalent height for a cube shaped hopper.

Impacts of Dispersity on the Mixture Concentration

The equilibrium concentration and the concentration at the onset of overflow (total concentration) are presented in Fig.14 and Fig.15 as functions of $\overline{\beta}$, where

$$\overline{\beta} = \frac{\overline{U}_T A}{Q} \quad , \quad \overline{U}_T = \frac{1}{N}\Sigma_{i=1}^{N} U_{T,i}$$

are introduced for plotting purposes. The curves for six values of dispersity (σ), as well as the analytical solutions for $\sigma = 1$ (i.e., Eq.24 and Eq.28), are presented for two values of total inflow concentration. The equilibrium concentration is normalized by the inflow concentration, and the concentration at the onset of overflow is normalized by the equilibrium concentration, the latter to more fully display the processes in polydispersions, because $c_\infty = c_\infty(c_0, \beta, m, \sigma)$. To obtain the concentration at the onset of the overflow normalized by the inflow concentration, the data in the graphs shown in Fig.14 and Fig.15 can be multiplied. Results are shown for clear ballast water conditions with $\tilde{h}_0 = 0.1$.

Strictly speaking, $\overline{\beta}$ is not universal, although calculations with various combinations of Q, A, and $U_{T,i}$, which collectively produce the same $\overline{\beta}$, provide nearly identical results, which is attributed to the weak nonlinearity introduced through R in Eq.7.

The results show that polydisperse mixtures behave similarly to monodisperse mixtures. The normalized equilibrium concentration is less sensitive to $\overline{\beta}$ as the dispersity increases. For $\overline{\beta} \geq 1$, the normalized concentrations at the onset of overflow are largest for monodispersions. This implies that hopper concentrations require a longer time to adjust with increasing dispersity (i.e., achieving equilibrium with many fractions is more intricate).

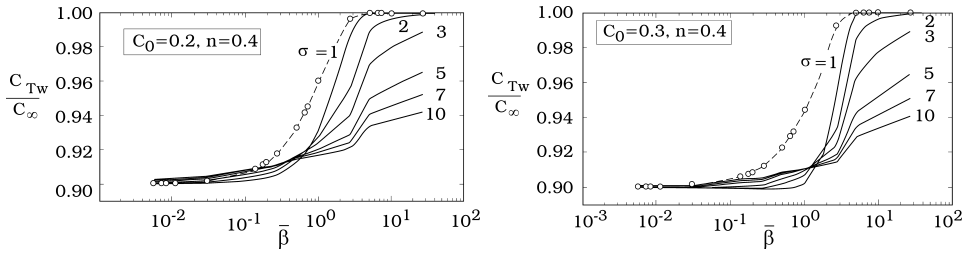

FIG. 15: Concentrations at the onset of overflow normalized by the equilibrium concentrations; lines denote numerical results and the dashed line with dots denotes the analytical solution

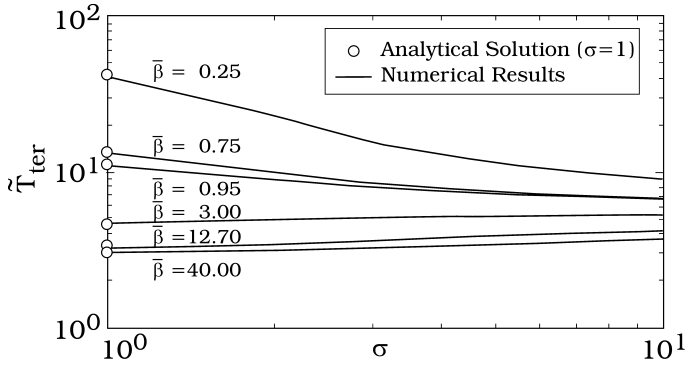

FIG. 16: Loading time with the dispersity, including the analytical solution (Eq.30) for $c_0 = 0.2$, $n = 0.4$, and $\tilde{h}_0 = 0.1$; note the double-logarithmic plot

Fig.16 shows the loading time, $\tilde{T}_{ter}$, as a function of dispersity for different $\overline{\beta}$. The analytical solution from Eq.30, valid for $\sigma = 1$, is also shown. The values for $\overline{\beta}$ are derived from actual hoppers and, thus, define a plausible range of scenarios. In accordance with the preceding results demonstrating slower adaptability as the dispersity increases, the loading time decreases as the dispersity increases if $\overline{\beta} \geq 1$. For $\overline{\beta} \leq 1$, the loading time is only a weak function of dispersity. When the dispersity of the material is high and $\overline{\beta} \leq 0.25$, the loading time decreases by a factor of four relative to that of monodisperse mixtures. The loading time reflects the efficiency of the hopper to trap sediment. The efficiency of small hoppers (with corresponding small $\overline{\beta}$) is therefore larger when dredging in material of high dispersity. For large hoppers, the efficiency becomes less reliant on the dispersity; if anything, the tendency is to reduce the efficiency as the dispersity increases.

The degree of kinematic coupling between fractions (Eq.5) was also investigated. A test in which $U_{c,i}$ was calculated sequentially was performed and

compared with the (implicit) solution obtained with the matrix solver, which, as previously noted, captures the effects of all other constituents on one constituent concurrently. The former test involved computing the settling velocity and associated vertical velocity of the largest constituent first and subsequently using this result (i.e., the vertical velocity) to calculate the settling of the second largest constituent, etc. In other words, a particle of a given size only feels a vertical velocity generated by larger particles. Insignificant differences were found between the settling velocities obtained with the two methods, which hints at the nature of the coupling. Conversely, significant differences were obtained by reversing the order, i.e., starting the sequence from the smallest constituent and then moving up. This is perhaps not surprising, given the imposing role of larger constituents on the settling processes. The small discrepancies between solutions obtained with the matrix solver and those of the sequential method (starting with coarser fractions) can be utilized in an analytical approach (e.g., in combination withEq.33) and are perhaps of interest for CFD modelers.

CONCLUSIONS

It has been demonstrated that an integrated two-layer approach, hinging on the distribution of concentration being uniform inside the hopper, is sufficient to capture overflow concentrations and bed growth. Although the concentration in the hopper is predominantly uniform, some degree of stratification in the vertical concentrations may occur locally, depending, in particular, on the inflow/outflow arrangement. If anything, the centroid of the concentration at the overflow section (away from the inflows) will be balanced slightly below middepth from gravity, and the overflow predictions will, in EIA terms, be slightly conservative. The good agreement between the modeled and measured concentrations and bed heights confirms that hindered settling is a key process in hoppers. Hindered settling and the derived effects from hindrance such as fluctuations in inflow concentrations and dispersity can potentially cause larger variations in bed growth when compared with the stratification effects. It is expected that predictions, in general, are sensitive to the choice of m and to the accuracy of σ. Neglecting dispersity will potentially overestimate overflow concentrations and underestimate bed growth. The model can readily include particle shape, interparticle collision effects, and nonuniformities in the density distributions as part of the fall velocity description. Assessments of plume excursions from the hopper overflow should include plausible error bars to accommodate uncertainties related to, e.g., oscillations in the inflow concentrations.

The model, apart from conveying an understanding of hopper sedimentation and the significance of governing parameters, can handle polydispersions and provide results without the rough discretization of the PSD curve typically required by CFD models. The model can be used as an auxiliary tool, providing dumping and dredge-plume modeling with improved source conditions in terms of concentrations, PSDs, and the durations of the spill and the loading. Accurate source conditions are crucial to plume modeling and thus to the delineation of impacts,

providing support to the EIA process as well as to the management and design of dredge campaigns.

APPENDIX. DISTRIBUTION OF CONCENTRATION IN A HOPPER MIXTURE

Consider a hopper mixture where sediment is being supplied continuously through the surface at a rate of $U_c c$. In this case, assuming horizontal uniformity and stationarity, the vertical profile of concentration,c', is governed by the following:

$$U_c c = U_c c' + \epsilon_s \frac{\partial c'}{\partial y} \quad \Rightarrow \quad 0 = U_c c_\Delta + \epsilon_s \frac{\partial c_\Delta}{\partial y}$$
$$with \quad c_\Delta \mid_{y=0} = max(0, c_b - c) \tag{34}$$

where $c_\Delta = c' - c$. This is a simplified, but realistic, representation of the sedimenting system, where sediments are supplied from above through the surface and where horizontal diffusion of the sediment in the surface layers ensures an even supply of sediment to the mixture below. Turbulent flows can potentially maintain volumetric concentrations of up to 0.35 [see the values of c_b in Zyserman and Fredsøe (1994)], but this only occurs under high bed shear stresses uncommon to settling basins and unenergetic hopper environments, where concentrations furthermore both overwhelm and dampen the carrying capacity of flow inside the hopper. Consequently, the solution to Eq.34 is $c_\Delta = 0$ for hopper conditions; i.e., the profiles of concentration are uniform over depth ($c' = c$), implying that the turbulent flux is zero (also at the interface of the bed). Whereas the horizontal diffusivity is active in mixing inflow sediments in surface layers, vertical diffusivity is redundant, irrespective of the turbulence level, as long as c_0 is large.

Nonuniform profiles can develop only if near-bed turbulence levels and their associated capacity for carrying sediments (as measured by the bed concentration,c_b) exceeds the capacity for keeping sediment supplied from above in suspension (as measured by the concentration,c). In this case, sediment will be prevented from depositing at the rate supplied from above, while the mixture accumulates/stores sediment. The accumulation in the profile continues until the larger capacity is filled. The depression at the inflow section observed in van Rhees experiments is interpreted as being the result of local scouring. This is a misconception, as scouring is an active morphological process. The hopper is a system adapting towards equilibrium through deposition, and the observed depression is caused by turbulence in the impinging jet (which is pronounced for single inflow arrangements) that prevents segregation within the confined area of impact. The bed outside this area is presumably accreting correspondingly more to alleviate any additional saturation.

ACKNOWLEDGMENTS

Mr. Louis Quist Poulsen is acknowledged for his development of the beta version of the numerical model. This work was supported by the Danish Ministry of Science, Technology, and Innovation through the Godkendt Teknologisk Service (GTS) grant Marine Structures of the Future.

REFERENCES

Batchelor, G. (1982). "Sedimentation in a dilute polydisperse system of interacting spheres. Part 1. General theory." *Journal of Fluid Mechanics*, 119.

Braaksma, J. (2008). "Model-based control of hopper dredgers." Ph.D. thesis, TU Delft, The Netherlands.

Camp, T. (1946). "Sedimentation and the design of settling tanks." *Trans. ASCE*.

Davis, R. and Gecol, H. (1994). "Hindered settling function with no empirical parameters for polydisperse suspensions." *AIChE journal*, 40(3).

Garside, J. and Al-Dibouni, M. (1977). "Velocity-voidage relationships for fluidization and sedimentation in solid-liquid systems." *Ind. Engng. Chem. Process. Des. Dev.*, 16, 206–213.

Koning, J. (1977). "Constant Tannage Loading of Trailing Suction Hopper Dredgers.

Kynch, G. (1952). "A theory of sedimentation." *Transactions of the Faraday society*.

Masliyah, J. (1979). "Hindered settling in a multi-species particle system." *Chemical Engineering Science*, 34(9), 1166–1168.

Miedema, S. (2009a). "A sensitivity analysis of the scaling of TSHD's." *WEDA XXIX & Texas A&M*, 40, 14–17.

Miedema, S. (2009b). "The effect of the bed rise velocity on the sedimentation process in hopper dredges." *Journal of Dredging Engineering*, 10(1), 10–31.

Miedema, S. and Rhee, C. V. (2007). "A sensitivity analysis on the effects of dimensions and geometry of Trailing Suction Hopper Dredges." *WODCON ORLANDO, USA*, (1970).

Ooijens, S. C. (1999). "Adding dynamics to the camp model for the calculation of overflow losses." *Terra et Aqua*, (76), 12–21.

Rhee, C. V. (2002). "On the sedimentation process in a trailing suction hopper dredger." Ph.D. thesis, TU Delft, The Netherlands.

Richardson, J. and Zaki, W. (1954). "Sedimentation and fluidisation: Part I." *TRANS. INSTN CHEM. ENGRS*, 32, S82–S100.

Schiller, L. and Naumann, A. (1933). "Uber die grundlegenden berechnungen bei der schwerkraftaufbereitungl." *Zeitung des vereins deutscher ingenieure*, 77, 318.

Steinour, H. (1944). "Rate of Sedimentation_suspensions of uniform-size angular particles." *Industrial & Engineering Chemistry*, 36(9).

Thompson, C. E. L., Amos, C. L., Angelaki, M., Jones, T. E. R., and Binks, C. E. (2006). "An evaluation of bed shear stress under turbid flows." *Journal of Geophysical Research*, 111(C4), C04008.

Vlasblom, W. (2003). *Lecture notes on dredging equipment and technology.*

Vlasblom, W. and Miedema, S. (1995). "A Theory for Determining Sedimentation and Overflow Losses in Hoppers." *Proc. WODCON IV, November.*

Wang, L.-P. and Maxey, M. R. (1993). "Settling velocity and concentration distribution of heavy particles in homogeneous isotropic turbulence." *Journal of Fluid Mechanics*, 256, 27–68.

Zyserman, J. and Fredsøe, J. (1994). "Data analysis of bed concentration of suspended sediment." *Journal of Hydraulic Engineering*, 120(9), 1021–1042.

CHAPTER 3

DETAILED MODELLING OF SEDIMENTATION AND OVERFLOW IN HOPPERS AND THE EFFECT OF INLET CONFIGURATIONS

In preparation as:
Saremi, S. and Jensen, J. H., (2014). Detailed modelling of sedimentation and overflow in hoppers and the effect of inlet configurations. To be submitted.

DETAILED MODELLING OF SEDIMENTATION AND OVERFLOW IN HOPPERS AND THE EFFECT OF INLET CONFIGURATIONS

Sina Saremi and Jacob Hjelmager Jensen

ABSTRACT

Overflow from Trailing Suction Hopper Dredgers is the source of turbidity plumes with potential impacts on marine environment. The rate of sedimentation and mixing of dredged material inside the hopper are the key parameters controlling the degree of overflow losses. A 3 dimensional two-phase mixture method has been used to model the detailed processes involved in the highly concentrated mixture inside the hopper. The benefit of such model is that it takes into account important dynamic interactions and volume exchange effects due to the settling particles in the flow and the accretion of the bed layer inside the hopper. The model has been validated successfully with experiment and has been used to study different processes critical to overflow losses. Termination of infilling has always been a point of debate between environmentalists and the dredging contractors. The capability of the model in resolving the slurry layer above the bed elucidates the behaviour of the overflow at the final stages of the filling cycle and assists the determination of when to terminate infilling. The placement of the inlet pipes along the length of the hopper, which is primarily arranged to balance the load distribution in the hopper, has been studied from the perspective of dredging efficiency. The results show large influences from the arrangement of the inlet pipes on the sedimentation rates, and the overflow losses in the hopper. Natural seabed material is composed by many fractions and the size and type of sediments change along and into the seabed. Variations in the material entering the hopper have been studied by assuming fluctuating inflow concentrations. The fluctuations impose a mean net change on the overflow concentrations. Whether these processes increase or decrease the overflow losses is determined by the non-dimensional parameter β, which is based on the characteristics of the hopper and the sediment type.

Keywords: hopper, dredging, overflow, sedimentation, two-phase modelling, mixture, CFD

INTRODUCTION

Coastal and offshore infrastructural development and maintenance projects are subject to increasing awareness, and demand towards sustainable development which have closely tied together the projects' economical, environmental

and political aspects. The disturbance of the marine ecosystem and aesthetic degradation are among the main potential impacts of dredging operations. Increase in the turbidity levels due to e.g. spillage of sediment during dredging activities is one of the main causes of the environmental impacts. The characteristics and magnitude of spill varies with the project and type of dredger. Trailing Suction Hopper Dredgers (TSHD) are often equipped with one or two suction pipes with dredge heads in the end, which are lowered down and trailed along the seabed. A mixture of sediment and water is pumped up in the retaining hopper. The sediment settles in the hopper while the excess mixture overflows until the capacity of the hopper is achieved. Overflow of excess mixture is part of the dredging process. Faster sedimentation of the dredged material inside the hopper results in lower overflow concentrations and earlier filling of the hopper. This means the turbidity caused by the overflow is less and the duration of the dredging is shorter and there is consequently both environmental and economical reasons to optimize the trapping efficiency of the hopper.

Hoppers are usually vessel-mounted containers following the shape of the hull (i.e. usually silo-shaped). In order to have an evenly distributed load along the hopper, usually more inlets are rigged along the hopper length. In small dredgers with one inlet pipe the pipe is placed at the center of the hopper to achieve a more evenly distribution of the material. The composition of the settled material inside the hopper is different from the dredged seabed material pumped into the hopper. This is due to i) the processes involved at the drag-head pump and along the inlet pipes (e.g. flocs break up) and ii) the heavier sediments settling inside the hopper and the remaining, mostly lighter fractions, flow overboard. Therefore the characteristics, concentration and size distribution of the overflowing mixture is totally different from the inflowing material to the hopper (see Jensen and Saremi (2014)). The overflow system usually consists of one or two circular weirs inside the hopper releasing the overflow mixture from the bottom of the vessel.The size range and concentration of the overflow mixture is a direct function of the sedimentation rate inside the hopper.

Sedimentation of solid particles is affected by various mechanisms. Among the main mechanisms are hindered settling pronounced in high concentrations, the mixing due to turbulence and the overall flow patterns in the hopper. Hindered settling is defined by a range of micro-scale dynamic processes which are approximated as functions of the concentration in the mixture. In case of cohesive sediments, flocculation and break up of the flocs take part in hindering. The other two mechanisms are functions of the hopper characteristics, namely the arrangement of the inlet pipes, the inflow rate and the dimensions and shape of the hopper. The hoppers are in general low energetic systems i.e. the velocities and the velocity gradients are relatively small.

The mixture inside the hopper is a two-phase system where solid particles settle in a liquid medium. In cases in which the mixture behaviour is dominated by one phase, the two-phase flow can be described by the single dominant phase and the effects of the other phase can be ignored (passive transport). On the other

end is the full two-phase modelling where none of the phases can be ignored due to their dynamic and kinematic influences on each other.

In general two-phase flows are either modeled by considering the two phases separately or by considering the mixture as a whole. In the first approach the mixture is described by conservation of mass and momentum for each phase and coupled by the phase-interaction terms. The main difficulty is providing accurate interaction terms describing and resolving the interfaces in between the phases and capturing the discontinuities associated with them. The second approach, also known as the "Mixture model" (Ishii 2006), solves the hydrodynamics of the mixture at the center of mass of the system. It is valid when the phases are strongly coupled. Mixtures of fine sand and smaller particles in the water, which have Stokes numbers much less than unity, fulfil such conditions. One set of momentum and continuity equations is solved for the mixture and an individual continuity equation is solved for the dispersed phase obtaining its volume fraction.

In cases where the dynamic and occupancy effects of the dispersed phase on the mixture are negligible except for that of the gravitational force, an intermediate approach is used known as the "Bousinesq approximation", which is based on the assumption that the density varies little, yet the buoyancy drives the flow, thus the variation in the sediment-water mixture density is neglected everywhere except in the buoyancy term.

However, the high levels of concentration inside the hopper indicates significant interaction between two phases and requires a fully two-phase modelling. The hindrance mechanisms become more pronounced and the hyper-concentrated region above the bed (slurry layer) is larger due to the constant feeding of highly concentrated mixture from above. The highly viscous mixture in this region and the dominance of frictional grain interactions creates a transition zone between the fluid-like mixture above and the bed below.

In this work, a two-phase mixture CFD (Computational Fluid Dynamics) model is set up to describe the sedimentation and concentration variations inside the hopper. One consequence of using such model is that the bed and the mixture is treated in same set of equations and moreover, interactions between the phases are captured implicitly. The model is used for studying the influence of inlet arrangements inside the hopper and the inflow variations on the overflow losses, but is equally suited to study other design aspects.

PREVIOUS WORKS

Analysis and modelling of hopper sedimentation and overflow calculations can be divided into two groups, the simple analytical models and the more sophisticated numerical models. In general, the numerical depth-resolving models have given better description of the local flow and sedimentation processes inside the hopper, although the simple models provide more quick and practical estimates of the solution and in some cases provide easy insight into the system which is not easily conveyed in more complex models. Majority of the existing analytical models are based on the idealized settling basin of Camp (1946) which was

originally developed for sludge settling tanks and is established on correlation between sedimentation rate inside the tank and the tank length scale. The main drawbacks of Camp's model being used for hopper sedimentation are the simple inlet-outlet system, uniform velocity profile inside the hopper and direct dependency of the sedimentation rate to the horizontal advection. However Koning (1977), Vlasblom and Miedema (1995), Ooijens (1999) and later again Miedema (2009) modified Camp's model by including hindered settling, turbulent diffusion, volume reduction (bed rise) and variable inflow rates to model the hopper sedimentation. Braaksma et al. (2007) proposed a model based on mass balance equations inside the hopper, but it had many calibrative parameters to be tuned by on-site measurements. Jensen and Saremi (2014) developed a more robust model based on mass balance equations inside the hopper through an integrated approach. The base assumptions in the model are i)pronounced horizontal and vertical uniformity exists inside the hopper and ii)the averaged concentration inside the hopper represents the overflow concentration. The former is a result of distributed inlet pipes along the hopper which is common in many dredgers. The model is established according to the retention time of particles inside the hopper rather than a geometrical length scale as in Camp's. The hindered settling was found to be critical to calculate the sedimentation rate and the average concentration inside the hopper. The agreement between the model and the experimental measurements confirmed the validity of the argument and shows the redundant effect of turbulent diffusion. The effect of the inlet arrangements though is clear when comparing the results from the analytical model (which is based on uniform distribution of inlets over the hopper) with the single inlet/outlet experimental setup of Rhee (2002).

The two dimensional vertical (2DV) numerical modelling done by Rhee (2002) is the only CFD modelling (to the authors knowledge) specifically done in the context of hopper sedimentation. He recognizes that the "Boussinesq approximation" can not be used in hopper sedimentation and proposed the use of two-phase mixture modelling. In his model, the continuity equation of the mixture discards the density variations and the momentum equation disregards the momentum exchange due to the relative motion of the dispersed phase. The turbulence closure is based on standard $k - \epsilon$ model including buoyancy effects, and the bed rise inside the hopper was modelled as an updating mesh so that the high concentrated regions close to the bed could be neglected. The predefined rate of the bed rise was then calculated as function of the net downward flux of the sediments including the hindered settling and particles size distribution effects. Rhee argued that the bed shear stress has a reduction effect on the bed rise velocity, therefore used a correction factor as function of Shields parameter. This may result in under-estimating deposition rates in low-energetic settling basins and hopper environments where a hyper–concentrated (slurry) layer exists above the bed and the bed shear stresses are small, the sediment is supplied from above, and the deposition is due to the over feeding of the carrier flow. The decay of turbulence is particularly efficient in mixtures of high concentration as a consequence

of sediment-induced turbulence damping. Significant damping of turbulence and thus diminution of the carrying capacity takes place by the mere presence of suspended sediments. The damping effects have been the subject of intense research.

The decay is particularly efficient in mixtures of high concentration as a consequence of sediment-induced turbulence damping. Significant damping of turbulence and thus diminution of the carrying capacity takes place by the mere presence of suspended sediments. The damping effects have been the subject of intense research. According to among others Dyer (1986), Thomsen and Gust (2000) and Thomsen (2006) a decrease in bed-shear stresses by up to $50\% - 70\%$ in well-mixed (i.e. non-stratified) mixtures of fine sediments takes place due to a thickening of the viscous sub-layer and a reduction of near-bed turbulence activity. The reduction is highest for high concentrations and moderate flow capacities. The bed shear stress with concentration was further analysed by Thompson et al. (2006). He showed that the bed shear stress variation itself does not fully account for the turbulence damping as the effect of the effective viscosity (which also increase with sediment concentration and increases the bed shear stress) masks the continued turbulence damping with concentration; the masking itself implying a laminarization. The damping and laminarization of flows to a degree where bed shear stresses are reduced by $50\% - 70\%$ is obviously important in modelling sedimentation processes inside hoppers.

Rhee (2002) did a comprehensive set of experiments providing valuable detailed observations in a scaled laboratory single-inlet hopper settings. The numerical results from his 2DV model were in good agreement with the measurements from the experimental setup. Unlike the situation in real hoppers where great deal of 3-dimensionality exists due to various inlet arrangements and the hopper shape, the single inlet/outlet experimental setup of van Rhee had a complete 2-dimensional design. Due to the well-documented and detailed information available from these experiments, they will be used as the validation data and a base-line for discussions in this paper.

PRESENT WORK

In common hopper configurations a multiple inlet arrangement provides uniform load distribution as well as significant three dimensionality. Detailed description of the sedimentation and concentration variations inside the hopper together with analysis of the influence of inlet arrangements requires a fully three-dimensional two-phase model. Considering particle size ranges from fine sand and smaller, which justifies the use of mixture two-phase modelling, the drift-flux theory described by Ishii (2006) is used as the basis of the numerical model in the present work. The performance of this method in density driven currents and settling tanks was evaluated thoroughly by Brennan (2001). In this work, hindered settling, effect of density variations on hydrodynamics of the mixture and development of the bed layer inside the hopper have been taken into account, first in a single fraction model and later extended to a multi-fraction model including kinematic coupling between the fractions. The work is limited

to the non-cohesive sediments. The results of the model are compared to the experimental measurements of Rhee (2002) and further analysis on the influence of the inlet arrangements on the sedimentation rate and overflow losses as well as the influence of variable inflow concentrations have been carried out.

MODEL DESCRIPTION

There are different methods in approaching the numerical modelling of the two-phase flows, where each one has its own advantages and drawbacks depending on the nature of the problem being modelled. The Eulerian mixture approach has been chosen in the present work based on i)the scale of the problem, ii)high degrees of coupling between the phases, iii) reduction in computational complexity due to inter-phase interactions. The mixture approach in two-phase modelling, also known as "Drift flux" modelling (Ishii 2006), describes the mixture as a whole and solves one set of equations for conservation of mass and momentum which are obtained by adding the two sets of conservation equations for each phase. The solution refers to the center of mass of the mixture due to the fact that quantities such as volume, momentum and energy are additive set functions of the mass. The model takes into account the dynamic and occupancy interactions of the two phases. The computational time is reduced considerably compared to the full two-phase models, and the uncertainties due to correct description of inter-phase forces become redundant. An additional continuity equation, which determines the volume fraction of the dispersed phase in the mixture, is solved alongside. The density of the mixture ρ_m is the volume averaged density of the two phases (Eq. 1).

$$\rho_m = c\rho_s + (1-c)\rho_w \tag{1}$$

where c is the volumetric concentration of the dispersed phase (sediment) and ρ_s and ρ_w are the densities of sediment and water respectively. As the solution, and therefore all of the hydrodynamic quantities of the mixture are defined at its center of mass, it is more natural to use the mass normalised concentration $\alpha = \frac{c\rho_s}{\rho_m}$ instead of the volume concentration of the dispersed phase. In this way the velocity of the center of mass of the mixture U_m can be defined as (mass) averaged velocity of the two phases (Eq. 2).

$$\overrightarrow{U}_m = \alpha \overrightarrow{U}_s + (1-\alpha)\overrightarrow{U}_w = \frac{c\rho_s \overrightarrow{U}_s + (1-c)\rho_w \overrightarrow{U}_w}{\rho_m} \tag{2}$$

where $\overrightarrow{U_s}$ and $\overrightarrow{U_w}$ are the velocities of the sediment and water phases respectively. The velocity of the mixture should be considered as an averaged representation of the velocities of the two phases due to the relative slip in between the two phases. The deviation from the mixture velocity for each phase can be defined as the relative velocity of that phase in respect to the mixture (Eq. 3), which has been illustrated in figure 1.

$$\overrightarrow{U}_{sm} = \overrightarrow{U}_s - \overrightarrow{U}_m \tag{3a}$$

$$\overrightarrow{U}_{wm} = \overrightarrow{U}_w - \overrightarrow{U}_m \tag{3b}$$

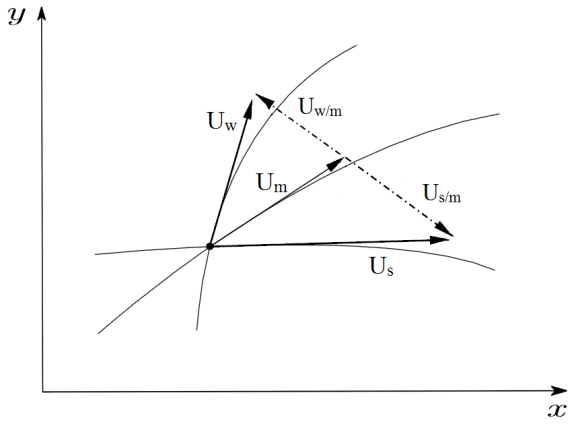

FIG. 1: Velocities in the mixture

In case of suspended sediment in water, the relative velocities are result of the gravitational fall velocity of the particles in water and it is assumed that in the horizontal direction the two phases respond simultaneously to accelerations and decelerations in the mixture (corresponding to small sediments). When adding the individual equations for each phase and using the definitions in equations 1,2 and 3, the equations of the conservation of mass and momentum for the mixture are as follows (Eq. 4 & Eq. 5).

$$\frac{\partial \rho_m}{\partial t} + \nabla.(\rho_m \overrightarrow{U}_m) = 0 \tag{4}$$

$$\frac{\partial \rho_m \overrightarrow{U}_m}{\partial t} + \nabla.(\rho_m \overrightarrow{U}_m \overrightarrow{U}_m) = -\nabla P_m + \nabla.(\tau_m + {\tau_m}^t + {\tau_m}^D) + \rho_m \overrightarrow{g} \tag{5}$$

The pressure inside the mixture P_m is assumed to act equally on both phases and the viscous shear stress in the mixture τ_m is a function of mixture velocity gradients and the mixture viscosity μ_m(Eq. 6).

$$\tau_m = \mu_m S = \mu_m \frac{1}{2}(\nabla \overrightarrow{U}_m + \nabla^T \overrightarrow{U}_m) \tag{6}$$

where S is the stress tensor and the superscript T denotes the matrix transpose. The presence of rigid particles induces extra resistance in dilatation movement of their surrounding fluid medium, equivalant to increased viscosity. Einstein (1906) developed a correction factor for fluids viscosity in dilute suspensions

as function of concentration. At higher concentrations and larger shear rates the particle collisions also play an important role in dissipation and transfer of momentum. Bagnold (1954) did a series of experiments measuring the forces (tangential and normal) in suspensions under various velocity gradients. Based on his experiments he defined two main rheological regimes (with a transitional regime in between); i) the inertia regime, where particle collisions are dominant, ii) the viscous regime, where the shear resistance can be modelled as an increased viscosity (apparent viscosity) in the mixture. In the low energy hopper systems, fine particles settle in velocity gradients which are small (even in the regions close to the unconsolidated rising bed). Roscoe (1952) modified Enstein's relation to account for mixtures with high concentrations and his relation has been used in the present work.(Eq. 7).

$$\mu_m = \mu_w (1 - c)^{-2.5} \tag{7}$$

where μ_w is the viscosity of clear water. The turbulent shear stress in the mixture ${\tau_m}^t$ takes into account the turbulent fluctuations, which depends on the turbulence closure; described later in this section. The third stress term ${\tau_m}^D$ is the mixture diffusion stress, accounting for the momentum exchange due to the relative velocities of the phases in respect to the mixture (Eq. 8).

$${\tau_m}^D = -\rho_m (\alpha \overrightarrow{U}_{sm} \overrightarrow{U}_{sm} + (1 - \alpha) \overrightarrow{U}_{wm} \overrightarrow{U}_{wm}) \tag{8}$$

The concentration of the sediment is obtained by solving the dispersed phase continuity equation (Eq. 9).

$$\frac{\partial \alpha \rho_m}{\partial t} + \nabla . (\alpha \rho_m (\overrightarrow{U}_m + \overrightarrow{U}_{sm})) = \nabla^2 (\alpha \mu_{SGS}) \tag{9}$$

where μ_{SGS} is the sub-grid scale turbulent eddy viscosity defined later in this section.

Particles fall velocity and hindered settling

In high-concentrated suspensions, the sedimentation velocity is less than that of the terminal velocity w_0, which is the Stoke's fall velocity of a single grain. The hindrance in sedimentation velocity is a result of both movement and presence of particles in the mixture. The downward movement of each particle results in an upward flux of water (displacement) which opposes the settling of other particles in its vicinity. As well the presence of particles in the mixture results in additional normal and shear stresses acting on them. Extensive experimental and analytical investigations have been done determining the hindrance rate of particles in suspensions (see the reviews by Felice (1995) and Scott (1984)) , which in general show the exponential reliance of hindrance rate on the mixture volumetric concentration (Eq. 10).

$$w_s = w_0 (1 - c)^b \tag{10}$$

where w_s is the hindered settling velocity and the exponent b is function of particles Reynolds number which the empirical relation developed by Garside and Al-Dibouni (1977) has been used in the present work to determine it (Eq. 11).

$$\frac{5.1-b}{b-2.7} = 0.1 {Re_p}^{0.9} \tag{11}$$

Particles in a suspension with concentration c, falling with velocity w_s, create an upward flux of water corresponding to a upward velocity v_f. In a frame of reference moving with the velocity of the center of volume of the mixture (e.g. from the view of a stagnant observer outside a fixed full tank of settling suspension), we have:

$$cw_s + (1-c)v_f = 0 \tag{12}$$

w_s and v_f are the relative velocities of the particles and the fluid in respect to the center of volume of the mixture. It should be kept in mind that in 2D or 3D situations the displacement flow does not necessarily become an upward flow. The relative velocity between the particles and the fluid (slip velocity) can therefore be defined as:

$$\overrightarrow{U}_{slip} = \overrightarrow{U}_s - \overrightarrow{U}_w = w_s - v_f = w_0(1-c)^{b-1} \tag{13}$$

The slip velocity as defined in equation 13, is the hindered falling velocity of the particles in the fluid excluding the hindrance due to the return flow. In other words it is the velocity of the particles from the point of view of an observer moving with them. By considering the occupancy effect of the particles in the continuity equation (which is often ignored in models dealing with low levels of concentrations), the effect of the return flow will implicitly be taken into account and the hindered settling function should be used cautiously to avoid double accounting of this effect. This over-calculation is often observed in literature using two-phase models. Re-writing the relative/slip velocity based on the definitions in Eq. 3, gives:

$$\overrightarrow{U}_s - \overrightarrow{U}_w = \overrightarrow{U}_{sm} - \overrightarrow{U}_{wm} \tag{14}$$

In a similar argument as above, in a frame of reference moving with the velocity of the center of mass of the mixture we can write the conservation of mass as:

$$\alpha \overrightarrow{U}_{sm} + (1-\alpha)\overrightarrow{U}_{wm} = 0 \tag{15}$$

Therefore based on equations 13,14 and 15 the relative velocities of particles and the fluid to the mixture can be defined as functions of the particles slip velocity (Eq. 16).

$$\overrightarrow{U}_{sm} = (1-\alpha)\overrightarrow{U}_{slip} \tag{16a}$$

$$\overrightarrow{U}_{wm} = -\alpha \overrightarrow{U}_{slip} \tag{16b}$$

Turbulence

Distribution of the turbulence and flow structures inside the hopper is three-dimensional. There are three main sources of turbulence inside the hoppers, which are the discharge pipe-turbulence injected into the hopper at the inlets, the generated turbulence by the inflow jet at the impinging area and finally the turbulence generated by the net flows through the hopper (Rhee 2002). The high levels of concentrations and the nearbed density driven currents in the mixture evens out the bed and influence the production and damping of the fluctuations and should be taken into account. The Large Eddy Simulation method (LES) has been used in the present work, allowing the large scale eddies in the mixture to be resolved and the sub-grid scale (SGS) eddies have been handled by the one-equation kinetic energy model, here taking into account the density variations in the mixture (Eq. 17).

$$\frac{\partial \rho_m k}{\partial t} + \nabla.(\rho_m k \overrightarrow{U}_m) = \nabla^2(\mu_{eff} k) + 2\mu_{SGS}(S:S) - \rho_m \frac{C_e}{\Delta} k^{3/2} \tag{17}$$

where μ_{SGS} is the sub-grid scale eddy viscosity (Eq. 18) and the effective viscosity is defined as $\mu_{eff} = \mu_m + \mu_{SGS}$.The filter size Δ is chosen to be function of the cube root volume of the computational cells.

$$\mu_{SGS} = C_k \rho_m \sqrt{k} \Delta \tag{18}$$

The constants C_e and C_k have the standard values of 1.084 and 0.094 respectively.

Bed rise inside the hopper

The bottom (bed) inside the hopper rises due to continuous sedimentation of the dredged material. From the mixture point of view, the bed is defined as part of the mixture where the concentration has reached the maximum packing limit of the particles and the flow through that area encounters higher resistance and dissipation due to the existing porous skeleton. In the depositing hopper systems with low bed shear stresses, the bed behaves as a continuously accreting layer and the occasional decrease in the bed rise (usually below the inlets) is merely due to the increased capacity of the mixture above the bed. Such specific behaviour allows us to simulate the bed inside the mixture by setting the particles fall velocity to zero when the concentration reaches the (pre-defined) packing limit and imposing an extra resisting force (as function of porosity) on the mixture in that region due to the porous structure of the bed. This has been incorporated in the model based on Darcy's relation for the resistance force on the flow in porous media (Engelund 1953).

Poly-disperse mixtures

Natural sediment is usually composed by widely varying particle sizes. The sedimentation in hoppers depends on the degree of size dispersity in the mixture. The upward flux of water induced by larger particles imposes higher hindrance on the finer particles and may overcome their downward settling velocity. More

detailed interactions, such as trapping of finer particles behind the coarser particles (and being dragged down) and the clustering of groups of particles also alter the sedimentation rate. The kinematic interactions between the particles due to the fluid displacement is the most pronounced influence of size distribution in the mixtures (see Batchelor (1982)), whereas the other hindrance effects are to great extend function of the total concentration of the mixture $c_T = \sum_{i=1}^{N} c_i$. Therefore to determine the particles fall velocity in a poly disperse mixture, the conservation of volume (Eq. 12) can be extended to the case for N different fractions (Eq. 19) and the slip velocity for the each individual fraction $U_{slip,i}$ can be defined as in equation 20.

$$\sum_{i=1}^{N} c_i w_{s,i} + v_f(1 - \sum_{i=1}^{N} c_i) = 0 \tag{19}$$

$$U_{slip,i} = U_{s,i} - U_w = w_{s,i} - v_f \tag{20}$$

where index i refers to the i_{th} constituent of the poly disperse mixture. By knowing the slip velocity of the particles, the equations 19 and 20 build a system of N equations and N unknowns for determining the hindered velocity of the particles ($w_{s,i}$) in a poly disperse mixture. A valid approximation for the slip velocity of the particles can be gained by an analogy to the mono sized mixtures which is as follows:

$$U_{slip,i} = w_{0,i}(1 - c_T)^{b_i - 1} \tag{21}$$

Defining the relative velocities of the particles to the mixture ($U_{sm,i}$) and the relative velocity of the fluid to the mixture (U_{wm}) in a poly disperse mixture can be done in a similar way as above (but based on Eq. 15) and the derived equations will become as follows.

$$U_{sm,i} = (1 - \alpha_i)U_{slip,i} - \sum_{j \neq i} \alpha_j U_{slip,j} \tag{22a}$$

$$U_{wm} = -\sum_{i=1}^{N} \alpha_i U_{slip,i} \tag{22b}$$

Numerical solution method

The model described above is implemented in the open source CFD code OpenFOAM based on finite volume approach. The Navier-Stokes equations for the mixture are solved by the PISO (Pressure implicit with splitting of operator) algorithm followed by the solution of the transport equation for the dispersed phase. In the poly-disperse case the solution should be obtained through the full implicit coupling between the fractions. Such approach increases the computational costs and complexity. The essence of the coupled solution in a multi fraction system is the kinematic interaction in between the particles due to the

fluid displacement. However, an explicit solution of the particles fall velocity, where the fractions are solved in decreasing order of their size, was proposed in Jensen and Saremi (2014) and provides excellent approximation to the solution obtained with the fully coupled system. The solution of the continuity and momentum equations for the mixture is a function of the mixture density, which is updated after solving each fraction's transport equation. Therefore to minimize the effects of the explicit solution of the multi fraction mixture, the transport equations are solved in decreasing order of particle diameters, while the pressure-velocity solution is updated after solving each fraction's transport equation. Wall boundary conditions have been used at the bottom and sides of the hopper and the top boundary is modelled by the slip condition representing the free surface.

MODEL VERIFICATION

The performance of the mixture model in simulating the sedimentation inside the hopper has been verified by modelling the physical tests done by Rhee (2002) in a laboratory scale hopper with a single inlet/outlet system. The model hopper had length of $4m$, width of $3m$ and depth of $2.5m$. The material used in the experiments was fine sand and had a size distribution with an averaged $D_{50} = 0.1mm$ and standard deviation of $\sigma \approx 2$. The inlet to the hopper had a constant flux but the concentration at the inflow had some variations in time. Further details of the experimental set-up can be found in Rhee (2002). The information about the size variations of the inflow material was sparse. An "overview particle size distribution" with 9 different sieve sizes which was used in the 2DV model of Rhee (2002) is given. In order to capture the effect of size variations in the sedimentation rate of the particles, resolving the distribution curve to at least 50 different fractions is necessary (Jensen and Saremi 2014). However, based on the available information and few trial and errors, a distribution curve of 10 different fractions has been constructed for tests 5 and 6, as more information is not available. The experiment is simulated as a rectangular basin with a downward inlet at one end and a horizontal outlet at the other. The test hopper was pre-filled with water up to around 50% of its height. The simulations started by having the hopper full of clear water. This means that the overflow begins in the model earlier, while in the experiments it started after the water level in the barge reaches the overflowing level. This time lag has been considered in comparing the results from the numerical model. The time series of overflow concentrations from the two tests $Test05$ and $Test06$ are shown in figures 2 and 3. The numerical model predicts the overflow concentration to a very good level of agreement with the experimental results.

Time series of the measured velocity and concentration profiles were presented in Rhee (2002) for $Test06$, which have been used here for comparison with the numerical model. The concentration profiles at five time spots were measured in the middle of the hopper. In figure 4 the profiles from the numerical model and the measurements are plotted. Both the measurements and the simulated results

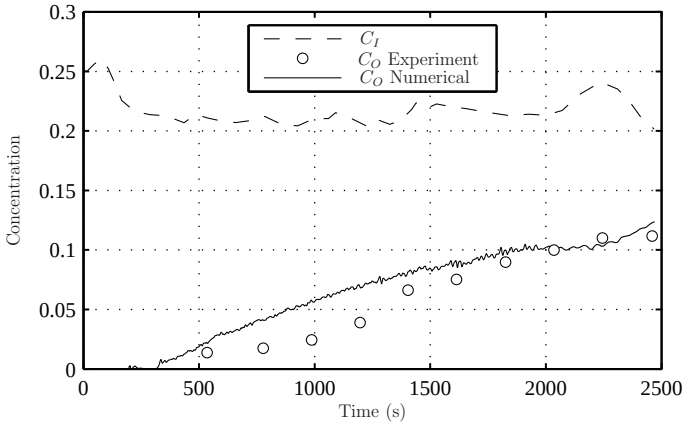

FIG. 2: Overflow concentrations from Test05

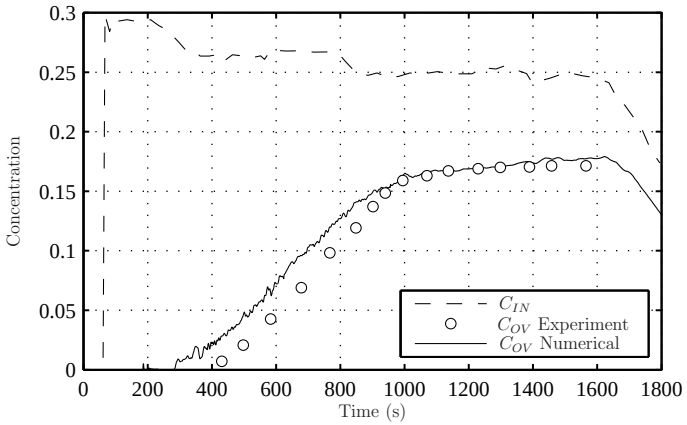

FIG. 3: Overflow concentrations from Test06

demonstrate the almost vertical (uniform) concentration profiles in the mixture layer above the bed. The onset of equilibrium stage which is after about 1000 seconds (see figure 3) can be distinguished by the almost similar profiles at the last plots in figure 4 where the average concentration inside the hopper remains almost constant. The numerical model also presents the slurry layer above the bed well in accordance to the measurements (see the last plot in 4).

The horizontal velocity inside the hopper was measured by probes which were fixed at a certain horizontal location and were raised during the experiment to follow the bed and not to be buried. van Rhee presented the time series of horizontal velocity from a probe which had vertical positions of 0.45 to 2.25 meters from the bottom of the hopper. The exact positions of the probe during

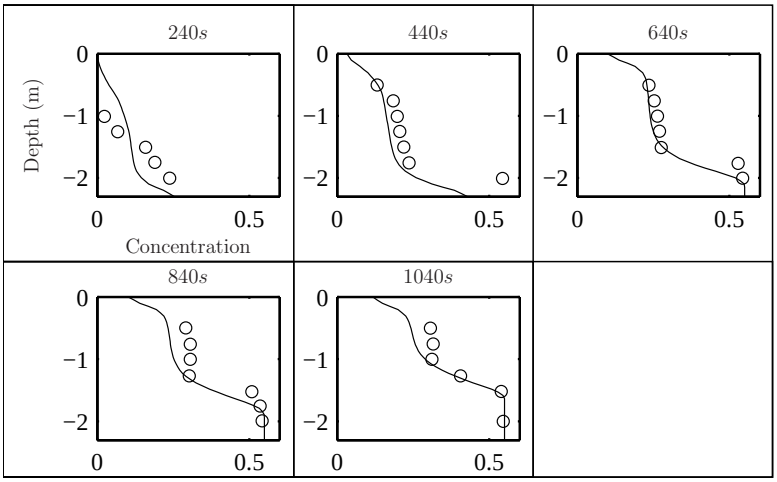

FIG. 4: Comparison between measured (circles) and computed (lines) concentration profiles in $Test06$

the experiment was not specified. In figure 5 the computed horizontal velocities at vertical distances of about 0.4 meters from the rising bed are plotted with the measured data of Rhee (2002). Although the probing positions of the experiment were not exact, it can be perceived that the numerical results are in the same order of magnitude of the measured velocities. The occasions of negative velocities indicate the density currents close to the bed being reflected from the end of the hopper, which presents the capability of the model capturing this feature.

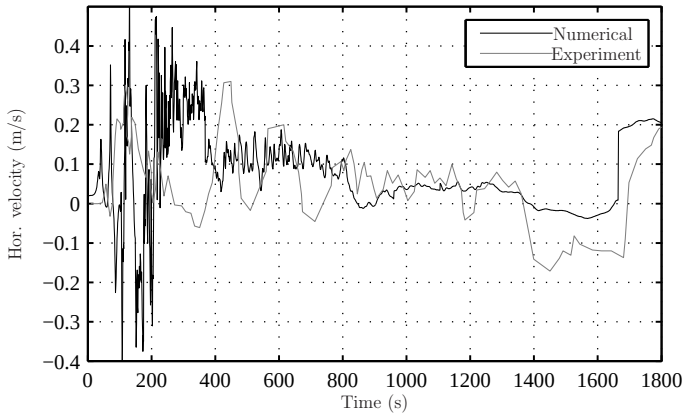

FIG. 5: Computed and measured horizontal velocity during Test06

INLET ARRANGEMENTS

The overflow concentrations are reasonably predicted with the model of Jensen and Saremi (2014), and within the uncertainties of the sediments at the seabed, its a perfect tool for the most environmental impact assessment (EIA) studies. The present model's sophistications enables a more detailed investigation of the dredgers and provides means for optimization of the hopper sedimentation system e.g. through the arrangement of the inlet pipes or the overflow structures.

The arrangement of the inlet pipes controls the load distribution in the hopper. Small hoppers usually have one or two discharge pipes which are placed either in the middle or one at each end. In bigger dredgers greater number of inlet pipes are used merely to control the load distribution along the hopper. Placement of the inlet pipes and the distribution of inflow rate among them have great impact on the distribution of sediment and the mixing level inside the hopper. In the following the effect of inlet arrangements and distribution of influxes on the overflow concentrations and the sedimentation rates in the hopper are investigated by simulating five different configurations (figure 6). The two extreme scenarios are the case with one row of inlet pipes at the far end of the hopper (case1) and the case with an inflow source distributed all over the hopper (case 5). The latter closely represents the conditions of the integrated approach of Jensen and Saremi (2014).

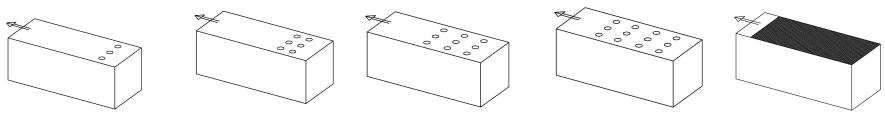

(a) Case 1 (b) Case 2 (c) Case 3 (d) Case 4 (e) Case 5

FIG. 6: Inlet configurations

Three different loading regimes (characterized by the non-dimensional loading parameter $\beta = \frac{Aw_s}{Q}$) have been considered to investigate the above configurations. The results from the analytical model of Jensen and Saremi (2014) have also been included. In figure 7 the time series of the overflow concentrations are presented until the point where the hopper is about 80% full. The overflow concentrations and the sedimentation rates vary differently under different inlet arrangements. Small values of β is an indication of excess influx of mixture in compare to the settling capacity in the hopper. It results in shorter retention times of sediments inside the hopper which means that in average particles will reach the overflow before settling. The dredging cycle is longer in this case due to higher overflow losses and slower bed growth rates. This situation can be enhanced when very fine sediments are pumped into the hopper at high volume rates. β values greater than unity represent the situation where the settling capacity in the hopper is higher than the feeding rate from the pipes. The retention time in the hopper

is long enough for the particles to settle before reaching the overflow. Coarser grains being pumped in at low volume rates perfectly represent this situation.

Depending on the loading regime, distributing the discharge points along the hopper can increase or decrease the overflow losses and the sedimentation rates. Keeping the total influx of material constant, but concentrating it in fewer inlet pipes at one end of the hopper (case 1) induces higher velocities and mixing in the hopper. With $\beta < 1$ this results in less settling rates and higher overflow losses whereas in $\beta > 1$, by further mixing of the sediments along the hopper (due to higher velocities) the particles will get extra time to settle. In figure 7 the described behaviour can be seen clearly where at $\beta < 1$ the overflow losses in case with the single rowed inlet rise immediately up to the inlet concentrations whereas the same case with $\beta > 1$ provides minimum losses when the influx of material is concentrated at fewer inlets.

The analytical model (Jensen and Saremi 2014) is based on the assumptions that the inlets are uniformly distributed all over the hopper, the concentration profiles in the mixture are constant and the average concentration inside the hopper is representative for the overflow concentration. In figure 8 the concentration profiles from all cases (including the analytical results) are shown at a probing point close to the overflow at time when all cases have reached the equilibrium stage. It can be seen that the concentrations are almost constant over the depth and by further distributing the inlet pipes along the hopper, the average concentration inside the barge get closer to the overflow values in figure 7. This supports the assumptions made in the analytical model.

Bed evolution and flow patterns

The injected turbulence from the discharge pipes into the hopper dies out soon by going further away from the impinging point below the inlet. Though at the impingement area it significantly decreases the sedimentation rate due to high velocities and intense diffusivity due to eddies. In figure 9 the iso-surface of the bed layer has been demonstrated for three different inlet configurations with $\beta \sim 1$. The results show the presence of depression areas located below the inlet pipes, which is more pronounced in case 1 where the velocities are higher. This should not be mistaken by an erosion mechanism as there were no bed layer to be eroded from, but just reduction in sedimentation rate due to higher flow capacity.

The common hopper configurations include multiple inlet pipes and in case of single inlet dredgers, the pipe is placed at the center which all result in significant levels of three dimensionality in the flow inside the hopper. In figure 10 the streamlines of the mixture velocity have been plotted over the bed layer in three different cases. At the surface there is a uniform flow pattern going towards the overflow, but deeper in the mixture the interactions between the eddies and the density currents in the mixture results in a fully 3 dimensional behaviour even in the first case with one row of pipes at the end of the hopper. This indicates that 3D modelling for optimizing hopper sedimentation is necessary.

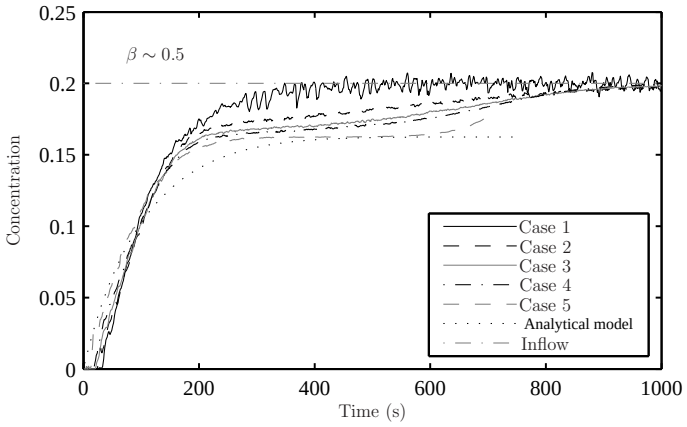

(a)

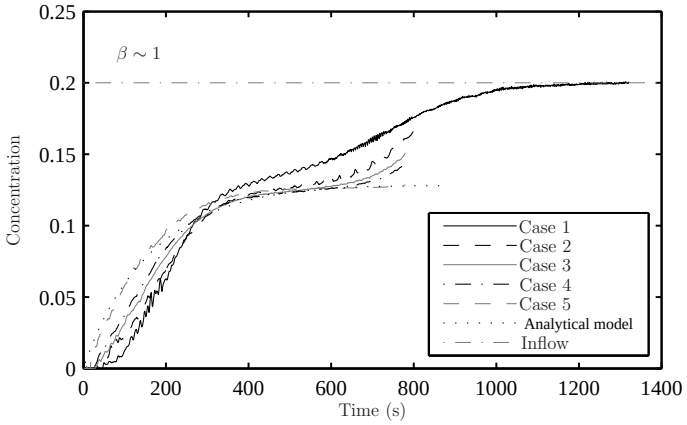

(b)

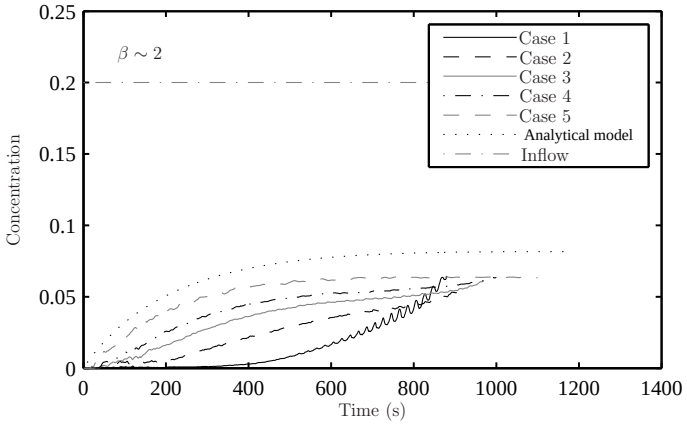

(c)

FIG. 7: Overflow concentrations until the bed level inside the hopper is 80%

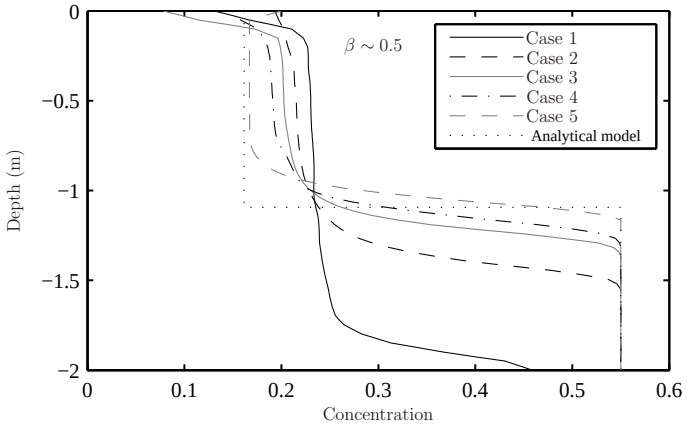

(a)

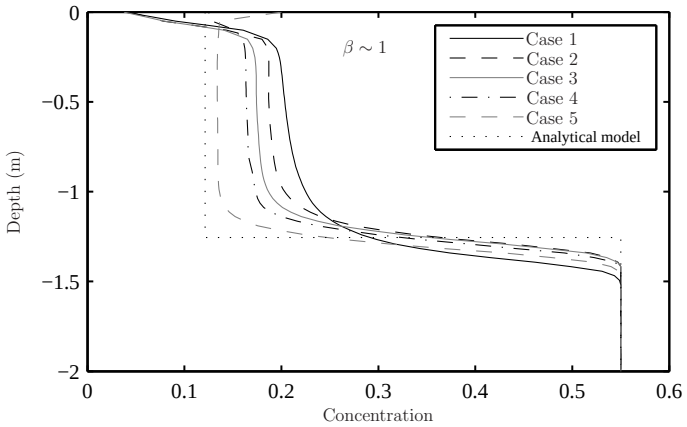

(b)

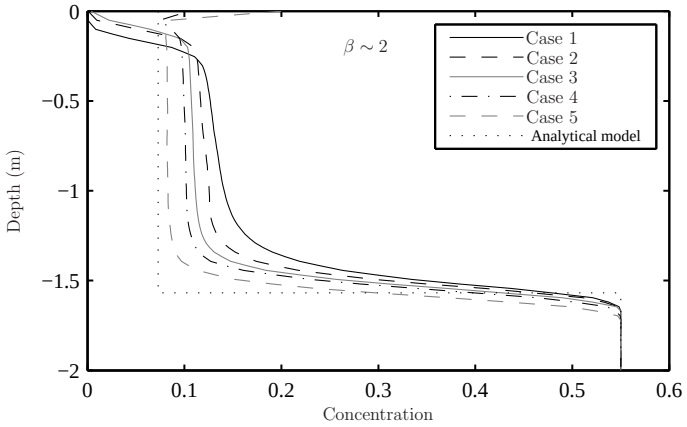

(c)

FIG. 8: Concentration profiles at a probe point close to overflow, at $t = 60\%T_{full}$

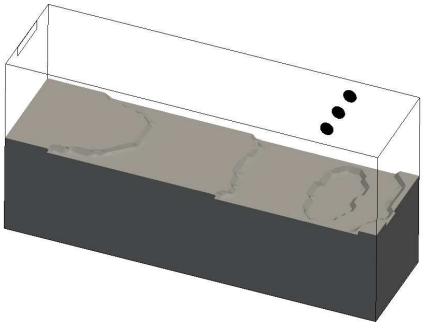

(a) Case 1

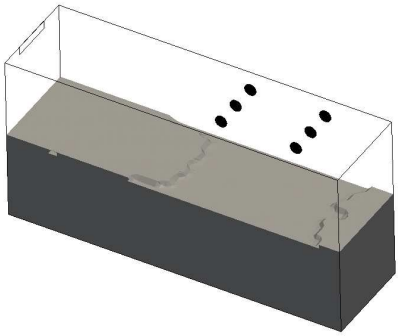

(b) Case 2

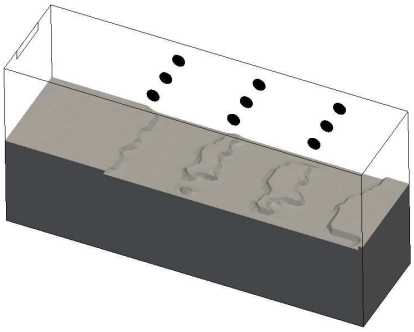

(c) Case 3

FIG. 9: Iso-surface of the bed layer for different inlet arrangements at $t = 60\%T_{full}$

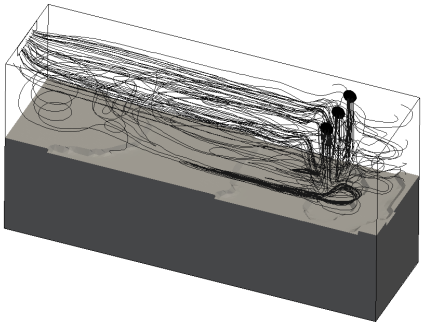

(a) Case 1

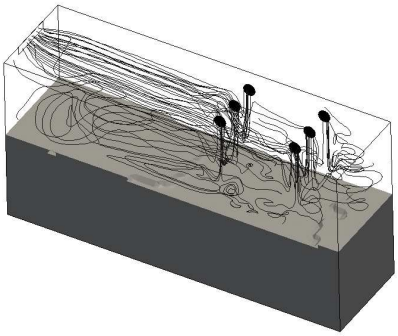

(b) Case 2

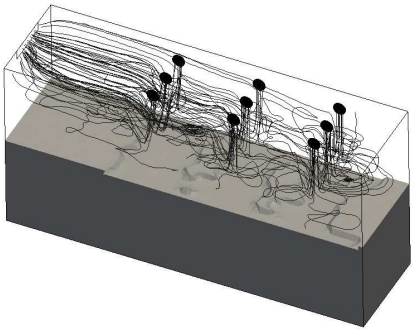

(c) Case 3

FIG. 10: Streamlines of the mixture velocities for different inlet arrangements at $t = 60\%T_{full}$

Filling capacity and the effect of slurry layer

Continuous feeding of the hopper with mixture of water and sediment results in constant overflow and bed growth. The increasing bed level reduces the height of the mixture in the hopper. By smaller available volume, the velocities increase and mixing level rises in the mixture. This will increase the overflow losses all the way up to 100%. At this stage the bed growth halts as whatever is being pumped in leaves the hopper directly. The transition from the stage where the overflow concentrations during infill attain equilibrium to the surpass of hopper capacity coincides with the time when the slurry layer above the bed reaches close to the overflow level. This phenomenon can be observed in the experimental results of Rhee (2002) at $Test08$ where the overflow concentration, after a period of equilibrium, begin to rise towards the inflow values. In the extreme situations where overflow losses reach 100% since the very early stages (e.g. case 1 with $\beta < 1$) the bed never develops and consequently the idea of slurry layer being exposed to the overflow level doesn't apply. It should be noted that formation of the slurry layer is due to highly hindered settling of particles close to the bed. Weak hindrance mechanisms in suspensions with coarse sediments are not able to trigger the formation of the slurry layer and there is a sharp interface between the bed and the mixture. In this case the overflow concentrations are at their lowest level due to fast settling of the particles. This situation occurs at large values of β and will be more pronounced at single inlet hoppers (e.g. case 1 with $\beta > 1$). The experimental results of Rhee (2002) at $test04$ where coarse sand where used in it clealry show this phenomenon.

In the analytical model the onset of the transition stage and the thickness and position of the slurry layer should be calculated explicitly. In order to include the transition behaviour of the mixture in the analytical results, the position of the slurry front can be estimated by the method of characteristics. The application of this method to the problem of particles sedimentation was first done by Kynch (1952). The low energetic and homogeneous nature of the hopper mixture with its uniform distribution of the material in cases with multiple inlets (corresponding to the assumptions made for the analytical model) justifies the validity of this method to approximate the rising rate of the concentration fronts along the depth. In the analytical model, the concentration inside the hopper is used as input for the calculation of the growth of concentration fronts. This has been calculated from the time of equilibrium onward and shown in figure 11. For the case with $\beta \sim 1$, the lines fanned from the origin display the evolve of higher concentration fronts of the slurry layer. The lines with the constant slope at the background represent the constant feeding of sediment in the mixture and the bold black line corresponds to the concentration front of the bed.

By estimating the position of the slurry front from the method of characteristics (see appendix for more details) it is then inserted into the results from the analytical model to obtain the onset of the slurry overflow period. According to the CFD results with conditions similar to the analytical model (case 5), the transition period is a short smooth rise of overflow concentrations towards the

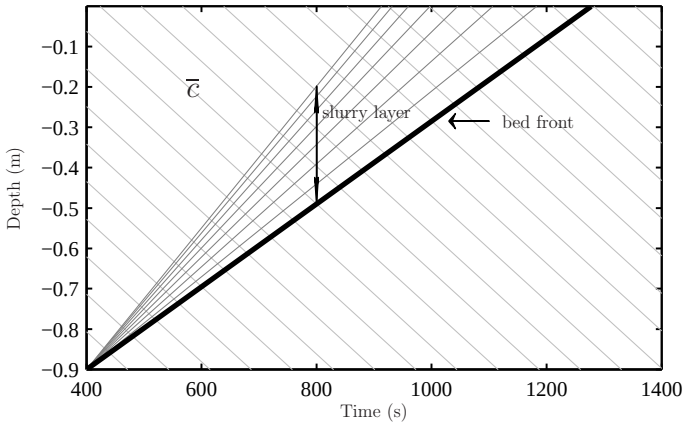

FIG. 11: Lines of characteristics for constantly fed mixture. The light lines are the concentration fronts in the mixture. The grey lines indicate the rising high concentrated fronts (slurry layer). The bold black line is the bed front

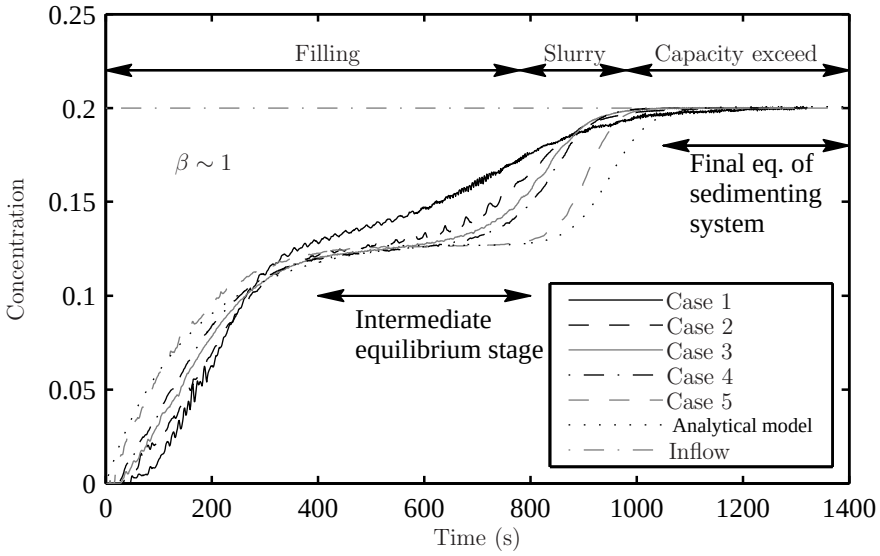

FIG. 12: Overflow concentrations over a longer period

inflowing values which in the analytical model can be approximated as a hyper tangential rise. In figure 12 the extended (in time) results from all cases with $\beta \sim 1$ including the results from the analytical model with the above described correction are plotted. Three different stages can be distinguished in the results. The first stage is the filling period where the overflow losses rise until reaching an intermediate equilibrium condition. The second is the transition stage where due to both shorter retention time and the exposure of the slurry layer to overflow, the losses begin to rise. The rise continues until a third stage is reached where the hopper capacity is exceeded and the overflow losses are 100%. In this stage the sedimenting system of the hopper has reached it's final equilibrium. The distinction between different stages is more clear in cases with more uniformly distributed inlets along the hopper.

VARIABLE INLET DISCHARGE

The natural composition of seabed material shows great variability in size, distribution and rheological properties both horizontally and vertically (various layers at the seabed). Such variability results in non-uniformities in material pumped into the hopper. Fluctuations in the inflow concentration has been modelled for an inlet arangment as in case 3 at different loading regimes to investigate the effects on sedimentation and overflow losses. The fluctuating component of the inflow concentration is described by a sinusoidal function with amplitude ε and frequency ω (Eq. 23).

$$c_{in} = \overline{c}_{in} + c'_{in} = \overline{c}_{in} + \varepsilon Sin(\omega t) \tag{23}$$

A situation where the amplitude of the concentration variations are 50% of the inflow concentration has been considered with periods varying from 10% to 60% of T_s, which is the time scale representing the time required for the sediments to settle over the depth of the hopper (Jensen and Saremi 2014). The oscillations in the inflow concentration result in i)fluctuating overflow concentrations, ii) net increase/decrease of the overflow concentrations. The oscillations in the overflow concentration have the same frequency as in the inflowing fluctuations, but the amplitude differs depending on the sedimentation regime of the hopper and the magnitude of ω. The net change in the overflow concentrations (under same ϵ values), depends only on the sedimentation regime inside the hopper (β value) and the frequency (ω) does not influence it. The effect of the frequency of inflow variations on the overflow concentrations can only be seen as higher/lower amplitudes in overflow fluctuations. Higher the frequency become, there will be less time for the mixture to react and consequently the overflow concentrations experience less variations (smaller amplitudes).

The time series of the overflow concentrations are presented in figure 13 for both non-oscillating and oscillating inflow concentrations ($\frac{2\pi}{\omega} \sim 20\%T_s$). The effect of the loading regime (β) on both the amplitude of the overflow fluctuations, and the net change in the overflow concentrations can be discussed according to the results in figure 13.

The reaction of the overflow losses to variations of the inflow concentration can be explained in terms of available retention time and the average concentration inside the hopper. In the case of lower beta values ($\beta < 1$), The retention time inside the hopper is short and the average concentration is high (often higher than inflow-see figure 8a). In order to describe the behavior of the mixture under concentration fluctuations, the two half periods of increasing ($c' > 0$) and decreasing ($c' < 0$) fluctuations are discussed separately. In the period with higher inflow concentration ($c' > 0$), due to the short retention time, any increase in the inflowing concentration will merely results in higher losses. In the period with lower inflow concentration ($c' < 0$), the inflowing flux of sediment mixture becomes positively buoyant and will be avoided from settling. Therefore, in total the variations result in a net increase in overflow losses (13c).

In case of higher beta values ($\beta > 1$), the retention time inside the hopper is long enough and the average concentration is low (often less than 50% of inflow, see figure 8c). In the period with higher inflow concentration ($c' > 0$), any increase in the inflowing concentration will increase the settling rate and the density currents towards the bed. The hindrance due to increase in the concentrations is in a lower order of magnitude than the effect of enhanced density gradients towards the bed. In the period with lower inflow concentration ($c' < 0$), the concentration of the inflowing mixture is still above the ambient concentration inside the hopper and will not cause any extra losses. Therefore, in total the variations result in a net decrease in overflow losses (13a). The contour lines of the mixture density at three consecutive phases under variable inlet discharge are plotted in figure 14. t_0 corresponds to the time where $c' = 0$, and therefore $t_0 + T/4$ represents the time when the inflow concentration has its maximum value, and $t_0 + T/2$ the time when the inflow concentration has its minimum value. The effect of the density variations on the mixture and the density currents are clearly visible in these figures. The concentration profiles at a point exactly below an inlet pipe are shown in figure 14g-h. It shows the effect of the variations on the slurry layer and the average concentration inside the hopper.

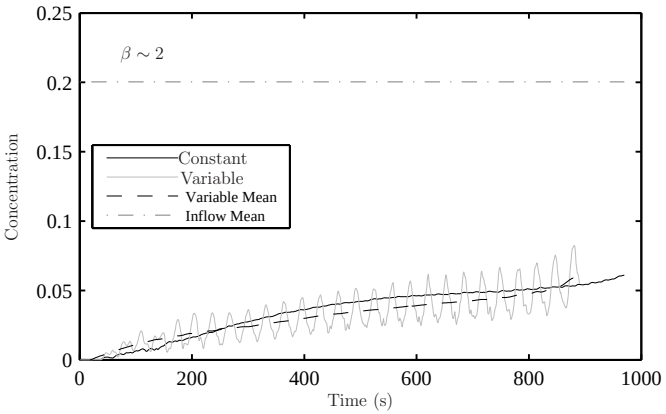

(a)

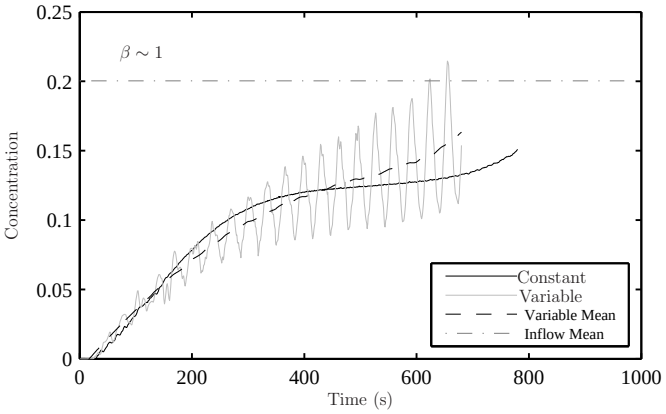

(b)

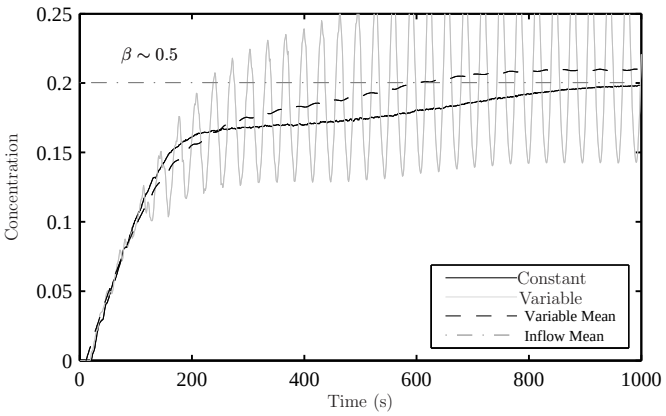

(c)

FIG. 13: Overflow concentrations for both varying and constant inflow

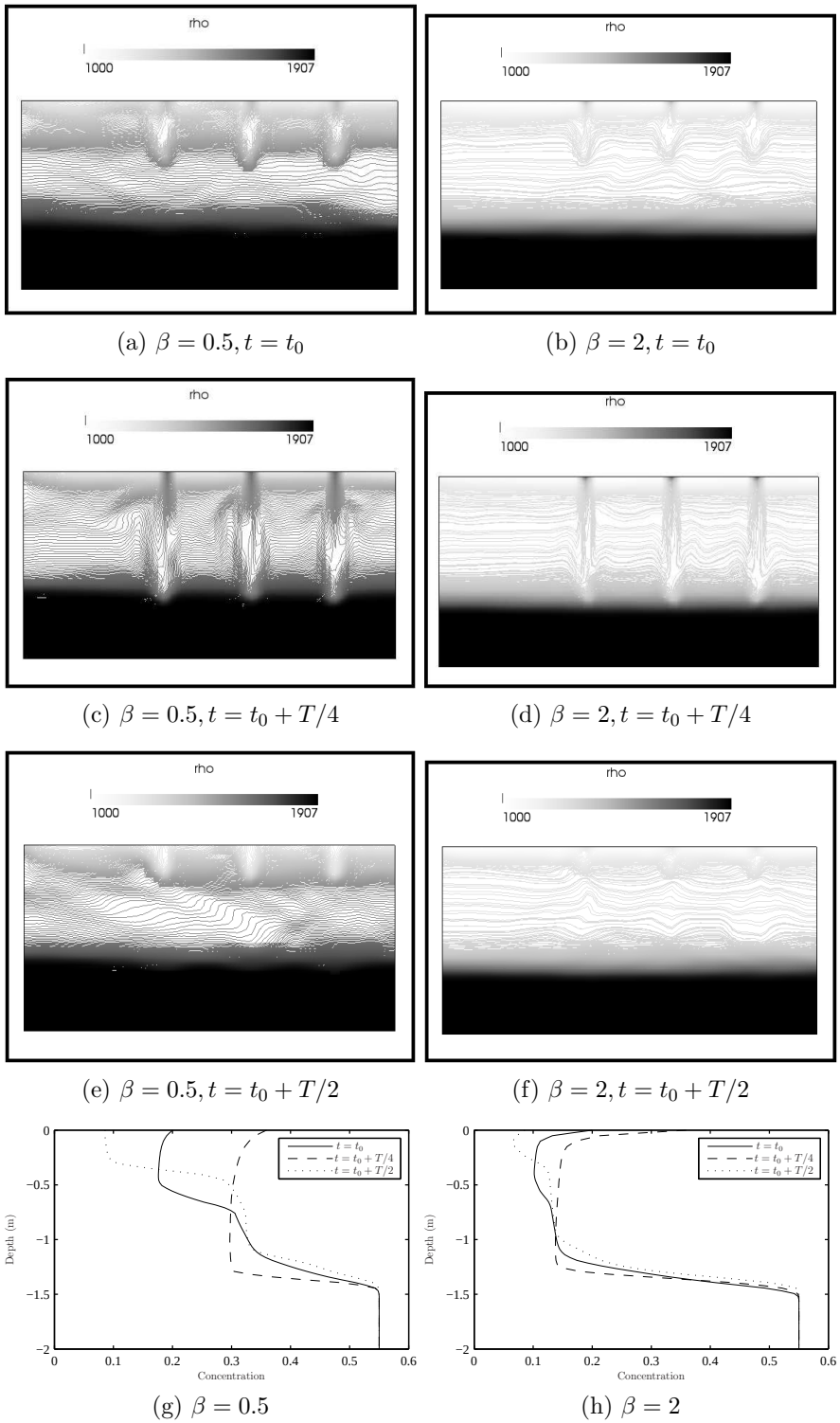

(a) $\beta = 0.5, t = t_0$ (b) $\beta = 2, t = t_0$

(c) $\beta = 0.5, t = t_0 + T/4$ (d) $\beta = 2, t = t_0 + T/4$

(e) $\beta = 0.5, t = t_0 + T/2$ (f) $\beta = 2, t = t_0 + T/2$

(g) $\beta = 0.5$ (h) $\beta = 2$

FIG. 14: a-f: Cross sections of the density contours inside the hopper(the overflow is at the top left corner). g,h: the concentration profiles below the middle inlet pipe.

CONCLUSIONS

The sedimentation of the highly concentrated dredged material in common hopper configurations which requires three dimensional coupled modelling has been successfully simulated by using the two-phase mixture approach. By using the poly disperse model the experimental results were reproduced well, which is also an indication of the effect of size variations on the overflow concentrations. The model should be considered as a perfect design tool investigating the processes involved in hopper sedimentation.

The ability of the model in resolving the highly concentrated regions above the bed (the slurry layer) reveals valuable information about the behaviour of the mixture at the final stages of the dredging cycle, which can be used to determine an optimum termination point corresponding to minimum overflow losses. In general the concentration of the mixture inside the hopper increases until reaching an (intermediate) equilibrium stage. Thereafter by rising of the bed and reduction in sediment retention time, the overflow losses begin to rise until the settling capacity of the hopper is surpassed and whatever is pumped in the hopper flows overboard, where the sedimenting system has reached its final equilibrium.

Termination of infilling has always been a point of debate between environmentalists and the dredging contractors. In the hoppers with a fixed overflow system, the infill continues until the ship reaches its maximum allowable draught. In hoppers with an adjustable overflow system, the infill continues while the maximum allowable draught is maintained by lowering the overflow weir. This phase is called the constant-tonnage phase. In this phase the overflow losses are typically higher and it continues until the losses become so high that it is no longer economically feasible to continue dredging, or the sand bed has reached the overflow weir (Braaksma 2008). The higher concentrations during the constant-tonnage phase are clearly due to the transition between the the intermediate and the final equilibrium of the sedimenting system inside the hopper and the exposure of the slurry layer to the overflow level. An optimum termination point, with the least overflow losses and at the same time most possible loading of hopper should be in the period between the onset of the transition stage and the beginning of the final equilibrium of the sedimenting system.

Arrangement of the inlets and distribution of inflowing material in the hoppers have been investigated from a new perspective, which is the effects on the overflow losses. The results show that the distribution of the inlets along the hopper has direct impact on the rate of sedimentation inside the hopper and the overflow losses. Depending on the hopper characteristics and the type of sediment (gathered in the non dimensional parameter β), the sediments retention time inside the hopper may increase or decrease under different inlet configurations. Therefore hoppers with multiple inlet pipes can benefit from adjusting the inflow configuration according to the inflow rate and type of sediment being dredged. The natural diversities found in the seabed introduce variations (in concentration, size and type of sediment) to the inflowing material. The investigation of concentration variations at the inlet shows that the average overflow losses may decrease or

increase depending on the hopper characteristics and the type of sediment (the β value). Assessments of plume excursions from the hopper overflow should include plausible error bars to accommodate uncertainties related to, e.g., oscillations in the inflow concentrations.

The results from the CFD model support the assumptions which the analytical model (Jensen and Saremi 2014) is based on and it perfectly matches the cases where the inlet pipes are distributed over the hopper. The analytical model however may under- or over estimate (depending on the β value)the overflow losses in hoppers with inlet arrangements which introduce minimum degree of uniformity over the whole area of the barge, such as a long hopper with a single inlet at one end, which usually is not the case in practical hoppers.

APPENDIX

In mixtures of coarse sediments (having higher settling velocities) or in cases with sufficiently low levels of concentration, a sharp interface between the bed and the mixture above it will develop (figure 15). In cases with high levels of concentrations and fine grained material, the interface is smeared by a slurry layer due to the hindrance.

In the analytical model of Jensen and Saremi (2014) the bed growth is assumed to be:

$$\frac{\partial h_b}{\partial t} = \frac{\overline{c} w_s}{1 - n - \overline{c}} \tag{24}$$

which provides an estimate of the time when the slurry layer is exposed to the overflow.

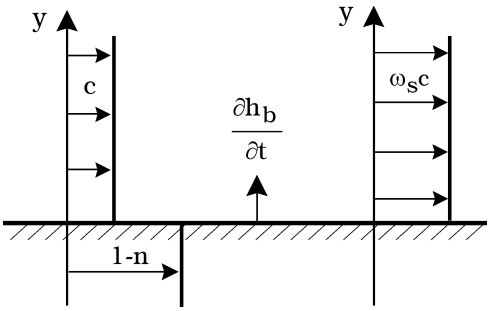

FIG. 15: Profiles of concentration and vertical sediment flux

In the numerical model though, there is no distinction between the bed and the mixture above it, and the concentration profile is a continuous transition between the value in the mixture to the bed packing limit c_b. Consider the concentration profile $\overline{c}$, and consequently the sediment flux profile to be defined as:

$$c = -(1 - n - \overline{c}) S(y - \omega t) + (1 - n) \tag{25a}$$

$$c w_s = \overline{c} w_s S(y - \omega t) \tag{25b}$$

where S is a (sigmoid) function representing the transition from mixture to the bed and ω is the growth rate (i.e. the bed rise velocity). S may attain a heaviside function (representing a sharp interface between the mixture and the bed, referred to as a first order discontinuity (Kynch 1952)) or a more smooth function such as arc-cosine or hyper-tangential functions (representing the presence of a smooth transition between the mixture and the bed, referred to as a second order discontinuity (Kynch 1952)).

As a first order approximation, it can be assumed that ω is constant in time and space. Therefore, by inserting the profiles from equation 25 into the the one-dimensional continuity equation for concentration (equation 26), the rate of bed rise (ω) can be upon inserting:

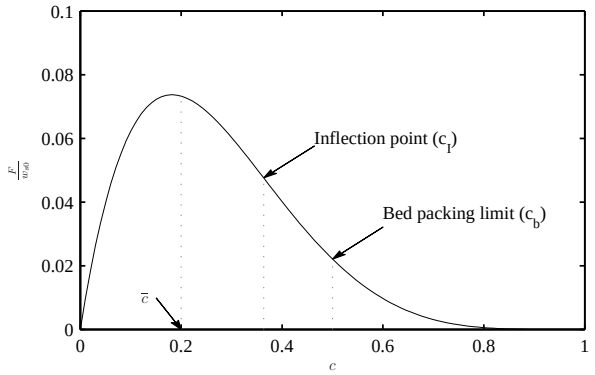

FIG. 16: Flux curve for suspension of fine sand with $b = 4.5$ and $\overline{c} = 20\%$

$$\frac{\partial c}{\partial t} = \frac{\partial c w_s}{\partial y} \tag{26}$$

$$\omega(1 - n - \overline{c})S' = \overline{c} w_s S' \Rightarrow \omega = \frac{\partial h_b}{\partial t} = \frac{\overline{c} w_s}{1 - n - \overline{c}} \tag{27}$$

The above implies that having a slurry layer which has a fixed thickness, does not influence the rate of bed level rise calculated as in equation 24. The thickness of the slurry layer, and therefore the shape of the function S is, however, not constant in time. This can be clearly seen when drawing the characteristic lines of different layers of concentration fronts rising in an initially homogeneous suspension.

The particles in a suspension with concentration c and hindered settling velocity of $w_s = w_{s0}(1 - c)^b$ (assuming that its valid all the way to the bed concentration) have a downward flux of $F = cw_s$. In a suspension with initial uniform concentration $\overline{c}$, the layers of higher concentration begin to develop from the bottom while the particles settle. The behaviour of the sedimentation flux function (F) depends on the value of power b which is function of grains diameter. Considering a suspension of fine sand and initial concentration of 0.2, the flux curve and the lines of characteristics of sedimentation and development of the bed layer with porosity of 0.5 are plotted in figures 16 and 17.

The position of the inflection point on the flux curve (fig. 16) indicates the concentration front with the highest growth rate (i.e. the slurry front). The position of the slurry front can therefore be calculated as:

$$\frac{\partial h}{\partial t} \mid_{slurry} = \frac{\partial F}{\partial c} \mid_{c_I} + c_I w_s = w_{s0}(c_I b - (1 - c_I)^2)(1 - c_I)^{b-1} \tag{28}$$

where c_I is the concentration at the inflection point of the flux curve. In case of coarser grains with smaller b values the point of inflection migrates forward and eventually falls after the packing limit (bed concentration). In this situation

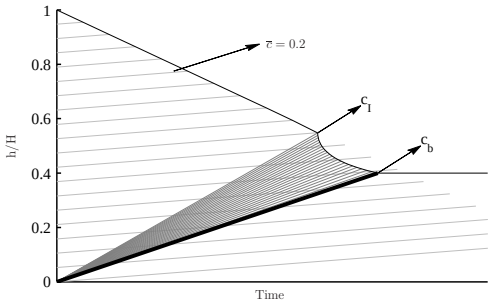

FIG. 17: Lines of characteristic for suspension of fine sand with $b = 4.5$ and $\overline{c} = 20\%$

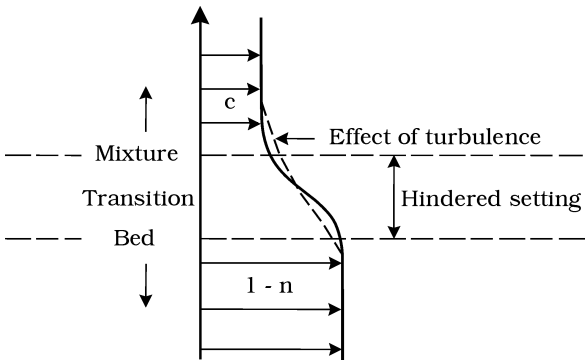

FIG. 18: Effect of turbulence on the shape of slurry layer

the bed front has the highest growth rate and does not allow formation of any other layers in between the mixture and the bed, resulting in a sharp interface between the bed and the mixture above it with no slurry layers.

The over/under-estimation of the bed rise velocity by equation 24 or the lower order version of it (equation 29), due to the presence of the slurry layer, are demonstrated in figure 19.

$$\frac{\partial h_b}{\partial t} = \frac{\overline{c} w_s}{1 - n} \tag{29}$$

In the mixture model however, the formation and changes in the slurry layer are taken into account implicitly. It should be noted that on top of the hindrance mechanisms which affect the behaviour of the slurry layer, the turbulent eddies may also play a role in expansion or compression of the slurry layer (figure 18). In hopper environment however, due to pronounced damping of the turbulent eddies, the effect from the turbulent diffusion on the slurry layer can be ignored.

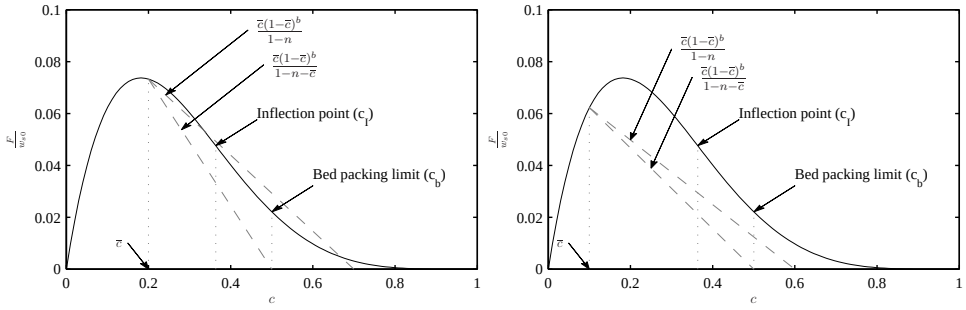

(a) $\overline{c} = 20\%$ (b) $\overline{c} = 10\%$

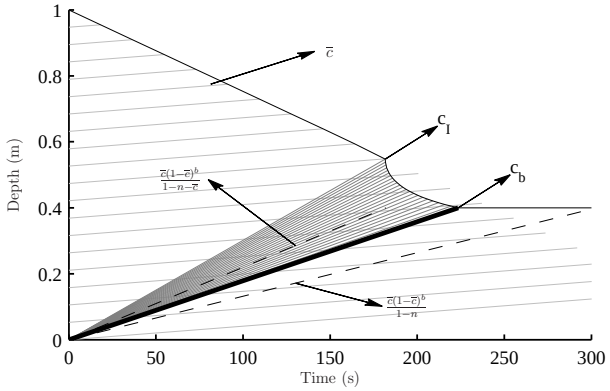

(c) $\overline{c} = 20\%$

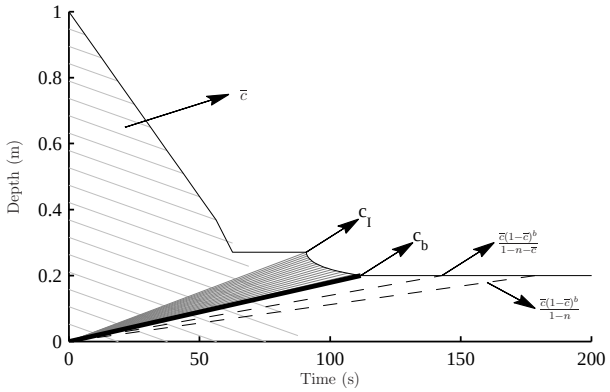

(d) $\overline{c} = 10\%$

FIG. 19: The flux curves and the concentration fronts of settling suspensions with 10% and 20% concentrations. In (a) and (b) the slopes corresponding to equations 24 and 29 are presented as well.

ACKNOWLEDGMENTS

The support of the Danish Ministry of Science, Technology, and Innovation through the Godkendt Teknologisk Service (GTS) grant Marine Structures of the Future is acknowledged.

REFERENCES

Bagnold, R. (1954). "Experiments on a gravity-free dispersion of large solid spheres in a newtonian fluid under shear." *Proceedings of the Royal Society A: Mathematical, Physical and Engineering Sciences*, 225.

Batchelor, G. (1982). "Sedimentation in a dilute polydisperse system of interacting spheres. Part 1. General theory." *Journal of Fluid Mechanics*, 119.

Braaksma, J. (2008). "Model-based control of hopper dredgers." Ph.D. thesis, Ph.D. thesis.

Braaksma, J., Babuska, R., Klaassens, J., and De Keizer, C. (2007). "A computationally efficient model for predicting overflow mixture density in a hopper dredger." *Terra et Aqua*, 106(106), 16.

Brennan, D. (2001). "The Numerical Simulation of Two-Phase Flows in Settling Tanks." Ph.D. thesis, Imperial College of Science, technology and medicine, Imperial College of Science, technology and medicine.

Camp, T. (1946). "Sedimentation and the design of settling tanks." *Trans. ASCE*.

Dyer, K. (1986). *Coastal and stuarine sediment dynamics*. Jouhn Wiley, New York, NY.

Einstein, A. (1906). "A new determination of molecular dimensions." *Ann. Phys*, 19(2), 289–306.

Engelund, F. (1953). "On the laminar and turbulent flows of ground water through homogeneous sand." *Transactions of the Danish academy of Technical sciences*, 3.

Felice, R. D. (1995). "Hydrodynamics of liquid fluidisation." *Chemical Engineering Science*, 50.

Garside, J. and Al-Dibouni, M. (1977). "Velocity-voidage relationships for fluidization and sedimentation in solid-liquid systems." *Industrial & engineering chemistry ...*.

Ishii, M. (2006). *Thermo-Fluid Dynamics of Two-Phase Flow*. Springer US, Boston, MA.

Jensen, J. and Saremi, S. (2014). "Overflow Concentration and Sedimentation in Hoppers." *Journal of Waterway, Port, Coastal, and Ocean Engineering*.

Koning, J. (1977). "Constant Tannage Loading of Trailing Suction Hopper Dredgers.

Kynch, G. (1952). "A theory of sedimentation." *Transactions of the Faraday society*.

Miedema, S. (2009). "A sensitivity analysis of the scaling of TSHD's." *WEDA XXIX & Texas A&M*, 40, 14–17.

Ooijens, S. C. (1999). "Adding dynamics to the camp model for the calculation of overflow losses." *Terra et Aqua*, (76), 12–21.

Rhee, C. V. (2002). "On the sedimentation process in a trailing suction hopper dredger." Ph.D. thesis, Ph.D. thesis.

Roscoe, R. (1952). "The viscosity of suspensions of rigid spheres." *British Journal of Applied Physics*, 3, 267.

Scott, K. J. (1984). "Hindered settling of a suspension of spheres." *Report no.*, Council for Scientific and Industrial Research, Pretoria, South Africa.

Thompson, C., Amos, C., Angelaki, M., Jones, T., and Binks, C. (2006). "An evaluation of bed shear stress under turbid flows." *Journal of Geophysical Research: Oceans (1978–2012)*, 111(C4).

Thomsen, L. and Gust, G. (2000). "Sediment erosion thresholds and characteristics of resuspended aggregates on the western european continental margin." *Deep Sea Research Part I: Oceanographic Research Papers*, 47(10), 1881 – 1897.

Vlasblom, W. and Miedema, S. (1995). "A Theory for Determining Sedimentation and Overflow Losses in Hoppers." *Proc. WODCON IV, November*.

CHAPTER 4

DETAILED MODELLING AND ANALYSIS OF NEARFIELD BEHAVIOUR OF THE OVERFLOW AND DISPOSAL PLUMES

In preparation as:
Saremi, S. and Jensen, J. H., (2014). Detailed modelling and analysis of nearfield behaviour of the overflow and disposal plumes. To be submitted.

DETAILED MODELLING AND ANALYSIS OF NEARFIELD BEHAVIOUR OF THE OVERFLOW AND DISPOSAL PLUMES

Sina Saremi and Jacob Hjelmager Jensen

ABSTRACT

The spillage of the highly concentrated sediment mixtures during dredging operations can result in creation of the turbidity plumes with negative impacts on the marine environment. The spatial and temporal extend of the overflow plumes is affected by the nearfield processes. A 3 dimensional two-phase mixture method has been used to model the detailed processes involved in nearfield entrainment, dilution and settling of the turbidity plumes. In order to resolve the entrainment and dilution mechanisms, the Large Eddy Simulation (LES) method has been implemented to directly solve the major flow structures and eddies responsible for the interactions between the mixture and the ambient fluid. The model is verified successfully with experiments and has been used to study the effects of governing parameters on the plumes behaviour, being in density driven or the mixing regime. The main parameters are the densimetric Froude number at the discharge point below the overflow pipe, velocity ratio between the overflow jet and the ambient current, and the water depth. The results from the CFD model have shown that presence of the dredgers propeller in the vicinity of the overflow plume increases the mixing rate, drags the plume towards the surface and retards its settling rate. The overflow material naturally compose of variety of sediment fractions which in average are finer/lighter than the parent material being dredged from the seabed, because the coarser/heavier grains settle inside the hopper and the remaining fine material flow overboard. The results from the polydisperse model show that the dispersity in size and weight of the mixture constituents affects the fate of overflow plumes, due to dynamic and kinematic interaction between the fractions. The numerical model is a perfect tool for conducting a parametrized study on the nearfield behaviour of the plume, which then provides boundary conditions for the larger scale farfield dispersion models.

Keywords: Overflow, particle clouds, dredging, turbidity plume, two-phase modelling, dumping, disposal, density currents .

INTRODUCTION

The environmental impact assessment (EIA) studies are important part of the coastal and offshore projects which involve dredging operations such as navigational channels maintenance, land reclamation, sand mining, offshore constructions and replacement of contaminated material. The formation of the turbidity plumes due to the spillage of fine sediments and the burial of the benthic marine life due to disposal of dredged material are among the most critical environmental impacts from dredging activities. The turbidity plumes are mainly caused by the overflow spill from the hoppers. The forward movement of the hopper (in the Trailing Suction Hopper Dredgers), presence of the local currents and few other factors cause the overflowing mixture to be exposed to further mixing and therefore can form a surface turbidity plume. The excess turbidity due to the overflow plume, if exceeds the background natural turbidity, can be harmful to the marine and benthic life. Depending on the material characteristics and the local conditions it can take from few minutes (coarser metrical) to few weeks (very fine material) for the overflow plumes to disperse, settle down and eventually disappear from the water column. This implies that good understanding of the key parameters influencing the plumes behaviour can to a great extend help reducing their possible adverse effects.

The sediment plumes in dredging activities can be divided into two types: i)the overflow plumes and ii) the disposal plumes.

The overflow mixture discharged into the open water during the dredging can be characterized as a buoyant jet entering the ambient water with downward velocity W (the momentum source of the overflow plume). One of the main parameters describing the nature of the overflow discharge, at the instance of entering the ambient water, is the non-dimensional densimetric Froude number F_d. Its the ratio between the inertial and buoyancy forces and can be considered as a measure of how buoyant the overflow plume is in beginning.

$$F_d = \frac{W}{\sqrt{gd\frac{\rho_m - \rho_w}{\rho w}}} \tag{1}$$

where d is diameter of the intruding buoyant jet into the open water (overflow pipe diameter), ρ_m is the overflow mixture density, ρ_w is the clear water density and g is the gravitational acceleration. The ambient water being stagnant, the densimetric Froude number can be a measure to indicate if the mixture entering the water is in a density driven regime ($F_d < 1$), where the plume settles towards the bed due to its negative buoyancy with the least diffusion and mixing in the water, or it is in a mixing regime ($F_d > 1$), where due to high levels of entrainment and dilution, the plume is dispersed into the water and lasts longer in suspension. The presence of the local currents or the trailing speed of the hopper, act as another governing parameter in determining the behaviour of the overflow plumes. The effect of ambient currents is presented by the non-dimensional velocity ratio ϵ, which is the ratio between the mean cross flow velocity (U) and the downward

velocity of the buoyant jet entering the open water (W).

$$\epsilon = \frac{U}{W} \tag{2}$$

The translation and shear dispersion caused by the ambient currents enhances the mixing and dilution mechanisms during the plumes fall. Higher the value of ϵ becomes, the overflow mixture will be mixed and translated further. Combination of high ϵ values and $F_d > 1$ results in fully mixed overflow plumes which can easily form surface turbidity plumes.

The second type of the plumes in dredging operations are the disposal plumes. The release of the dredged material in a quasi-instantaneous manner in open water, which happens at the relocation sites (e.g. from the split hoppers), acts as a (negative) buoyant plume forming a particle cloud. The behaviour of the released material can be divided into four distinct phases: 1) convective descent, 2) dynamic collapse, 3) density current over the bed and 4) passive diffusion. During the descent, the high entrainment rate due to the shear, density gradients (concentrations are much higher than overflow mixtures) and lack of momentum source incorporate the mixture in a spherical (ring) vortex resembling an upside down mushroom, which falls faster than the individual grains velocity. Provided with sufficient time (sufficient depth), the expansion and dilution of the plume reaches a point where the plume enters the dispersive phase and particles begin to rain out of the cloud. In this case the collapsing stage and formation of density currents over the bed do not exist. The minimum depth (the fallout height) depends on the plumes initial density and the fall velocity of the individual grains.

The water depth is another local parameter influencing the fate of the sediment plumes. Under calm water conditions ($\epsilon = 0$), deeper the water becomes, the entrainment processes have more time and further dilute the plume before collapsing into the bed. In $\epsilon > 0$, deeper the water becomes, the plume undergoes further translation and dispersion over the depth. If the water is deep enough, the plume reaches to a level of dilution where it doesn't act as a uniform mixture and the individual particles begin to fall out with their own fall velocities (Bush et al. 2003). Coarse grains, due to their high fall velocities, rain out of the plume soon, but in case of fine material this happens in very late stages of the plumes dispersion which is not of importance in nearfield studies.

Marine dredging operations most often take place under calm sea conditions where extreme wave events don't exist. Therefore the effect of the waves on the plumes behaviour is limited to the helical displacements beneath the crests and troughs and the net effect of this motion on the overall descend and dispersion of the plume is negligible.

The computational fluid dynamics (CFD) tools are extensively being used to model the far field plumes excursions. However, these models lack the well-resolved nearfield modelling of the plume source, which significantly affects the farfield behaviour of it. In the context of dredging, due to high levels of the solid concentrations in the mixture, the solution requires full coupling of the

two contributing phases of water and sediment to capture the detailed processes involved in nearfield behaviour of the plumes.

PREVIOUS WORKS

Settling behaviour of sediments released into water recently has become subject of extensive studies both experimentally and numerically. The experimental works can be divided into two groups; the physical models of overflowing mixture (under currents and calm water conditions) and the experimental studies of material release into ambient water (dumping) as negatively buoyant particle clouds. Winterwerp (2002) presented the experimental results of the nearfield behaviour of dredging spill in shallow waters, where the behaviour of the laboratory scale overflow plumes was observed and categorized into three different regimes based on the Richardson number ($R = \frac{1}{F_d^2}$) and the velocity ratio (ϵ): density driven, mixing and transitional. Decrop et al. (2013) also did similar sets of experiments, measuring the path of overflow plumes under ambient currents. The majority of existing experimental work however is focused on the material release (disposal) and particle clouds. Jiang et al. (1997) conducted laboratory scale disposal experiments, observing the radial expansion of the density driven turbidity current over the bed and measuring the concentrations and velocities close to the collapsing point of the released material. Similar exercise (under still water conditions) were carried out by Boutin (2000) and Burel and Garapon (2002).Ruggaber (2000) did cmprehensive set of laboratory experiments on particle clouds and Bush et al. (2003) did series experiments of negatively buoyant particles released into ambient water and developed equations for predicting the bulk parameters of the plume such as plumes falling speed, width and density. Gensheimer et al. (2013) studied the behaviour of the released plumes under ambient currents, measuring the effect of the current on the plumes landing position. Zhao et al. (2012) studied the effects of regular surface waves on the descent of instantaneously released sediments. Their results show that the motion of the plumes centroid and the growth rate of the descending plume are not affected by the waves.

The numerical methods can be divided into two groups of Eulerian and Lagrangian approaches, where the later has its computational limitations. Oda and Shigematsu (1994), Gotoh and Fredsøe (2000) and Shakibaeinia and Jin (2012) modelled the sediment release in still water by the Lagrangian approach and showed acceptable results comparing with experiments. Jiang et al. (1997) used an Eulerian single phase model corrected with the Bousinesqe approximation to reproduce their experimental results. Their model though, was not able to capture the detailed entrainment processes. This is due to disregarding of the volume occupancy and momentum exchange of sediments which has considerable effects through the fulfilment of the continuity equation and dynamics of the plume in high concentrations. As a result, the single-phase models with the Boussinesq approximation typically fail to capture and resolve detailed aspects of the plume evolution such as the creation of vortex rings, meandering behaviour

of the plume during the descent and the characteristic double peak observed in the concentration. These shortcomings compromise the use of two-phase models in plumes modelling. Nguyen et al. (2012) illustrated the mentioned shortcomings of the models using the passive (Bousinesq approximation) approach. They used the two phase numerical model developed by Drew and Lahey (1993) which solves the mass and momentum conservation equations for each phase separately. The turbulent stresses were modelled by Reynolds Averaging method and sophisticated closures were implemented for inter phase momentum transfer terms. However, their model (possibly due to the turbulence modelling) failed to resolve the instabilities produced by the entrainment mechanisms during the descending stage, which resulted in less accurate representation of the plume evolution, particularly the dilution. De Wit (2010) used a three dimensional numerical model based on the mixture approach and LES (Large Eddy Simulation) method for resolving the turbulent eddies to model the overflow plumes. He investigated the effect of water depth on the experimental results of Winterwerp (2002). Burel and Garapon (2002) also developed a numerical model to reproduce their experiments. Their model was based on single phase passive solution therefore was not able to represent the descending plume well.

PRESENT WORK

In the present work the near field behaviour of the overflow plumes and the instantaneous release of dredged material has been studied by the means of two-phase mixture modelling (Ishii 2006) which takes into account the coupling between the two phases (water and sediment) both in terms of dynamic and occupancy interactions. Details of the interactions between the entraining eddies and the density driven mixture is captured by postulation of the Large Eddy Simulation (LES) method. The performance of the model has been verified by the data from two type of laboratory scale experiments; Overflow from the hopper under both calm water and currents (Winterwerp 2002) and the instantaneous disposal of highly concentrated mixture from a container (Burel and Garapon 2002). Thereafter the effect of key parameters in determining the plumes behaviour (F_d, ϵ and depth) has been investigated by the model. In addition to the mentioned factors, there exists few other processes such as the air entrainment at the overflow pipe and the effect of the dredger's propeller which may also affect the plumes behaviour. In the present work the presence of the the dredger's propeller has been modelled in a simple way to investigate the possible effects of it. The seabed material poses great deal of variability in size, type and porosity. The material which flow overboard the hopper has quite a different characteristics in compare to what is being fed into the hopper. Great portion of the coarse and heavier grains settle immediately in the hopper and the overflow mixture consists mostly of finer fractions of the distribution curve of the inflow material. Therefore the numerical model has been used to investigate the effect of particles size variations on the plumes behaviour, which also elucidates the possible error in the farfield dispersion models if using the seabed material as a source for the

plume.

MODEL DESCRIPTION

The high levels of sediment concentration in the overflow and disposal plumes indicates significant dynamic and occupancy interactions in between the two phases which requires a two-way coupled solution. The application of the so called "Boussinesq" approximation, which approximates the effects of the heavier dispersing phase only to that of the excess gravitational force on the flow, is insufficient. Including the displacement effects of falling sediments in the continuity equation and the inclusion of density gradients in the momentum equations are necessary for detailed calculation of the displacement effects and the excess momentum transfer due to the falling particles in the fluid.

The mixture method (Ishii 2006) is used to model the near field behaviour of the turbidity plumes. Its advantage to the fully two-phase models is in reduced computational costs and complexity (due to the difficulties in resolving the interfaces between the two phases). The method solves the equations of conservation of mass and momentum for the mixture as a whole, by simply adding the conservation equations of each phase. The mixture parameters are defined at the center of mass of the total material due to the fact that quantities such as volume, momentum and energy are additive set functions of the mass. The density of the mixture ρ_m is defined as the volume averaged density of the two phases (Eq. 3).

$$\rho_m = c\rho_s + (1-c)\rho_w \tag{3}$$

where c is the volumetric concentration of the dispersed phase (sediment) and ρ_s and ρ_w are the densities of sediment and water respectively. The equations of the conservation of mass and momentum for the mixture are as follows (Eq. 4 & Eq. 5).

$$\frac{\partial \rho_m}{\partial t} + \nabla.(\rho_m \overrightarrow{U}_m) = 0 \tag{4}$$

$$\frac{\partial \rho_m \overrightarrow{U}_m}{\partial t} + \nabla.(\rho_m \overrightarrow{U}_m \overrightarrow{U}_m) = -\nabla P_m + \nabla.(\tau_m + {\tau_m}^t + {\tau_m}^D) + \rho_m \overrightarrow{g} \tag{5}$$

The pressure inside the mixture P_m is assumed to be continuous and to act equally on both phases. The viscous shear stress in the mixture τ_m is function of mixture velocity gradients and the mixture viscosity μ_m(Eq. 6).

$$\tau_m = \mu_m S = \mu_m \frac{1}{2}(\nabla \overrightarrow{U}_m + \nabla^T \overrightarrow{U}_m) \tag{6}$$

$$\mu_m = \mu_w (1-c)^{-2.5} \tag{7}$$

where S is the stress tensor, and T is the matrix transpose operator. The viscosity of the mixture is defined based on the concept of apparent viscosity

initially introduced by Einstein (1906) for dilute suspensions. The expression developed by Roscoe (1952) which counts for high concentration mixtures (Eq. 7) is used in the present work, where μ_w is the viscosity of clear water. U_m is the velocity of the mixture which should be considered as an averaged representation of the velocities of the two phases due to relative slip velocities in between them. The deviation from the mixture velocity for each phase can be defined as the relative velocity of that phase in respect to the mixture (Eq. 8).

$$\overrightarrow{U}_{sm} = \overrightarrow{U}_{s} - \overrightarrow{U}_{m} \tag{8a}$$

$$\overrightarrow{U}_{wm} = \overrightarrow{U}_{w} - \overrightarrow{U}_{m} \tag{8b}$$

where $\overrightarrow{U_s}$ and $\overrightarrow{U_w}$ are the velocities of the sediment and water phases respectively. ${\tau_m}^t$ is the turbulent shear stress and ${\tau_m}^D$ is the mixture diffusion stress, which is the momentum transfer due to the relative velocities of the phases in respect to the mixture (Eq. 9).

$${\tau_m}^D = -\rho_m(\alpha \overrightarrow{U}_{sm} \overrightarrow{U}_{sm} + (1-\alpha)\overrightarrow{U}_{wm} \overrightarrow{U}_{wm}) \tag{9}$$

The transport equation for the dispersed phase is solved based on the mass-averaged concentration $\alpha = \frac{c\rho_s}{\rho_m}$ of sediments (Eq. 10).

$$\frac{\partial \alpha \rho_m}{\partial t} + \nabla.(\alpha \rho_m(\overrightarrow{U}_{m} + \overrightarrow{U}_{sm})) = \nabla^2(\alpha \mu_{SGS}) \tag{10}$$

where μ_{SGS} is the sub-grid scale (SGS) turbulent eddy viscosity (equation 13). The fall velocity of solid particles in water is defined as $w_s = w_0(1-c)^b$, where b is function of the grain size (Garside and Al-Dibouni 1977) and w_0 is the stokes fall velocity. The relative velocities of the sediment and water to the mixture ($\overrightarrow{U}_{sm}$ and $\overrightarrow{U}_{wm}$) are defined based on the continuity of volume and mass, as below.

$$U_{sm} = (1-\alpha)U_{slip} \tag{11a}$$

$$U_{wm} = -\alpha U_{slip} \tag{11b}$$

where $U_{slip} = w_0(1-c)^{b-1}$. The settling and dilution of sediment plumes is strongly dependant on the entrainment process and interactions between the particles and the turbulent eddies in the flow. This implies that fluctuations of both velocity and concentration play an important role in driving the plume. Therefore application of averaged turbulence models may not resolve all the features involved in evolve of the turbidity plumes. In present work the Large Eddy Simulation method (LES) has been implemented to take account for the turbulent fluctuations in the flow. The sub grid scales have been modelled based on the one equation kinetic energy method including the density variations in the mixture.

$$\frac{\partial \rho_m k}{\partial t} + \nabla.(\rho_m k \overrightarrow{U}_m) = \nabla^2(\mu_{eff} k) + 2\mu_{SGS}(S:S) - \rho_m \frac{C_e}{\Delta} k^{3/2} \qquad (12)$$

where the effective viscosity is defined as $\mu_{eff} = \mu_m + \mu_{SGS}$.The filter size Δ is chosen to be function of the cube root volume of the computational cells.

$$\mu_{SGS} = C_k \rho_m \sqrt{k} \Delta \qquad (13)$$

The constants C_e and C_k have the standard values of 1.084 and 0.094 respectively. The model described here is implemented in the open source CFD code OpenFOAM based on finite volume approach. The Navier-Stokes equations for the mixture are solved by the PISO (Pressure implicit with splitting of operator) algorithm followed by the solution of the transport equation for the dispersed phase.

MODEL VERIFICATION

The performance of the mixture solution in modelling the descend and dispersion of sediment plumes has been evaluated by simulating two sets of laboratory experiments. The first experiment which was done by Boot (2000) and later presented by Winterwerp (2002), is a laboratory scale hopper with an overflow pipe at its bottom. The setup was placed in a shallow laboratory flume. The purpose of the experiment was to observe the behaviour of the overflow plume during the dredging and after the termination of the overflow, in calm water and in the presence of cross currents. The scaling was done based on the Froude number, due to the fact that inertial forces are dominating. With an scale ratio of $\lambda = 100$, a $18000m^3$ hopper in $20m$ water depth was modelled as a $1.5 \times 0.425m$ hopper with $0.13m$ draught in a $0.33m$ deep laboratory flume. The overflow pipe had $0.025m$ diameter and the overflow flux lasted for 10 seconds. The overflow mixture had density of $\rho_m = 1033 \frac{kg}{m^3}$ and consists of fine grains with $D50 = 10\mu m$. The type of material being used was China Clay, which is up to 85% kaolinite and the cohesive behavior can be ignored in freshwater. The results of the experiment were reported as visual observations of the average radial expansion rate of the density current at the bottom of the flume after the plume reached the bed. It was not clarified by which concentration threshold the plume diameters were registered. Correlation between visual turbidity in water and the corresponding concentration depends on type of the material and the local conditions. Thackston and Palermo (1998) presented the results of experiments correlating the turbidity (in Nephlometric Turbidity Units NTU) to the concentration (Total Suspended Solids TSS) for different sediment types. The visual turbidity is much less than $50NTU$ (Strausberg 1983) which according to the overall data of Thackston and Palermo it corresponds to TSS of about 100 to $500mg/L$. This roughly acquired concentration threshold ($300mg/L$ used in present work) has been considered for determining the plume diameter in the numerical model. Winterwerp (2002) characterized the experiments by two non-dimensional parameters, the velocity ratio (ϵ) and the Richardson number (R) which is simply the reciprocal of the

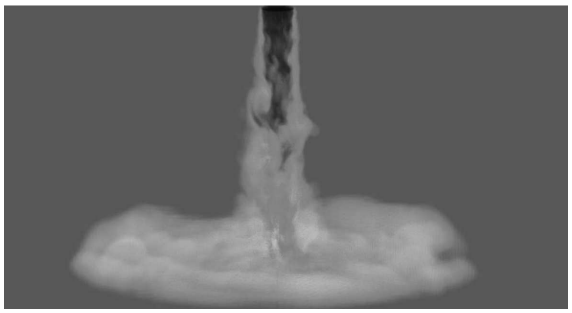

FIG. 1: 3D view of the volumetric concentration contours, $\epsilon = 0$ and $F_d = 2.2$. The contours have threshold of $300mg/L$.

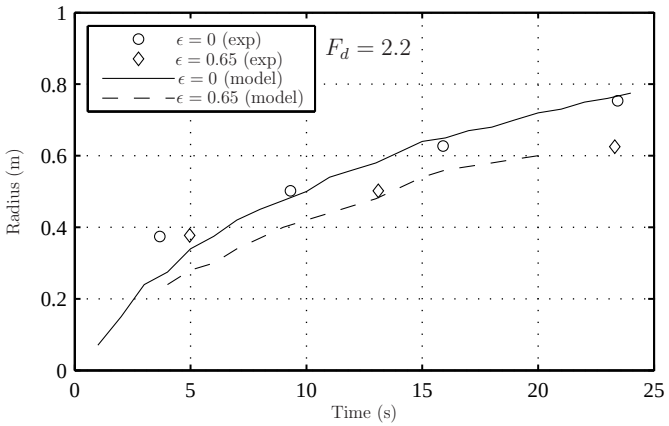

FIG. 2: Comparison between the experimental (Winterwerp, 2000) and numerical values of the plume radius

square of the densimetric Froude number. The experiments were done at different velocity ratios and Richardson numbers. Here the results for two test cases, with same Richardson numbers ($R = 0.2$) and different velocity ratios of $\epsilon = 0$ and $\epsilon = 0.65$ ($W = 0.2m/s$) have been compared with the simulation results from the numerical model. In figure 1 a 3D view of the concentration volume contours from the numerical model ($\epsilon = 0$) has been depicted. A cross section view of the descending plume under the influence of the cross flow ($\epsilon = 0.65$) has been demonstrated in figure 3 and a 3D view of the concentration volume countours are presented in figure 4. The numerical results for both the stagnant water and the case with cross flow show good agreement with the experimental data (figure 2).

The second experimental setup simulated by the numerical model is the material disposal case done by Burel and Garapon (2002). A cylindrical container

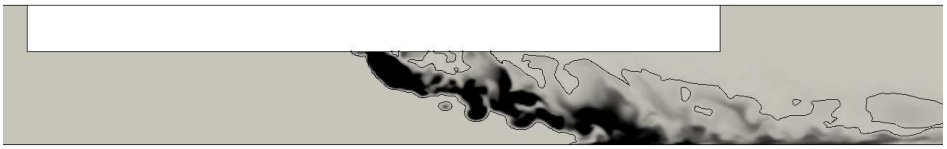

FIG. 3: Cross section view of the overflow plume under the hopper, $\epsilon = 0.65$ and $F_d = 2.2$

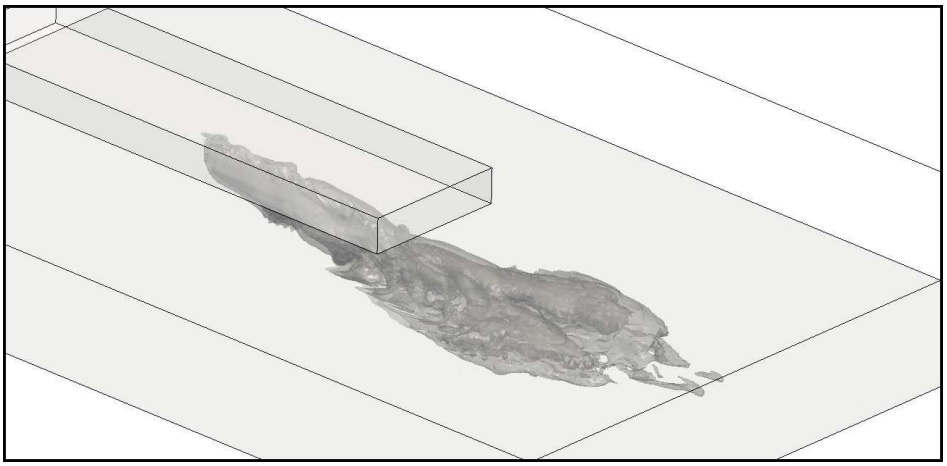

FIG. 4: 3D view of the volumetric concentration contours, $\epsilon = 0.65$ and $F_d = 2.2$

filled with mixture of sand and water was placed at the water surface in a laboratory flume. The opening of the container was at its bottom and submerged. The flume which the testing facilities were mounted on, had a length of $80m$ and width of $1.5m$. The cylindrical container was $172mm$ wide and $200mm$ long, filled with a mixture of $200g/L$. The material used in their experiment had a grain diameter of $90\mu m$ and the density of $2650\frac{Kg}{m^3}$. The purpose of the experiment was to observe the descending and entrainment processes of the plume after its instantaneous release and the propagation of the density current at the bottom. The behaviour of the plume was reported by visual measurements of the plume diameter with a specified concentration threshold of $5g/L$. In general the release of the mixture into water does not happen from a completely at rest situation due to the disturbances from the opening devices. The numerical results also are sensitive enough to the way the release process is modelled. In present work the opening of the container is modelled as a finite varying (reducing) flux boundary condition. The rate of the incoming material is calculated based on the total mass inside, the height and the area of the container. The entrainment of sur-

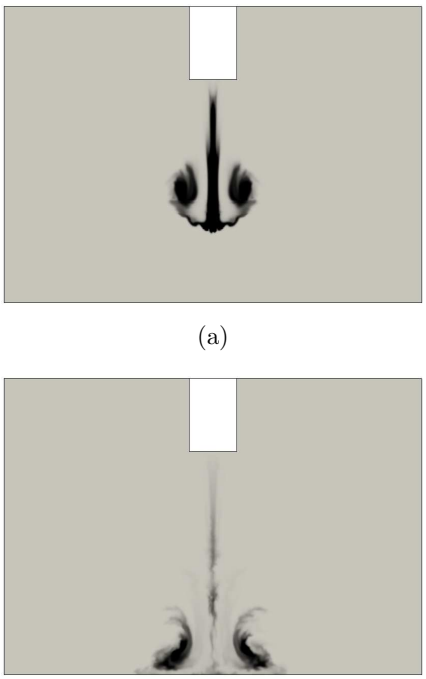

(a)

(b)

FIG. 5: Cross-section of the descending plume before (a) and after (b) the collapse

rounding fluid into the released mixture and formation of a mushroom like plume due to the vortex rings before reaching the bottom is a characteristic behaviour which has been captured well by the numerical model. In figure 6 a cross section view of the descending plume at the midway before collapsing into the bed is demonstrated. The formation of the vortex ring surrounding the plume is visible in this figure. Figure **??** is a 3D demonstration of the simulation results.

In figure 7 the computed and measured plume diameters have been compared together which shows good agreement. The results present the initial stage where the plume expands due to entrainment of surrounding fluid, then there is the collapsing stage where the diameter remains almost constant, and finally the spreading of the mixture as a density current at the bottom. The model resolves the behaviour of the plume perfectly during the descend and the collapsing stage, but overestimates the spreading velocity over the bed. This might be due to the fact that at this stage the combination of high concentrations and the high velocity gradients over the bed results in enhanced particle collisions and therefore the inertial rheological regime dominates. The collisional interaction between the particles and the dissipation due to them is not included in the present model.

Including the density variations and both the dynamic and occupancy cou-

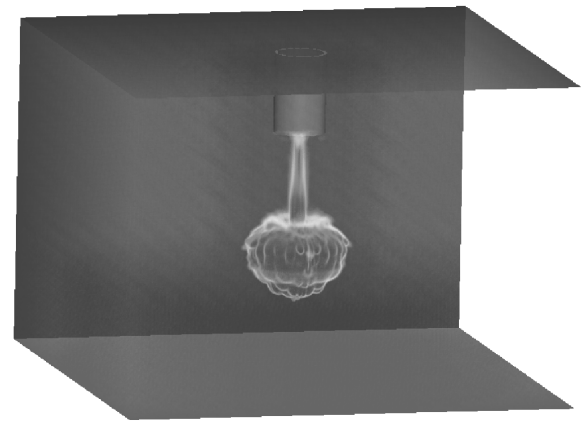

(a)

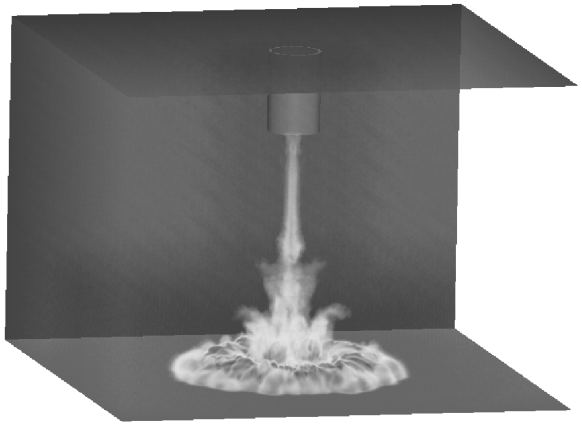

(b)

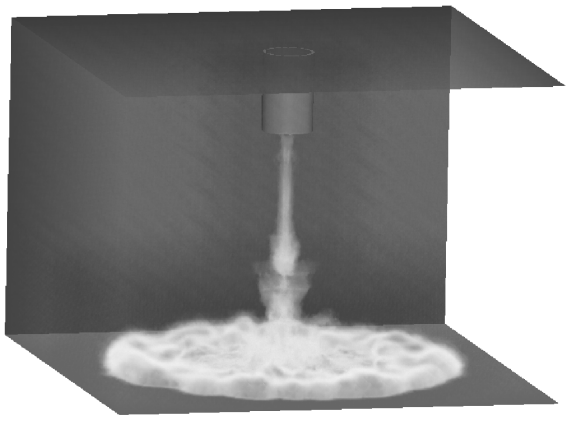

(c)

FIG. 6: 3D view of the volumetric concentration contours of the CFD modelling of material disposal

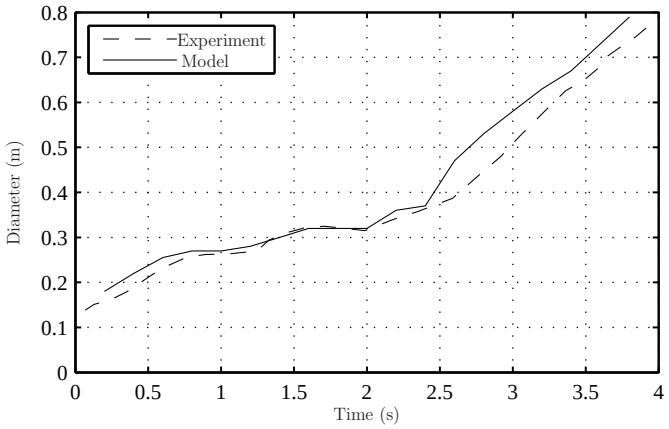

FIG. 7: Comparison between the experimental (Burel and Garapon, 2000) and numerical values of the plume radius

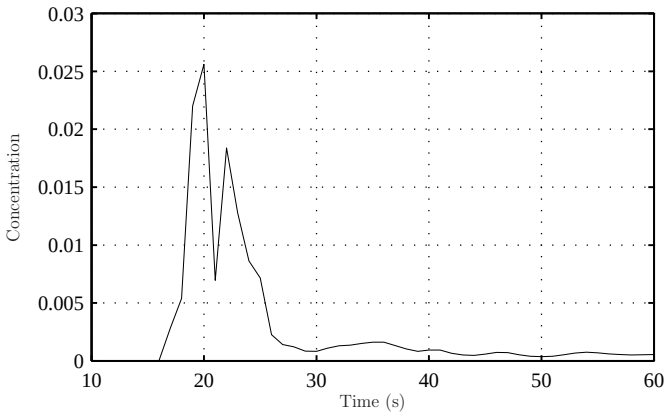

FIG. 8: Time-series of the concentration at a probing point in radial distance of $0.09m$ from the collapsing point and $0.063m$ above the bed.

pling between the two phases has enabled the model to capture the detailed entraining mechanisms which drive the plume. The induced flow field due to the entraining vortex ring at the time of collapse interacts with the initial spreading of the density current over the bed and results in the occurrence of a double peak in concentration time series close to the collapsing point. This feature could not be resolved in numerical models based on the Bousinesq approximation (Jiang et al. 1997), but was captured in the Lagrangian models (Gotoh and Fredsøe 2000). In figure 8 the concentration time series at $r = 0.09m$ from the point of collapse has been shown where the formation of the double concentration peak is clearly visible.

APPLICATION OF THE MODEL

The near field behaviour of the overflow plumes affects their later far field mode. The two main parameters which distinguish the state of the overflow plumes between buoyancy dominated and mixing dominated, are the densimetricc Froude number (F_d) at the point of release and the velocity ratio (ϵ). In addition to these two main parameters, the water depth and other external elements such as the dredgers propeller also have impacts on nearfield behaviour of the plumes. In order to study the effect of the mentioned parameters on the settling and dispersive behaviour of the overflow plumes, a down scaled model ($\lambda = 100$) corresponding to a $18000m^3$ TSHD at $20m$ water depth and a single overflow pipe with diameter of $2.5m$ has been modelled as a $1.5 \times 0.425m$ hopper with $0.13m$ draught in a $0.33m$ depth under different conditions and the results are presented in terms of the position of the centroid of the plume during the overflow and after the termination point when there is no discharge of sediment from the overflow pipe. The overflow mixture in the simulations has density of $\rho_m = 1033\frac{kg}{m^3}$ and consists of fine grains with $D50 = 10\mu m$.

Velocity ratio (ϵ) and densimetric Froude number (F_d)

The behaviour of the overflow plume under different velocity ratios has been studied by simulating the down-scaled model at $F_d = 2.2$. The flux of sediment/water mixture from the overflow pipe has been kept constant while different cross current velocities have been applied. Figure 9 presents the position of the centroid of the plume under different cross flow velocities,where both the horizontal and vertical distances have been normalized by the overflow pipe diameter (d). At higher velocity ratios the plume is distracted earlier and the settling rate is reduced, whereas at smaller velocity ratios, the plumes reaction to the cross flow is weaker. The centroid of the overflow plume reaches an equilibrium position as long as the source (the discharge from the hopper) is maintained. As soon as the discharge is stopped (corresponding to the termination of dredging), the plume's behaviour is then determined by the dominant regime (either mixing or buoyant) and it's centroid will either fall down or keeps on remaining in suspension until the plume is diluted and dispersed away. This can be seen in figure 10 , where the vertical and horizontal position of the plumes centroid is plotted in time.

The other characteristic parameter which describes the state and the behaviour of the plume, is the densimetric Froud number, F_d. The densimetric Froude number is function of the density of the mixture being overflowed and the flow rate of which it enters the ambient water. The latter is less variable, because it strongly depends on the dimensions of the overflow pipe and the rate which the hopper is being filled. The density of the overflow mixture however is direct function of the overflow concentration, which is more variable based on the type of material being dredged. To investigate the effect of the Froude number on the behaviour of the plumes, three different cases, with the same inflowing velocities, but different concentrations have been simulated. In figure 11 the horizontal and

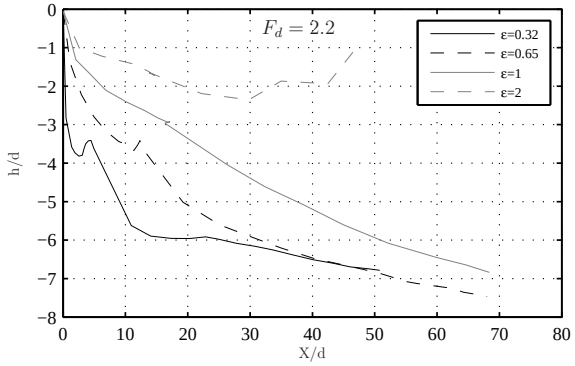

FIG. 9: Path of the centroid of the plume, at different ϵ values with same F_d

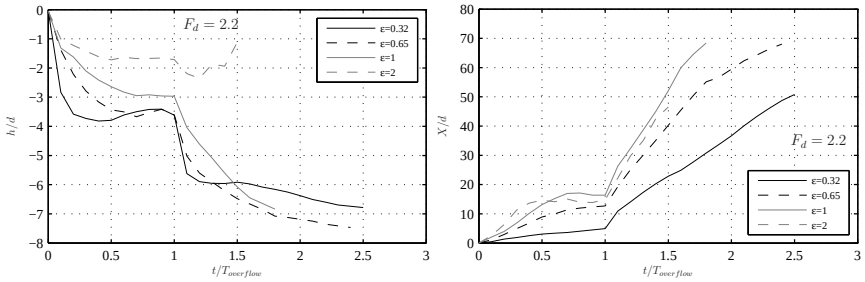

(a) (b)

FIG. 10: Time-series of the vertical (a) and horizontal (b) position of the centroid of the plume,normalized with the overflow pipe diameter d. $T_{overflow}$ represents the time when the overflow discharge stops.

vertical position of the centroid of the plume has been plotted. In the presence of cross currents, densimetric Froude numbers less than unity represent the dominance of buoyancy forces, which causes the plume to settle soon. On the other hand, higher values of F_d indicates a mixing driven plume which remains in water column until complete dilution of the plume. In figure 12b, the horizontal extend of the plumes are plotted against time. It shows the plumes with lower Froude numbers have higher expansion rates. This is merely due to the strong density currents created on the bed in cases with small F_d, because of higher concentrations and faster reaching the bed before any dissipation of the momentum (as can be seen in figure 12a).

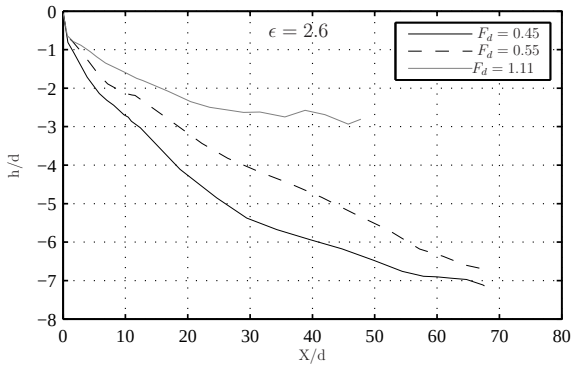

FIG. 11: Horizontal and vertical position of the centroid of the plume, at different F_d values with same ϵ.

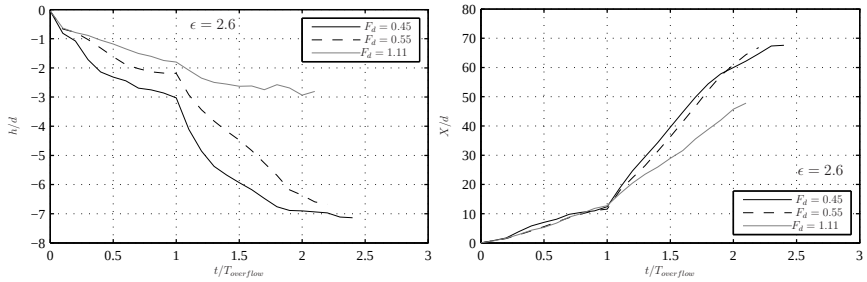

(a) (b)

FIG. 12: Time-series of the vertical (a) and horizontal (b) position of the centroid of the plume,normalized with the overflow pipe diameter d. $T_{overflow}$ represents the time when the overflow discharge stops

Water depth

The effect of the water depth on plumes behaviour can be seen as the time available for either the overflow plume (as a buoyant jet) or the disposal material (as a buoyant plume) to undergo further entrainment and dilution. The effect of the water depth on the settling and dispersion rate of the overflow plumes have been investigated under two different conditions of $\epsilon = 0$ (stagnant water) and $\epsilon > 0$ (presence of cross flow). Under calm water conditions, the buoyant jet of the overflow mixture penetrates directly towards the bed. After the collapsing stage it begins to expand radially over the bed as a density current. Deeper the water becomes, the jet has more time to dilute and disperse out due to entrainment processes, occurrence of the instabilities and the meandering effects. Further dilution of the plume at the time it reaches the bed, alleviates the collapsing stage and results in weaker density currents spreading over the bed. In figure 13

(a) $D/d = 8$

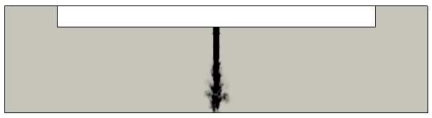

(b) $D/d = 16$

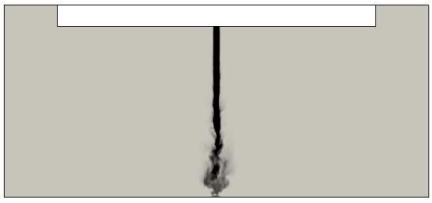

(c) $D/d = 32$

(d) $D/d = 64$

FIG. 13: Overflow buoyant jet under calm water condition ($\epsilon = 0$, $F_d = 2.2$), in different depths

the overflow jet under calm water conditions has been depicted at the moment of collapse in four different water depths. It can be seen, deeper the water becomes, the mixture undergoes further dilution.

In the presence of cross currents, the effect of the velocity ratio (ϵ) becomes important. Depending on the magnitude of ϵ, the centroid of the overflow plume reaches an equilibrium position as long as the overflow flux is retained. At $\epsilon < 1$

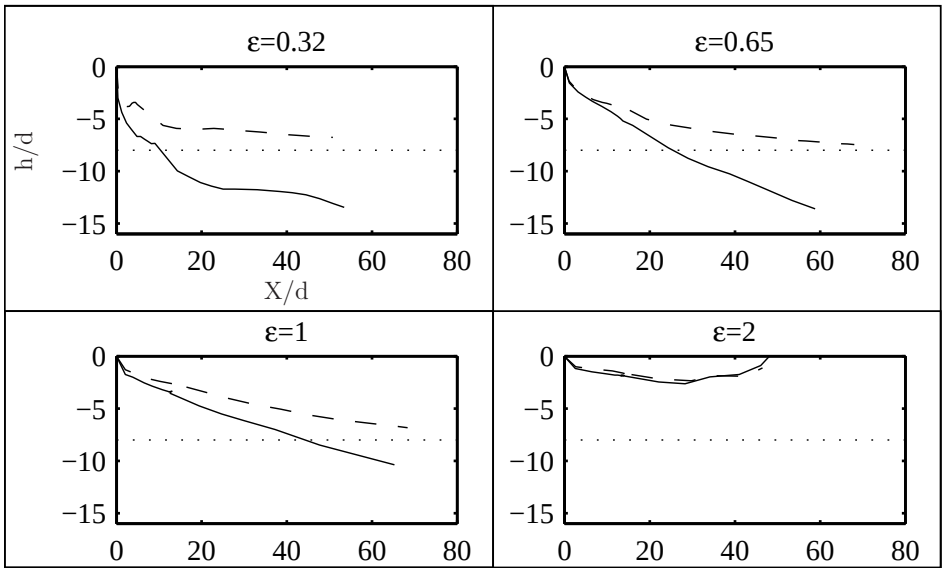

FIG. 14: Horizontal and vertical path of the plume centroid at two water depths, $D/d = 8$ (dashed line) and $D/d = 16$ (solid line). The dotted line represents the position of the bed in the shallow case. $F_d = 2.2$

because the buoyancy is dominating, the descent of the plume follows the available water depth. However, at $\epsilon \geq 1$ the behaviour of the plume begins to ignore the depth, and no matter how far below the bed is, the centroid of the plume follows the same path. In figure 14 the path of the centroid of the overflow plume (normalized with the overflow pipe diameter d) is plotted for two different water depths, $D/d = 8$ and $D/d = 16$. It can be seen that the water depth has no effect on the horizontal spreading of the plume, whether its in density driven regime ($\epsilon = 0.32$) or in fully mixing regime ($\epsilon = 2$). This has been shown more clearly in figure16. The vertical displacement of the plume however is affected by the water depth, depending on the magnitude of ϵ. In buoyancy dominated situations, the plume travels through the whole water depth and reaches the bed whereas in mixing dominated situations, the plume never feels the depth and remains close to the surface. In figure 15, where the time series of the plumes (centroid) vertical position is plotted, it can be clearly seen that by increasing the velocity ratio, the plumes behaviour eventually becomes independent of the water depth.

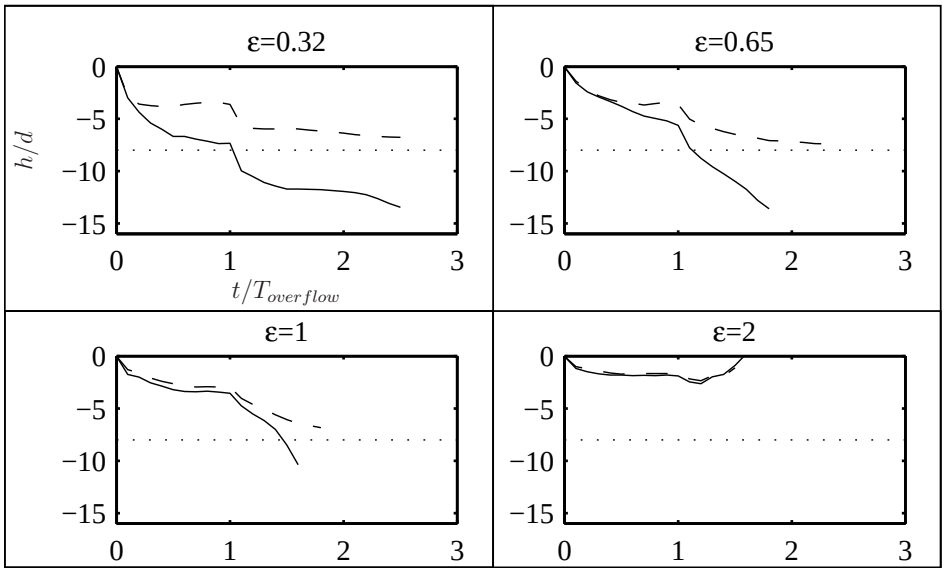

FIG. 15: Time series of the vertical position of the plume centroid at two water depths, $D/d = 8$ (dashed line) and $D/d = 16$ (solid line). The dotted line represents the position of the bed in the shallow case. $F_d = 2.2$

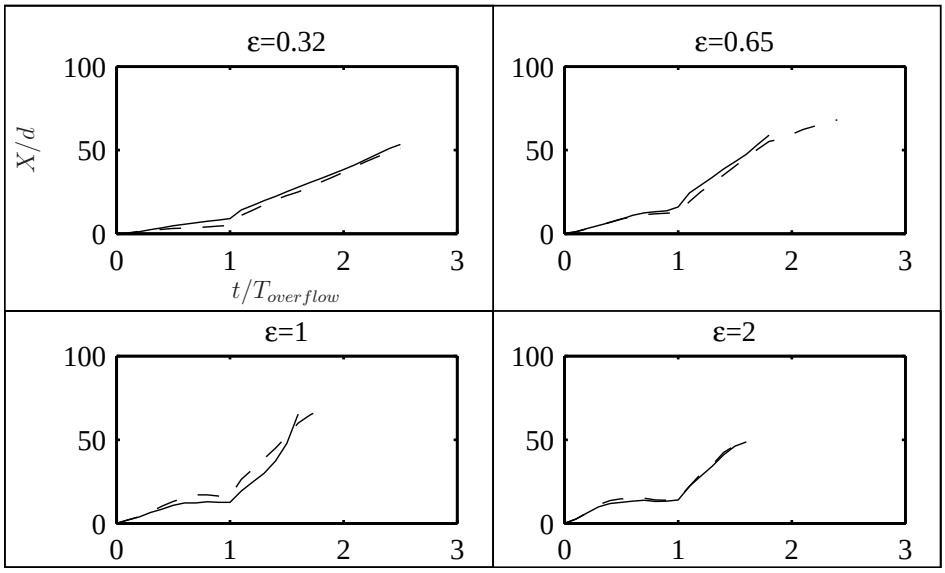

FIG. 16: Time series of the horizontal position of the plume centroid at two water depths, $D/d = 8$ (dashed line) and $D/d = 16$ (solid line). The dotted line represents the position of the bed in the shallow case. $F_d = 2.2$

Dredgers propeller

The overflow begins as soon as the hopper is filled with the dredged mixture and lasts till the end of the operation. The forward motion of the TSHD during dredging is similar to the situation where the overflow mixture is introduced to the ambient current. Movement of the dredger means continuously running propellers. The induced flow field due to the propellers and the wake behind them enhance the mixing process and drags the plume centroid closer to the surface.

Detailed modelling of the propellers requires significantly fine computational mesh and resolving the detailed geometry of the rotating blades. In the present work the goal is to investigate the significance of the propellers effect (if any) on dispersing plumes. Therefore a first order method has been used to model the effect of the propeller beneath the hopper. The actuator disc method (Sørensen and Shen 2002) has been implemented in the numerical model to account for the normal forces induced by the propeller on the water body. A typical jumbo trailer with capacity of $18000m^3$ has a pair of 4-bladed propellers with diameter of about $4.5m$. During the course of dredging the propeller speed is around $125RPM$. By applying the same scaling ratio as in previous section, the model propeller has a diameter of $0.045m$ and speed of $1250RPM$. The absolute advance ratio for such propeller with forward speed of $0.2m/s$ becomes $J = 0.068$ and according to the Kramer diagrams (Kramer 1939) the thrust and power coefficients become $C_T = 1.5$ and $C_P = 2.0$ respectively for 75% propeller efficiency.

The effect of the propeller has been investigated in two different situations; a buoyancy dominated and a mixing dominated case. The path of the plumes centroid is plotted in figure 17, where the propeller position (end bottom corner of the hopper) is at $\frac{X}{d} = 30$ and $\frac{h}{d} = 0$. The results show that the presence of the propeller causes the vertical position of the plume to be lifted slightly. In the mixing regime, the centroid of the plume is shifted directly towards the surface in the final diluting stages. The excess mixing due to the dredgers propeller drags the plume further towards the surface which in the mixing regime should be considered as a factor that enhances the surface turbidity.

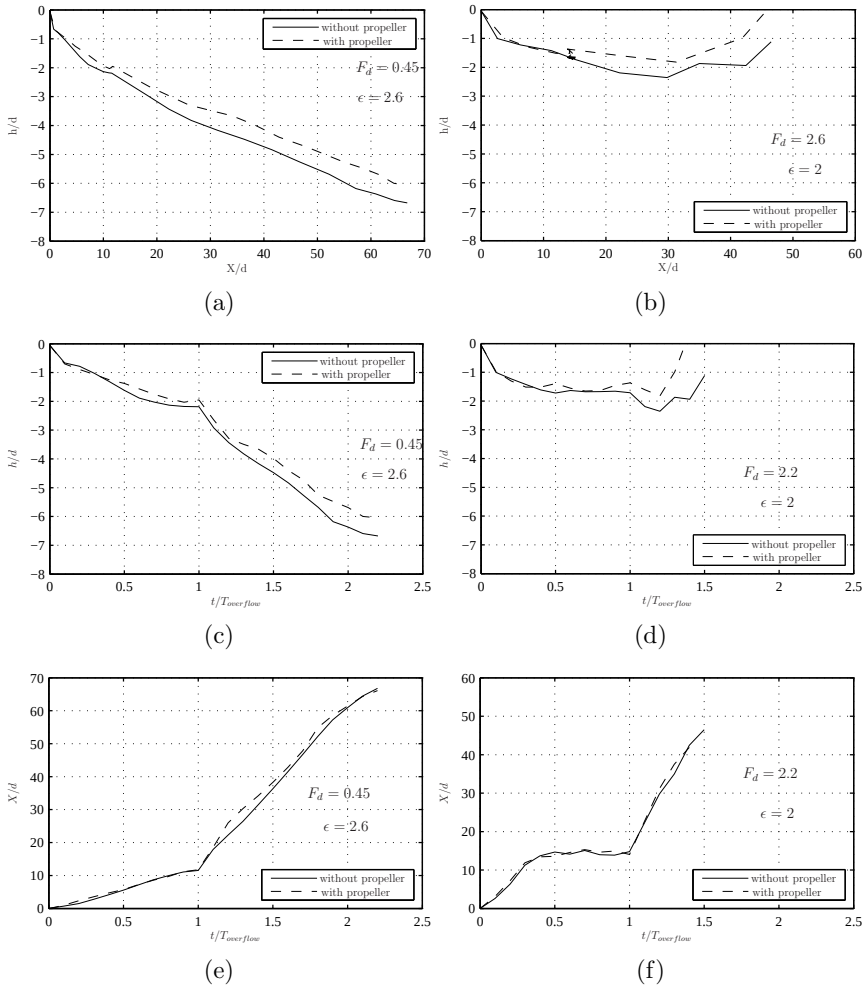

FIG. 17: Centroid of the plume under the influence of the dredger's propeller, in two regimes: Density driven (a-c-e) and Mixing (b-d-f)

Sediment variations in the overflow

The dredged material being pumped into the hopper often consist of wide range of sediment types varying in size and weight. Most of the coarse and heavier material settle inside the barge and the remaining fine and lighter grains flow overboard because their settling time scale exceeds the hoppers retention time. The average material characteristics of the overflowing mixture therefore differs from the parent material at the seabed. This has been investigated and discussed thoroughly by Jensen and Saremi (2014). Overlooking the mentioned mechanism will result in overestimation of the grain size and density of the material being

used as the source for the overflow plume.

In order to investigate the effect of variations in sediment type, three types of sediment have been considered (see table 1), type 1 representing fine silt and clay (but neglecting the cohesive properties), type 2 representing fine sand and type 3 which represents heavy volcanic sands.

TABLE 1: Sediment groups and their share in each mixture case

Type	$D_{50}(\mu m)$	$\overline{\rho}_s(\frac{Kg}{m^3})$	Case1	Case2	Case3
1	20	1800	0	50%	0
2	100	2500	100%	50%	50%
3	400	2700	0	0	50%

The total concentration and the inflow velocity of the overflow mixture are as described in the previous section. The position of the plumes centroid for the three cases have been plotted in figures 18 and 19. The results show that lighter mixture (case 2) remains above the other two cases, but the average vertical position of the heavier mixture (case 3) does not fall below the medium mixture (case2). The heavier mixture (case 3) has a slightly higher horizontal extend due to stronger density currents at the bed. In order to see whether the buoyancy is the dominating parameter causing the differences between the different cases, or the displacement effects, a fourth case (case 4) has been simulated with only the sediment type 2, with no other constituents. This means the total concentration of case 4 is half of the other cases. In figure 20 the position of the centroid of only the type 2 sediment in all cases has been plotted. Comparing the path of the type 2 sediments in case 1 and case 3 shows the dominant effect of displacement flow (lighter fractions being pushed up because of the downward movement of heavier fractions), as the centroid of type 2 sediments in case 3 lays above that of case 1 (figure 20). Although the mixture in Case 3 is heavier, but due to displacement effect, the lighter constituents are remained higher in water column and therefore the average position of the whole mixture stays close to case 1 (see figure 19a). However, the effect of buoyancy can be seen by comparing the vertical position of type 2 sediments in Case 2 and Case 4 (see figure 20). The mixture in Case 2 is heavier than the case 4, and therefore the type 2 constituents of it settles further down in compare to case 4.

The results confirm that by neglecting the dispersity of the mixture constituents (using a mono-sized model), the settling rate of the plume can be overestimated, as can be seen in figure 18, due to the omission of the combined effects of buoyancy and displacement on the plumes. The results also confirm that ignoring the trapping effect of the hopper (which results in considering a heavier overflow mixture than what actually is) causes an underestimation in the calculation of plumes dispersion rate.

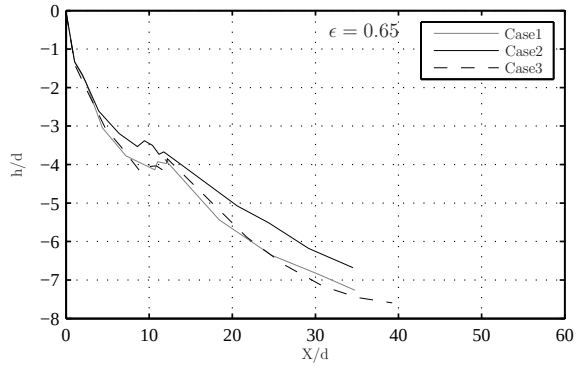

FIG. 18: Path of the centroid of the plume

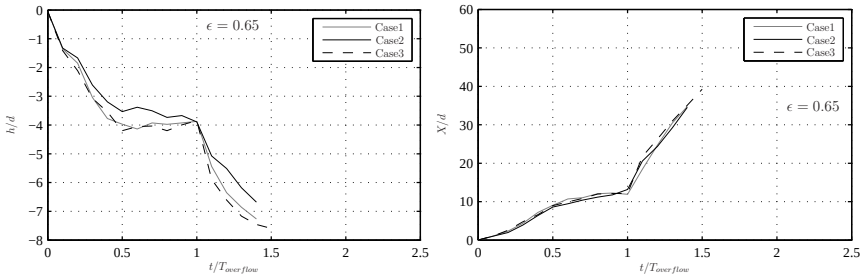

(a) (b)

FIG. 19: Time-series of the vertical (a) and horizontal (b) position of the centroid of the plume,normalized with the overflow pipe diameter d. $T_{overflow}$ represents the time when the overflow discharge stops

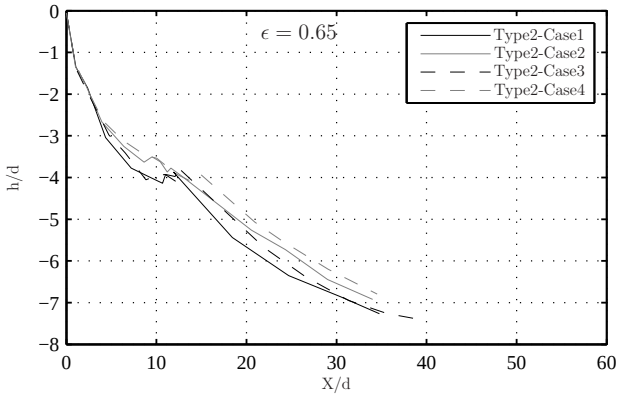

FIG. 20: Path of the centroid of the type 2 sediment in different mixture cases

CONCLUSION AND REMARKS

The nearfield behaviour of the overflow plumes during dredging operations has successfully been modelled by the mixture method which takes into account the dynamics of the plume due to density variations, the momentum exchange (due to relative motion of the particles and the fluid in the mixture) and the displacement effects due to volume exchange from settling. The peripheral entertainment mechanisms which are responsible for the dilution and expansion of the plume are resolved by using the LES method, so that the large entraining eddies are solved directly. The model is tested with experiments for two different problems, the overflow during dredging and the disposal of dredged material. It has been then used to investigate the effect of main driving parameters on the overflow plumes behaviour, namely the densimetric Froude number of the overflow mixture at the point of release (F_d), the velocity ratio between the ambient current and the overflow jet (ϵ) and the water depth. The results show that the mixing/density-driven behaviour of the overflow plume is dependant on both the mixture buoyancy and the ambient current. The combination of less buoyant plume ($F_d > 1$) and high velocities of ambient current ($\epsilon > 1$) drives the overflow into mixing regime and possibly results in creation of surface turbidity plumes.

The influence of the dredgers propeller on the overflow plume behaviour has been approximated by including the force field corresponding to the propeller (actuator disc method) in the computational domain. The results show that in both density driven and mixing regimes, the propeller can reduce the settling rate of the plume. However, further investigations with more detailed modelling of the flow field around the propellers is required.

Constituents of the overflow mixture are different from that of the parent material being dredged from the seabed. This is due to the trapping of coarser and heavier grains inside the hopper, which results in overflow mixture composing of lighter and smaller grains. Ignoring the mentioned mechanism, results in overestimation of the average size and density of the overflowing material, which overestimates the nearfied and farfeild settling rate of the plume. The dredged material naturally has size and to some extent density variations, which their settling and dispersion are affected due to both kinematic and dynamic interactions in between different fractions. The results from the numerical model shows that the presence of heavier material in the plume, increases the overall buoyancy, but due to displacement effect, the lighter constituents are pushed upward. The presence of lighter fractions , decreases the overall buoyancy and therefore the settling rate of the plume. Therefore, ignoring the size variations in the plume also results in miscalculation of its settling and dispersion rate.

The ability of the numerical model to resolve the dynamic and occupancy effects of sediments in the overflow plume, combined with the usage of the LES method and inclusion of polydisperse mixtures, provides a perfect tool in studying the nearfeld behaviour of the plumes and providing boundary conditions for the farfield large scale models.

ACKNOWLEDGMENTS

The support of the Danish Ministry of Science, Technology, and Innovation through the Godkendt Teknologisk Service (GTS) grant Marine Structures of the Future is acknowledged.

REFERENCES

Boot, M. (2000). "Near-field verspreiding van het overvloeiverlies van een sleephopperzuiger." M.S. thesis, TU Delft, The Netherlands.

Boutin, R. (2000). *Dragage et rejets en mer: les produits de type vase*. Presses de l'école nationale des ponts et chaussées.

Burel, D. and Garapon, A. (2002). "3D numerical modeling of dredged material descent." *Coastal Engineering*.

Bush, J. W. M., Thurber, B. a., and Blanchette, F. (2003). "Particle clouds in homogeneous and stratified environments." *Journal of Fluid Mechanics*, 489, 29–54.

De Wit, L. (2010). "Near field 3d cfd modelling of overflow plumes." *Proceedings of the 19th World Dredging Conference (WODCON XIX)*.

Decrop, B., Mulder, T. D., and Troch, P. (2013). "Experimental investigation of negatively buoyant sediment plumes resulting from Dredging operations." *CoastLab 2012*, (3).

Garside, J. and Al-Dibouni, M. (1977). "Velocity-voidage relationships for fluidization and sedimentation in solid-liquid systems." *Industrial & engineering chemistry ...*.

Gensheimer, R., Adams, E., and Law, A. (2013). "Dynamics of particle clouds in ambient currents with application to open-water sediment disposal." *Journal of Hydraulic Engineering*, (February), 114–123.

Gotoh, H. and Fredsøe, J. (2000). "Lagrangian Two-Phase Flow Model of the Settling Behavior of Fine Sediment Dumped into Water." *Coastal Engineering*, ASCE, 3906–3919.

Ishii, M. (2006). *Thermo-Fluid Dynamics of Two-Phase Flow*. Springer US, Boston, MA.

Jensen, J. and Saremi, S. (2014). "Overflow Concentration and Sedimentation in Hoppers." *Journal of Waterway, Port, Coastal, and Ocean Engineering*.

Jiang, Q., Kunisu, H., and Watanabe, A. (1997). "Numerical modeling of the settling processes of dredged material disposed in open waters." *International Offshore and Polar Engineering*, 510–515.

Kramer, K. (1939). "The induced efficiency of optimum propellers having a finite number of blades." *NACA, TM*, 884.

Oda, K. and Shigematsu, T. (1994). "Developemenet of a Numerical Simulation Method for Predicting the Settling Behaviour and Deposition Configuration of Soil Dumped into Waters." *Coastal Engineering*, 3305–3319.

Roscoe, R. (1952). "The viscosity of suspensions of rigid spheres." *British Journal of Applied Physics*, 3, 267.

Ruggaber, G. J. (2000). "Dynamics of Particle Clouds Related to Open Water Sediment Disposal." Ph.D. thesis, MIT, USA.

Shakibaeinia, A. and Jin, Y.-C. (2012). "Lagrangian multiphase modeling of sand discharge into still water." *Advances in Water Resources*, 48, 55–67.

Sørensen, J. N. and Shen, W. Z. (2002). "Numerical modeling of wind turbine wakes." *Journal of fluids engineering*, 124(2), 393–399.

Strausberg, S. (1983). "Turbidity interferes with accuracy in heavy metals concentrations.." *INDUST. WASTES.*, 29(2), 16–21.

Thackston, E. and Palermo, M. (1998). "Improved methods for correlating turbidity and suspended solids for dredging and disposal monitoring.

Winterwerp, J. (2002). "Near-field behavior of dredging spill in shallow water." *Journal of Waterway, Port, Coastal, and Ocean Engineering*, (April), 96–98.

Zhao, B., Law, A. W., Huang, Z., Adams, E. E., and Lai, A. C. (2012). "Behavior of sediment clouds in waves." *Journal of Waterway, Port, Coastal, and Ocean Engineering*, 139(1), 24–33.

CHAPTER 5

NUMERICAL MODELLING OF EFFECT OF THE GREEN VALVE ON AIR ENTRAINMENT AT HOPPER OVERFLOW

In preparation as:
Saremi, S. and Jensen, J. H., (2014). Numerical modelling of effect of the green valve on air entrainment at hopper overflow. To be submitted.

NUMERICAL MODELLING OF EFFECT OF THE GREEN VALVE ON AIR ENTRAINMENT AT HOPPER OVERFLOW

Sina Saremi and Jacob Hjelmager Jensen

ABSTRACT

The air entrainment at hopper overflow structures results in further mixing and slower settling of the sediment plume due to the positive buoyancy effects of the entrained bubbles. The hydraulics of the classic dropshafts (being in close resemblance to the hopper overflow structures) has been studied for better understanding of the air entrainment process and the driving parameters. A two-phase numerical model, based on the Volume of Fluid (VOF) method, has been established to simulate the process of overflow and the air entrainment in circular dropshafts, which has been verified successfully with the experimental data. The model has been used to simulate the performance of the so called Green Valve, as being a mitigation method in reducing the air entrainment in overflow pipes. The numerical results confirm the effectiveness of the valve in reducing the rate of entrainment of the air bubbles into the overflowing material. The model also provides information about the draw backs of this mitigation method, which is mainly the reduced rate of the overflow. The results however show that reduction in the overflow rate can be acceptable considering the significant reduction in air entrainment.

Keywords: Green valve, dropshaft, air entrainment, CFD, volume of fluid, dredging, overflow

INTRODUCTION

The operation of Trailing Suction Hopper Dredgers (TSHD) is based on continuous loading of dredged material into the hopper, which is most often appended with the overflow of excess mixture of water and fine sediment. The overflow results in generation of plumes, potentially inducing high levels of turbidity around the dredger, which may have severe impacts on marine and coastal environments. Earlier the overflow structure in TSHDs was simply of the weir-type, arranged on the sides of the hopper, where the mixture was released into marine waters. Since then, increased environmental awareness has prompted the design of more environment friendly systems that help reducing the temporal and spatial extend of the turbidity caused by the plumes. One of the first innovations was to relocate

the release point further down below the water surface, by installing one or more dropshafts along the hopper. These shafts are usually circular and equipped with telescopic weir providing adjustable overflow rates during the dredging operation (figure 1).

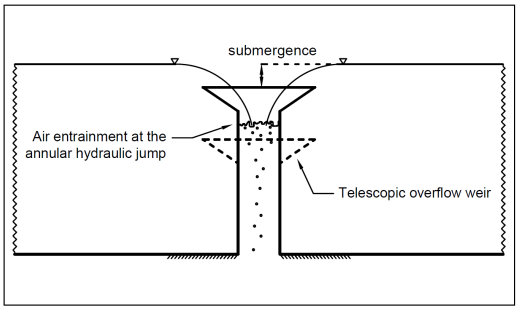

FIG. 1: Schematic representation of the overflow structure

The axial flow in dropshafts provokes air entrainment. In hoppers the trapped air in the overflow mixture, once discharged from the bottom of the dredger, tends to segregate owing to its buoyancy and rises towards the open water surface. This induces an upward stream of bubbles counteracting with the settling solid particles in the mixture. The extra mixing and hindrance due to the rising bubbles rectifies the near field spreading of the plume and drags it towards the surface, increasing the period of impact.

To understand the problem of air entrainment and the mitigation methods adopted to avoid air entrainment, it is beneficial to revisit the classic dropshaft hydraulic research. The nature of the annular flow through the overflow shaft is governed by the non-dimensional Froude number at the weir and the submergence level of the intake (Khatsuria 2004). At small submergence levels (low flow rates or large diameters of the shaft), the flow inside the shaft clings to the walls as a thin sheet leaving an open channel of air in the middle of the shaft all the way down to the plunging point at the bottom. The shear at the air water interface determines the air entrainment rate, which increases by increasing the flow velocity inside the shaft. Further increase in the flow rate reaches a point where the sheet of water is thick enough to completely seal the air passage at the lower end of the shaft. This latter situation is characterized by an annular hydraulic jump which moves up in the shaft by increasing flow rate. In this case the air entrainment rate decreases by increasing flow rate until it ceases at the point where the weir is fully submerged. Extensive studies on air entrainment in the vertical dropshafts have shown that the flow rate and shaft dimensions (gathered in the non-dimensional Froude number) and the submergence level at the intake are the main parameters in determining the rate of air entrainment in such structures. Jain et al. (1978) did series of experiments to investigate the air entrainment in radial flows through circular intakes. They proposed an empirical

relation (Equation 1) which determines the minimum (critical) submergence at which below that air entrainment begins. It is a function of the Froude number and the shaft diameter. Their experimental setup was a cylindrical tank with a vertical pipe as the intake in the tank bottom. The intake was equipped with guidance vanes to ensure fully radial flow into the overflow pipe.

$$\frac{S_c}{d} = 0.47F^{0.5} \tag{1}$$

Earlier, Harleman et al. (1959) did also similar experiments but without using any guiding vanes at the intake. Their empirical relation (Equation 2) is quite similar to the one proposed by Jain et al. (1978) but gives a higher threshold for the onset of air entrainment. This might be due to the extra circulations and vortices at the intake which were diminished in Jains experiments by using the guide vanes.

$$\frac{S_c}{d} = 0.47F^{0.4} \tag{2}$$

In the above equations S_c is the critical submergence, d is the shaft diameter and F is the non-dimensional Froude number defined by the diameter and the velocity inside the shaft. Air entrainment takes place when the submergence level of the overflow weir becomes smaller than the critical value which begins to show itself by creation of a gulping type flow at the water surface over the intake. Further decrease in the submergence level is then characterized by a descending annular hydraulic jump in the shaft. To avoid air entrainment, one should assure that the water level above the intake is more than the critical submergence value. In other words, the critical submergence level should be as small as possible. This can be achieved (according to equations 1 and 2) by either reducing the Froude number inside the shaft or decreasing the shaft diameter.

Overflow pipes in the hoppers should be able to handle different ranges of flow rates depending on the type of the dredging activity. Therefore the shaft diameter usually has its maximum required size based on the hoppers capacity and number of overflow pipes in it. Regarding this limitation, then it's more feasible to reduce the critical submergence level by reducing the flow velocity inside the shafts. A common way assuring that water level at the intake is above the critical submergence value, is to increase the hydraulic resistance inside the shaft. Jan de Nul (2003) developed the so called green valve (also known as the turbidity valve) which is an adjustable butterfly-type valve rigged inside the overflow shaft. The overflow is choked and leads to further submergence of the overflow weir.

Parys et al. (2000) studied the performance of the green valve by measuring the turbidity levels. The studies showed that by incorporating the valve, turbidity caused by the overflow plume was reduced to about 40% of the values registered from the case with no usage of the valve. It also showed a 30% reduction in the time required for the natural background turbidity to return. These results

confirm the pronounced effect of air entrainment on the turbidity caused by the overflow plumes. In the present work a numerical model is established to study the air entrainment rate at the overflow shafts and evaluating the effect of the green valve by modelling the hydraulic processes involved.

In the following the numerical model is described and is verified by simulating the laboratory experiments carried out by Whillock and Thorn (1973), who measured the rate of air entrainment in dropshafts. Thereafter the model is used to analyse the air entrainment in circular overflow shafts and investigating the effect of the green valve.

NUMERICAL MODEL DESCRIPTION

The dynamics of the two-phase (air and water) flow is modelled by solving one set of the equations of conservation of volume and momentum where the volume of fluid (VOF) method (Hirt and Nichols 1981) is implemented as the interface capturing scheme.

$$\nabla.(\overrightarrow{U}) = 0 \tag{3}$$

$$\frac{\partial \rho \overrightarrow{U}}{\partial t} + \nabla.(\rho \overrightarrow{U}\,\overrightarrow{U}) = -\nabla P + \nabla^2(\mu_{eff} U) + \rho \overrightarrow{g} + f_s \tag{4}$$

$$\frac{\partial c\rho}{\partial t} + \nabla.(c\rho \overrightarrow{U}) = 0 \tag{5}$$

Here P is the total pressure and is assumed to act equally on both phases. The effective viscosity μ_{eff} is sum of the dynamic viscosity and the sub-grid scale turbulent eddy viscosity which is defined later in this chapter. The density ρ and the dynamic viscosity μ are defined as functions of the volume fraction of the liquid phase c in the following equations (6 and 7).

$$\rho = c\rho_l + (1-c)\rho_g \tag{6}$$

$$\mu = c\mu_l + (1-c)\mu_g \tag{7}$$

The subscripts l and g stand for the liquid and gas phases respectively. The last term on the right hand side of the equation 4 is the surface tension force at the interface which is based on the continuum model of Brackbill et al. (1992).

$$f_s = \sigma\kappa\nabla(c) \tag{8}$$

The surface tension force is defined as function of the gradient of the liquid volume fraction. It indicates that the force is active at the interface regions as in the other regions the gradient of c is zero. Here σ is the surface tension for the air-water interface which is about $0.07 N/m$ at the temperature of $25°C$. The surface tension force is function of the curvature of the interface as well, which is defined as below.

$$\kappa = \nabla(\frac{\nabla c}{|\nabla c|}) \tag{9}$$

The problems due to the boundedness and conservativeness of the phase fractions at the sharp interface between water and air (corresponding to the VOF method) have been mitigated by the method developed by Berberović et al. (2009), where the equation 5 is replaced by the equation 10 below.

$$\frac{\partial c\rho}{\partial t} + \nabla.(c\rho\overrightarrow{U}) + \nabla(\rho c(1-c)U_r) = 0 \tag{10}$$

Here U_r is the relative velocity of the two phases at the interface. The additional convective term has the role of keeping the interface sharp and has the designated name of "the compression term" which means that it compresses the interface towards a sharper one and has nothing to do with the compressible flows. For detailed description of the compression term read Berberović et al. (2009). The turbulence in the flow is handled by the Large Eddy Simulation (LES) method, where by using a filter (based on the computational mesh resolution) the large exclusive eddies are resolved and the small universal sub-grid scales are represented by the one-equation kinetic energy model.

$$\frac{\partial k}{\partial t} + \nabla.(k\overrightarrow{U}) = \nabla^2(\mu k) + 2\mu_{SGS}(S:S) - \frac{C_e}{\Delta}k^{3/2} \tag{11}$$

Here k is the sub-grid scale (SGS) kinetic energy, μ_{SGS} is the SGS turbulent eddy viscosity defined in equation 12, S is the deformation rate (equation 13) and the constant C_e has the value 1.048.

$$\mu_{SGS} = C_k\rho\sqrt{k}\Delta \tag{12}$$

$$S = \mu_m\frac{1}{2}(\nabla\overrightarrow{U} + \nabla^T\overrightarrow{U}) \tag{13}$$

The filter size Δ is chosen to be the cubic root volume of the computational cells and the constant C_k has the value 0.094. The superscript T in equation 13 denotes the matrix transpose function.

The numerical model is implemented in the open source CFD code OpenFOAM based on the finite volume method. The PISO (Pressure Implicit with Splitting of Operator) pressure-velocity coupling algorithm is used and the pressure equation is solved by the multi-grid technique. The choice of the above described model has been first confirmed by showing that its capable of simulating the entrainment process and giving acceptable results in compare to the measured laboratory data. However the authors are aware of the known issues with the interface compression method specially the problem of spurious velocities at the sharp interfaces (Deshpande et al. 2012), but the aim of the present study is to use the model as a screening tool to evaluate the relative performance

of the mitigation methods on the process of air entrainment. Therefore, detailed resolving of the physics of the air bubbles are out of the scope of the present work.

MODEL VERIFICATION

Whillock and Thorn (1973) designed an experimental system to study the air entrainment due to the plunge in dropshafts and to quantify the relationship between the air demand of the system at different scales. Besides being well described and documented, the novelty of their experimental setup was the elimination of as many as possible variables in the system. The two-dimensional vertical plunge was consisted of a constant-head water inlet at the top and a submerged outlet tunnel at the bottom. The closed volume of air inside the shaft was then connected to an air inlet with a gauge (Figure 2).

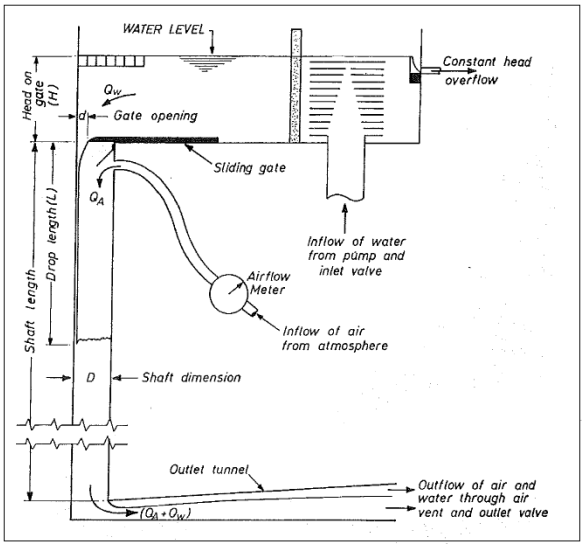

FIG. 2: Experimental setup of Whillock and Thorn (1973)

The air-water emulsion at the plunging point entrains the air bubbles into the water column. Depending on the plunge and the shaft characteristics, a portion of bubbles have the chance to rise up again and leave the water. The remaining trapped bubbles then follow the flow through the outlet tunnel. The rate of air entrainment is then registered by the air gauge at the top of the shaft which is responsible for replacing the lost volume of air (trapped air) back into the free space inside the shaft. The numerical simulation of the experimental setup is done by modelling the dropshaft with constantly inflowing water from the top and an outlet tunnel at the bottom of the shaft. The airflow meter has been modelled as an open inlet/outlet boundary which then the air flux through it was calculated. In figure 3 the 3-dimensional computational domain is presented.

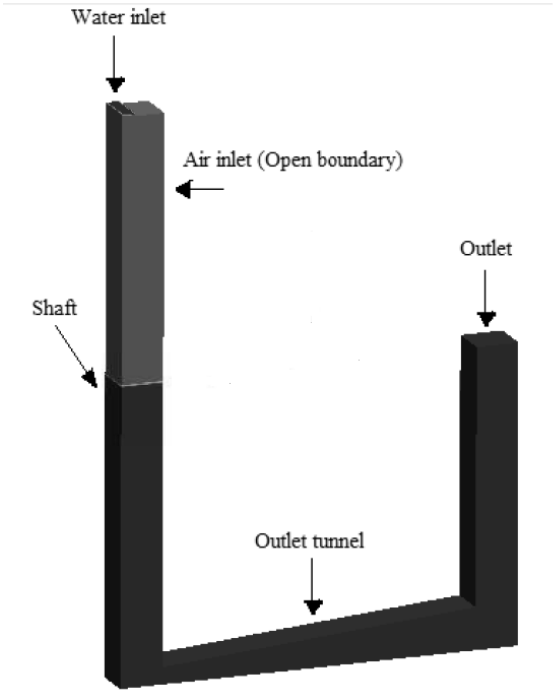

FIG. 3: The computational domain for simulation of the experiment

Whillock and Thorn, based on the model and prototype observations, reported a consistent predominance of bubbles with 1-5 mm equivalent diameter. This has been the basis for choosing the grid resolution in the numerical model. An important point is that although the experimental setup had a fully two-dimensional design, but due to three-dimensionality of the entrainment phenomenon and bubbles behaviour, a 2D model is not able to correctly predict the entrainment rate. The test case with $44.5mm$ inlet gate opening and discharge of $0.0125m^3/s$ has been simulated by both the 2D and 3D numerical model, where the ratio of air flux to the water flux at the outlet has been calculated. In figure 4 it can be seen the difference in the results from a 2D and 3D model. The good agreement between the 3D numerical results and the measured experimental data indicates that the model is capable of capturing the entrainment processes, therefore can be used for further investigation of the problem.

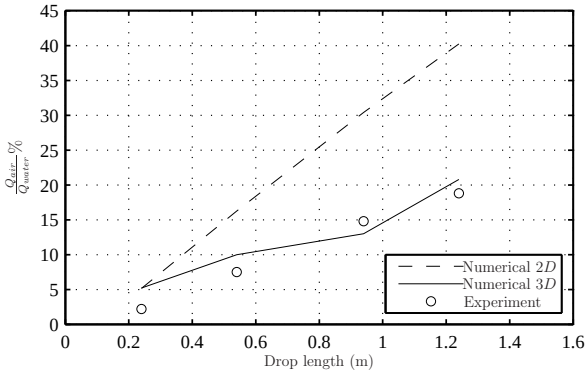

FIG. 4: The air entrainment ratio at different drop lengths; measurements by Whillock and Thorn (1973) (circles), 3D numerical results (full line) and 2D numerical results (dashed line)

AIR ENTRAINMENT IN CIRCULAR SHAFTS

The dependency of air entrainment on the submergence level and the Froude number inside the shaft is defined based on the empirical relation of Jain et al. (1978) and Harleman et al. (1959) for critical submergence . Their expressions were derived from experimental data on a circular dropshaft which is the common configuration of overflow system in the hoppers. The numerical model has been used to setup a 3-dimensional circular tank with an overflow shaft placed in the middle. The dimensions of the model has been scaled down to about 10% of a real hopper overflow as a payoff to the computational costs of having a mesh which is refined enough to capture the entrainment processes. This is justified by keeping the Froude number in the same range as in the prototype. The free surface flow enters the tank radially from all sides and overflows through the pipe in the middle. The entrainment rate is then determined by calculating the flux of the air phase at the bottom outlet of the shaft. A representation of the computational domain is depicted in figure 5.

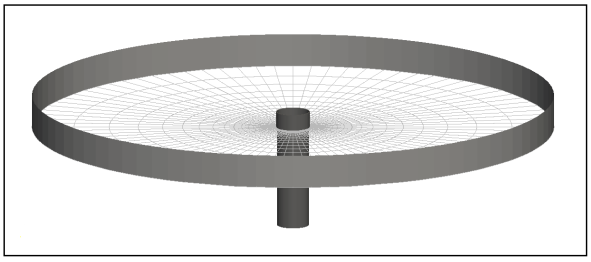

FIG. 5: Computational domain for simulation of circular dropshaft

The entrainment rate has been registered with different submergence levels and Froude numbers by adjusting the flow rate approaching the shaft or the shaft diameter. The results in terms of occurrence of air entrainment have been plotted against the Jains and Harlemans empirical thresholds (Figure 6). The cases where air entrainment occurs fall in the same region which empirical relations assign. This shows that the dependency of the entrainment on the submergence level and the Froude number is recognized by the numerical model as well.

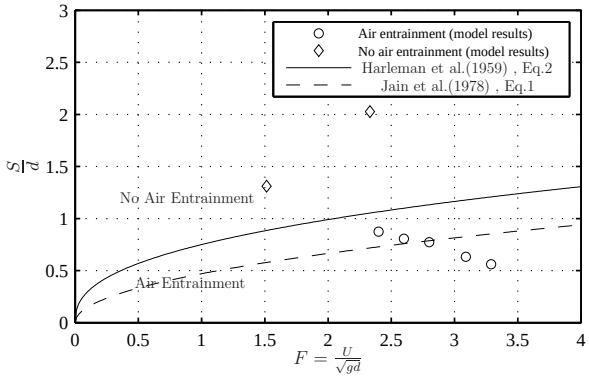

FIG. 6: Empirical thresholds for critical submergence (lines) and the simulation cases with and without air entrainment (circles and diamonds)

GREEN VALVE

The air entrainment at the overflow system in the hoppers results in enhanced mixing and dilated existence of the turbidity plume. The rate of the air entrainment, as shown in previous section, decreases by increasing submergence of the overflow weir, decreasing the shaft diameter or reducing the Froude number inside the shaft. In general moving above the lines of the empirical thresholds (Figure 6) results in reduction or even cease of the air entrainment. The physical constraints in the hoppers and the case specificity of different dredging projects limit the adjust-ability of the submergence level at the overflow and the shaft diameter. Therefore a more feasible solution is to increase the hydraulic resistance inside the shaft in order to decrease the Froude number and as a consequence decrease the critical submergence limit. Such practice is already being used in the sewers and waste water systems, known as the baffle/cascade dropshafts. This concept has been exercised in dredging industry by rigging a butterfly-type valve midway in the overflow shaft which creates a controllable hydraulic resistance inside the shaft by choking the flow. The effect of using the so called green valve on the turbidity levels induced by the overflow plumes has been reported by Parys et al. (2000) from a 5-years monitoring project The MOBAG 2000. They reported up to 60% reduction in the turbidity levels after using the green valve in a TSHD overflow system. Such a considerable reduction highlights the significance of the

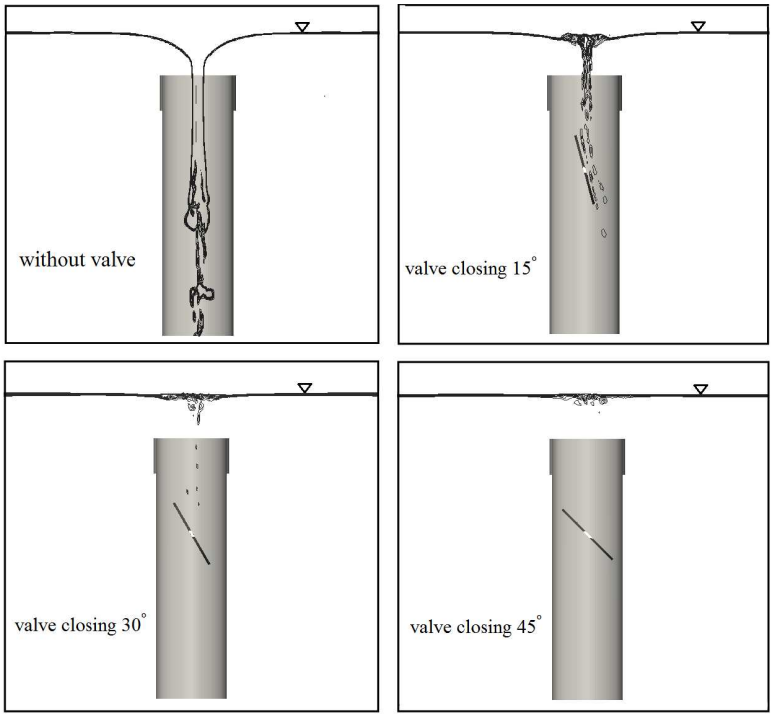

FIG. 7: Demonstration of air-water interface at the reference case (without valve) and three different valve openings

green valve in mitigating the environmentally adverse effects of the turbidity plumes.

The effect of the butterfly-type valve inside the circular overflow shaft has been simulated by the numerical model. A circular solid plate, representing the valve, is placed inside the shaft with three different opening angles. In order to investigate the effect of the green valve, first a case without the valve (the reference case) has been simulated and then by placing the valve in the model, the results have been compared with the reference case. In the reference case $\frac{S}{d} = 0.56$ and $F = 2.8$, which according to figure 6 is in the entrainment region. Three different cases have been simulated with different valve openings and the demonstration of the air water interface of different test cases at their equilibrium state is shown in figure 7. It is clearly visible that the placement of the valve results in elevation of the annular hydraulic jump all the way up to the surface. In this case even the slightly closed valve (15 degrees from vertical) chokes the flow enough to almost cease the air flow from the bottom.

The presence of the valve causes an extra hydraulic resistance to the flow passing through the shaft and reduces the flow rate. This reduction results in smaller Froude numbers inside the shaft and therefore reduces the critical sub-

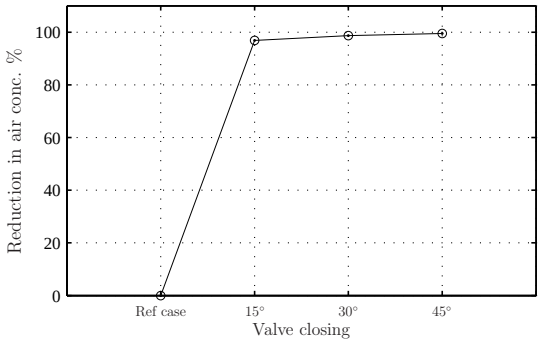

FIG. 8: Reduction in air concentration at the shaft outlet at different closings

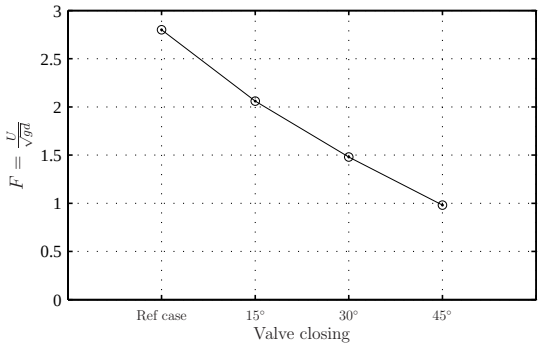

FIG. 9: Froude number inside shaft at different closings of the valve

mergence at the shaft intake which then results in less air entrainment. It can be seen in figure 7 that reduction in critical submergence and the air entrainment is accompanied by the elevation of the annual hydraulic jump at the plunge towards the surface. In other words, the resistance due to the valve causes the water level inside the shaft to rise. In figure 8 the reduction in the air entrainment relative to the reference case (with no valve) has been plotted for the three different valve openings. It shows a significant reduction in the air fraction leaving the shaft even with the slightly closed valve.

According to figure 6 the air entrainment ceases when we are above the critical line. The role of the green valve is to move the conditions at the intake towards the non-entrainment region (figure 6) by reducing the Froude number inside the shaft. In figure 9 the Froude numbers for the four cases has been plotted where it shows the reduction as the valves closes further. The reduced Froude numbers in cases with the Green Valve (which all have $\frac{S}{d} = 0.56$) are above the empirical thresholds.

The reduction in the flow rate inside the shaft caused by the green valve has always been considered as a drawback by the dredging contractors. Its therefore

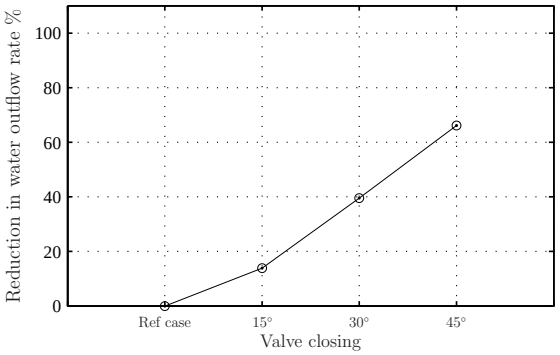

FIG. 10: Reduction in the flow rate through the shaft at different closings

desired to find an optimum closure of the valve which has the most reduction in air entrainment and the least reduction of the flow rate. In figure 10 the reduction in flow rate has been plotted for the three different closings of the valve. The results from the numerical model show that in the case with 15 degrees of valve closure which gives up to 96% reduction in air entrainment, the reduction in overflow rate is less than 20%.

CONCLUSION AND REMARKS

The overflow structures in the hoppers closely resemble the hydraulic dropshafts. The entrainment of the air bubbles into the overflowing mixture results in further mixing and slower settling of the sediment plumes which is totally undesirable from the environmental point of view. The effect of different parameters on rate of air entrainment in dropshafts has been investigated by the two-phase interface capturing numerical model based on the VOF method. The ability of the model in resolving the entrainment process is successfully verified by 3-dimensional simulation of the experimental work of Whillock and Thorn (1973) using the Large Eddy Simulation (LES) method. The performance of the green (turbidity) valve has been then investigated by the numerical model, where the results clearly confirm the reductive effect of the valve on the rate of air entrainment. The results from the numerical model also show the reduction in the flow rate through the shaft, which has always been considered as a draw back of using the green valve. However, the results tell that the rate of reduction in the air entrainment due to closure of the valve is far more higher than the relative reduction in the flow rate for the corresponding valve closure. For example, according to figures 8 and 10, by closing the valve about 15 degrees, the air entrainment almost ceases where the reduction in the flow rate at this situation is less than 20%. This implies that an optimum closure point can be found to have the most reduction in the air entrainment with the least choking of the flow through the overflow pipe. It requires more detailed sensitivity analysis based on the shape of the valve and the intake of the overflow shaft.

ACKNOWLEDGMENTS

The support of the Danish Ministry of Science, Technology, and Innovation through the Godkendt Teknologisk Service (GTS) grant Marine Structures of the Future is acknowledged. The simulation of the experimental case and part of mesh generations were performed by Ms. Hale Al-Mousavi under guidance of the authors.

REFERENCES

Berberović, E., van Hinsberg, N., Jakirlić, S., Roisman, I., and Tropea, C. (2009). "Drop impact onto a liquid layer of finite thickness: Dynamics of the cavity evolution." *Physical Review E*, 79(3).

Brackbill, J., Kothe, D., and Zemach, C. (1992). "A continuum method for modeling surface tension." *Journal of computational physics*.

Deshpande, S. S., Anumolu, L., and Trujillo, M. F. (2012). "Evaluating the performance of the two-phase flow solver interFoam." *Computational Science & Discovery*, 5(1), 014016.

Harleman, D., Morgan, R., and Purple, R. (1959). "Selective withdrawal from a vertically stratified fluid." *Proc. 8th Congress Int. Assoc. Hydraulic Res.*

Hirt, C. and Nichols, B. (1981). "Volume of fluid (VOF) method for the dynamics of free boundaries." *Journal of Computational Physics*, 39(1), 201–225.

Jain, A. K., Garde, R. J., and Ranga Raju, K. G. (1978). "Air entrainment in radial flow towards intakes." *Journal of the Hydraulics Division*, 104(9), 1323–1329.

Jan de Nul (2003). "SPECIALISED ALTERNATIVE DREDGING METHODS." *3er Congreso Argentino de Ingenieria Portuaria*.

Khatsuria, R. M. (2004). *Hydraulics of spillways and energy dissipators*. CRC Press.

Parys, M. V., Dumon, G., Pieters, A., Claeys, S., Lanckneus, J., Lancker, V. V., and Vangheluwe, M. (2000). "Environmental monitoring of the dredging and relocation operations in the coastal harbours in Belgium : MOBAG 2000." *WODCON XVI*, Vol. 32, Kuala Lumpur, Malaysia.

Whillock, A. and Thorn, M. (1973). "Air Entrainment in Dropshafts.

DTU Mechanical Engineering
Section of Fluid Mechanics, Coastal and Maritime Engineering
Technical University of Denmark

Nils Koppels Allé, Bld. 403
DK- 2800 Kgs. Lyngby
Denmark
Phone (+45) 4525 1360
Fax (+45) 4588 4325
www.mek.dtu.dk
ISBN: 978-87-7475-389-6

DCAMM
Danish Center for Applied Mathematics and Mechanics

Nils Koppels Allé, Bld. 404
DK-2800 Kgs. Lyngby
Denmark
Phone (+45) 4525 4250
Fax (+45) 4593 1475
www.dcamm.dk
ISSN: 0903-1685